SOLAR PHOTOVOLTAIC ENERGY SYSTEM ANALYSIS USING LINEAR QUADRATIC REGULATOR AND MODEL REFERENCE ADAPTIVE CONTROL TECHNIQUES

A THESIS

BY

ABRAHAM, IDARESIT ISAAC
20194196588
(CONTROL ENGINEERING OPTION)

SUBMITTED TO

THE DEPARTMENT OF ELECTRICAL AND ELECTRONIC ENGINEERING,
SCHOOL OF ELECTRICAL SYSTEMS ENGINEERING TECHNOLOGY (SESET),
FEDERAL UNIVERSITY OF TECHNOLOGY, OWERRI (FUTO)

In Partial Fulfilment of the requirement for the Award of the Master of Engineering (M.Eng.) Degree in Electrical and Electronic Engineering (Control Engineering option).

SUPERVISORS

ENGR. DR. C. C. MBAOCHA
ENGR. DR. S. O. OKOZI

DECEMBER, 2023.

Certification

I certify that this work, "**Analysis of Solar Photovoltaic Energy System using LQR and MRAC Techniques**" was carried out by **Abraham, Idaresit Isaac (20194196588)** in partial fulfilment of the requirements for the award of the M.Eng. degree in Control Engineering in the Department of Electrical and Electronic Engineering, School of Electrical Systems Engineering Technology, Federal University of Technology Owerri.

.....
Engr. Dr. C. C. Mbaocha
(Lead Supervisor)

20/4/24
Date

.....
Engr. Dr. S. O. Okozi
(Co-Supervisor)

22-04-2024
Date

.....
Engr. Dr. N. Chukwuchekwa
(Head of Department)

22/4/24
Date

.....
Engr. Prof. M. C. Ndinechi
(Dean, SESET)

30/7/24
Date

.....
Prof. D. O. Esonu
(Dean, Postgraduate School)

.....
Date

.....
External Examiner

22/4/24
Date

Engr. Prof. Chigozie Ihekweaba

Acknowledgements

Let me first of all acknowledge God Almighty, the author and finisher of my faith for his unmerited grace, which has made this work a reality amidst all challenges. I hereby express my heartfelt gratitude to my loving and amiable supervisors, Engr. Dr. C. C. Mbaocha and Engr. Dr. S. O. Okozi, whose positive and resourceful guidance, encouragement, kindness and patience, have enabled me to go this far.

I cannot fail to appreciate the Dean of the School of Electrical Systems Engineering Technology, Engr. Prof. M. C. Ndinechi, the Head of the Department of Electrical and Electronic Engineering, Engr. Dr. N. Chukwuchekwa, my lecturers, Engr. Prof. D. O. Dike, Engr. Dr. O. J. Onojo, Engr. Prof. L. O. Uzoechi, Engr. Dr. I. O. Akwukwaegbu, Engr. Dr. M. Olubiwe, Engr. Dr. O. C. Nosiri, and other distinguished academic staff of the department; Engr. Prof. (Mrs) G. N. Ezeh, Engr. Prof. (Mrs) G. A. Chukwudebe, Engr. Prof. E. N. C. Okafor, Engr. Prof. F. K. Opara, Engr. Prof. I. E. Achumba, Engr. Dr. L. S. Ezema, Engr. Dr. A. O. Akande, Engr. Dr. C. K. Agubor, Engr. R. O. Opara, Engr. Dr. C. K. Joe-Uzuegbu, Engr. Dr. N. C. Onuekwusi, Engr. R. C. Okpara, Engr. C. F. N. Ubbonu, Engr. C. J. Onwuagba, Engr. E. U. Ekwueme, Engr. C. F. Paullinus-Nwammuo, Engr. E. Ezeugwu for their outstanding academic and moral support, advice and encouragement in the course of this work.

I also seize this opportunity to thank all other academic and non-academic staff in the deparment whose names are too numerous to mention here, for their academic and moral support throughout the period spent to achieve this feat. I cannot forget my father, Elder Isaac Abraham and my siblings, whose prayers have supported me during this great task. I also specially thank my colleagues and friends, most especially Mfonobong Eleazar Benson, for their great supports in one way or the other.

Dedication

This work is dedicated to my mother, Late Mrs. Ekaette Isaac Abraham and other contributors.

Table of Contents

List of figures

List of tables

ABSTRACT

This work presents solar photovoltaic energy system analysis using incorporated linear quadratic regulator (LQR) and model reference adaptive control (MRAC). Solar photovoltaic (PV) energy system is one of the renewable energy applications, which operates by tracking energy from the sun and converting it into useful electrical energy. However, harnessing the generated energy has been the major concern of the engineers hence the adoption of various control strategies for efficient control of the generated power. The idea is to transfer the optimal generated power to the output considering the fact that PV energy produced may have been affected by irradiation and temperature conditions. To avoid the unstable output power, there is need to deploy an efficient control scheme. Most of the conventional control techniques are not optimal to resolve power inaccuracies in the system and they have shortcomings. The control methods employed in this work involved the combination of LQR and MRAC to investigate the control performance. The results obtained by simulation on MATLAB/Simulink software, show that the average tracking efficiency for LQR control scheme was 95.92% compared to MRAC Type with an average tracking efficiency of 73.41% while the integrated MRAC-LQR control has a tracking efficiency of 94.45%. Rise time was used to measure the speed of convergence for the control schemes. LQR has a rise time of 1.95ms while MRAC and MRAC-LQR have 1.323s and 0.156ms respectively. LQR control does not adapt to the changing conditions of the environment but MRAC and MRAC-LQR have adaptive features, which enables the system adjust itself at varying environmental conditions. Moreover, LQR-MRAC accepts a higher adaptation gains ($0.2 < \Gamma < 900$) compared to the MRAC-type with $0.1 < \Gamma < 2$. The duty cycles for LQR, MRAC and LQR- MRAC were also determined to be approximately 0.6, 0.7 and 0.6 respectively. Considering its unique features such as appreciable tracking efficiency, rise time, duty cycle and the ability to adapt even at higher adaptation gain values, LQR- MRAC control scheme is recommended over the other two (LQR and MRAC).

Keywords: Adaptive control scheme, Improvement, Linear quadratic regulator, Maximum power point, Model reference, Solar photovoltaic energy, Tracking

CHAPTER ONE

INTRODUCTION

1.1 Background of study

The issue of greenhouse emission which is caused by the use of the traditional energy sources has given the researchers a great concern. To reduce the greenhouse effect, renewable energy has recently become one of the major research areas across the globe. Fossil fuels like gas and oil are not renewable, unclean and they are not eco-friendly source of energy. Unlike the traditional energy, solar energy is clean, inexhaustible and free (Dolara, Faranda & Leva, 2009). Solar energy is one of the most important renewable energy sources. To harness this energy to the fullest, there is need to build a photovoltaic (PV) system capable of tracking maximum power. PV system is divided into two categories: Stand-alone and Grid connected PV system. For places that are away from the utility grid, stand-alone PV systems are used at those places. In these systems, the performance of a PV system relies on the operating conditions. The maximum power extracted from the PV source depends strongly on three factors such as irradiation, load profile and temperature (Salas, Olıas, Barrado & Lazaro, 2006). The photovoltaic (PV) power system is becoming increasingly important as the most available renewable source of energy since it is clean with little maintenance, low cost and without any noise, which is as a result of the absence of moving parts. Nevertheless, one of the issues associated with PV systems is the nonlinear characteristics of the power curve which change the amount of electric power generated (Dolara et al., 2009). Photovoltaic (PV) systems are a critical component in addressing the national mandates of achieving energy independence and reducing the potentially harmful environmental effects caused by increased carbon emissions (Khanna, Zhang, Stanchina, Reed & Mao, 2014).

Moreover, the interest in Distributed Energy Systems (DES) is increasing (Philipson, 2000). DES is a decentralized approach towards energy management system and it entails using many small generators with output of 2-50 MW, situated at numerous strategic points throughout cities and towns, so that each provides power to a small number of consumers nearby. Larger power

plants have become uneconomical in many regions because of strict environmental regulations and security issues, and this has led to lack of corridors for building high voltage transmission systems hence the need for DES. Photovoltaic systems have become increasingly popular and are ideally suited for distributed systems. Additionally, recent technological advances in small generators, power electronics, and energy storage devices have provided a new opportunity for distributed energy resources that are located closer to loads. Many governments have provided the much needed incentives to promote the utilization of renewable energies, encouraging a more decentralized approach to power delivery systems. In spite of their relatively high cost, there has been very remarkable growth in installed Photovoltaic systems. According to the International Energy Agency (2001), recent studies show an exponential increase in the worldwide installed photovoltaic power capacity. There is ongoing research aimed at reducing the cost and achieving higher efficiency. Furthermore, new regulatory laws mandating the use of renewable energy have expanded this market around the world. PV energy is adopted as one of the most important energy sources for the future.

It is important to operate PV energy conversion systems in the maximum power point (MPP) to maximize the output energy of PV arrays. This is not possible if a tracking algorithm is not integrated into the system, hence the need for maximum power point tracking (MPPT) control to extract this maximum power from the PV arrays. Typically, MPPT algorithms are integrated into power electronic converter systems, where the duty cycle of the converter is controlled to deliver maximum available power to the load (Brunton, Rowley, Kulkarni & Clarkson, 2010; Mastromauro, Liserre, Kerekes & Dell'Aquila, 2009). A large number of techniques have been proposed for tracking the maximum power point (Manel & Hfaiedh, 2016) and they are discussed in the literature. Due to the various MPPT methods, different researchers in PV systems have presented a comparative analysis of MPPT techniques. These techniques vary in complexity, cost, speed of convergence, sensors required, hardware implementation, and effectiveness.

The control strategy of Perturbation and Observation (P&O) method requires external circuitry to repeatedly perturb the array voltage and subsequently measure the resulting change in the output power. P&O is seen as an inexpensive and relatively simple method but the algorithm is however

inefficient in the steady state because it forces the system to oscillate around the maximum power point (MPP) instead of continually tracking it. Furthermore, the P&O algorithm fails under rapidly changing environmental conditions, because it cannot discern the difference between changes in power due to environmental effects versus changes in power due to the inherent perturbation of the algorithm (Jainand & Agarwal, 2004). This therefore calls for the need to search for other control algorithms that can provide a more efficient result. This work therefore focuses mainly on the performance effect of linear quadratic regulator (LQR) and model reference adaptive control (MRAC) techniques on solar PV systems.

Whitaker et al. in 1958 originally proposed the MRAC method for effective control. In this control scheme, the controller parameters are allowed to be adjusted through an adjusting mechanism designed in the feedback control law to give a plant output performance similar to that of the reference model. An adaptive controller, unlike a fixed gain controller, is capable of achieving good performance in the presence of significant parametric uncertainties, and even without the full knowledge of the plant (Yucelen & Calise, 2011). A fast adaptation can be achieved because the performance index measurements are obtained simply by a direct comparison of the output with the reference model and the plant. Thus, this method does not require the identification of the plant dynamic performance, although a certain apriori knowledge of the plant structure is necessary to implement the adaptive control system (Astrom, 1983; Hang & Parks, 1973; Landau, 1973). Although a high gain control ensures a faster response in theory, it may cause instability due to excitation of unmodeled dynamics. Furthermore, a high gain controller requires a high fidelity system dynamics, which can be difficult to obtain. Therefore, the adaptive gains are generally kept small to avoid instabilities (Ghaffar & Richardson, 2015). In order to allow the model reference adaptive controller to make a stable correction to compensate for unmodelled parametric changes without the occurrence of instability due to high gain, an LQR technique should be incorporated. The response of a system controller with LQR controller is very good when the plant is similar to how it was modelled initially. However, if there are significant changes in the plant parameters LQR controller fails to operate as designed. To provide a viable solution for the limitations involved in using only one of these control techniques the combination of both LQR and MRAC is important. It is expected that the controller is capable of benefitting from the optimal response of LQR controller in the nominal

case, as well as providing self-correction features from adaptive controller when there are changes in the plant parameters.

1.2 Statement of problem

The nonlinear characteristic of the photovoltaic system which arises as a result of variations in solar irradiation, temperature and the profile loads, has been a great challenge faced by researchers over the past decades. Due to these variations, photovoltaic systems do not continually deliver the optimal power to the load. The amount of power generated from any PV panel varies based on the resistive load applied across the panels, and as a result brings about a reduction in the generated power, even at the same solar irradiance and temperature. To minimize the power losses, maximum power point tracking (MPPT) devices are required to enable the photovoltaic system to adapt to environmental changes so that adjustment in the voltage operating point is obtained hence delivering the optimal power. This challenge calls for the proper design of MPPT algorithm capable of achieving such an objective. Therefore, this work is bent on making relevant contribution in this research area by investigating the performance of photovoltaic system based on linear quadratic regulator (LQR) and model reference adaptive control (MRAC) algorithms.

1.3 Objectives of the study

The main objective of this research is Solar Photovoltaic Energy System Analysis using Linear Quadratic Regulator (LQR) and Model Reference Adaptive Control (MRAC). The specific objectives are as follows:

(i) To design a Linear Quadratic Regulator (LQR)

(ii) To design a Model Reference Adaptive Control (MRAC) system.

(iii) To combine the model designs of the LQR and MRAC controllers.

(iv) To simulate the system through the application of MATLAB/Simulink software package.

(v) To analyze and validate the results with the conventional control schemes, with respect to the performance characteristics such as adaptability, stability, tracking speed and efficiency.

1.4 Justification of the study

In recent time there has been a global move to protect our beloved planet against global warming, which in addition to other causes, owes greatly to greenhouse emission. This move has correspondingly mandated an industrial revolution which has seen an increased level of appreciation and integration of clean energy sources in the industries since the past decade. Solar energy could be one of the significant sources as an alternative energy for the future. In regard to endless importance of solar energy, it is worth saying that photovoltaic energy is the best prospective solution for energy crisis. However, key issues like intermittency in supply, resource location and cost of renewable energy materials are the main roadblocks preventing it from entering the mainstream energy. At this level, producers, policy makers and governments have an important role to play in addressing the challenges associated with the development of renewable energy. To push for the success of this great move means in a way to delve deeply into researches that seek to incorporate power generated by solar energy sources which is in abundance naturally in Africa into the available national grids. This research is therefore significant as it deems to contribute usefully to the development of an algorithm that can be used in building the suitable MPPT controller for photovoltaic system. Both researchers and power system engineers will benefit from this work immensely.

1.5 Scope of study

This work was limited to the analysis of solar photovoltaic energy system using linear quadratic regulating (LQR) algorithm incorporated with model reference adaptive control (MRAC) technique. The system model was limited to a boost converter based control system architecture through which the process to be controlled was designed using the specifications from the MITSUBISHI Electric Photovoltaic Module Specification Sheet, with the model $PV-MLU255HC$. The work was finally validated by comparing the performance results of the control scheme with the ones gotten from the existing methods.

CHAPTER TWO

LITERATURE REVIEW

2.1 Overview of solar photovoltaic (PV) system

The dispersed character of rural populations and their low commercial energy consumption result in poor capacity utilization efficiency for transmission and distribution systems and other energy infrastructure (Goldemberg, 2000). More specifically, the close relationship between the proximity of energy resources to the potential users coupled with the high cost of conventional energy sources have led to a considerable interest in the development and application of renewable energy resources. Although research and development activities are still being seriously undertaken in various aspects of renewable energy utilizations, a number of the technologies have since been shown to be feasible and ready, for adoption into the economy (Kreith & Goswami, 2007). Globally, current patterns of energy consumption are polluting and unsustainable (Nkue et Njomo, 2009). With world economic development and growing demand for energy, the conventional energy sources have become increasingly unable to meet the world demand for the energy (Kreith & Goswami, 2007).

Global warming, exhaustion and high cost of fossil fuels dictates the exploitation of alternative sources of energy such as wind and solar energies (Mboumboue & Njomo, 2013). Renewable sources of energy acquire growing importance due to enormous consumption and exhaustion of fossil fuel experienced globally. Renewable energy is abundant, free, sustainable and clean, and can be harnessed from different sources in the form of wind, solar, tidal, hydro, geo-thermal and biomass (Kreith & Goswami, 2007). Energy is an essential ingredient for socio-economic development and economic growth. Energy is critical to achieving virtually all the Millennium Development Goals (Brundtland, 1987). Energy in all its forms is required to achieve various purposes such as electricity for schools or clinics, energy for the delivery of health, education and sanitation, services, clean fuel to reduce indoor pollution, energy for pumping water or heat for cooking food and boiling water. Currently a high proportion of the world‘s total energy

output is generated from fossil fuels such as oil and coal (Mboumboue & Njomo, 2013). On the other hand, photovoltaic (PV) generation systems are actively being promoted in order to mitigate environmental issues such as the greenhouse effect and air pollution. Solar energy is the world's major renewable energy source and is available everywhere in different quantities. Photovoltaic panels do not have any moving parts, operate silently and generate no emissions. Another advantage is that solar technology is highly modular and can be easily scaled to provide the required power for different loads (Gwinyai Dzimano, 2008).

2.1.1 Components of solar PV system

Solar PV system generally consists of a solar PV array, a charge controller, a battery bank, an inverter, and so on. These components have to be correctly installed for harnessing the energy captured from the sun. Figure 2.1 shows a typical solar PV system with its components and how these components are connected to each other so as to deliver the power generated by the solar panel to the loads.

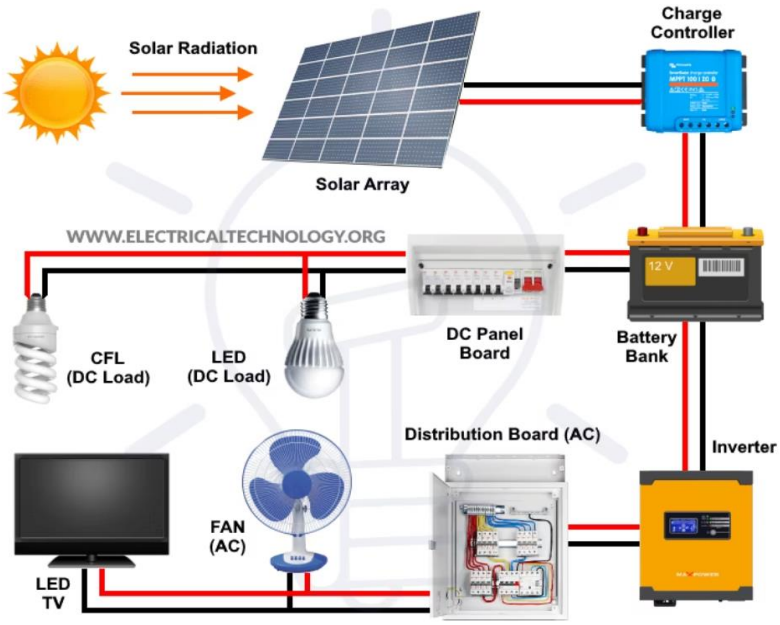

Figure 2.1: Solar PV system with its components.

2.1.2 Classifications of photovoltaic systems

Photovoltaic systems are composed of interconnected components designed to accomplish specific goals ranging from powering a small device to feeding electricity into the main distribution grid. The two main general classifications of the PV system are the stand-alone and the grid-connected systems (Messenger & Ventre, 2003). The main distinguishing factor between these two systems is that in stand-alone systems the solar energy output is matched with the load demand. To cater for different load patterns, storage elements are generally used and most systems currently use batteries for storage. If the PV system is used in conjunction with another power source like a wind or diesel generator then it falls under the class of hybrid systems. The balance of system (BOS) components are a major contribution to the life cycle costs of a photovoltaic system. They include all the power conditioning units, storage elements and mechanical structures that are needed. They especially have a huge impact on the operating costs of the PV system (Gwinyai, 2008). According to Dzimano (2008), the classifications of PV systems are as illustrated in figure 2.2.

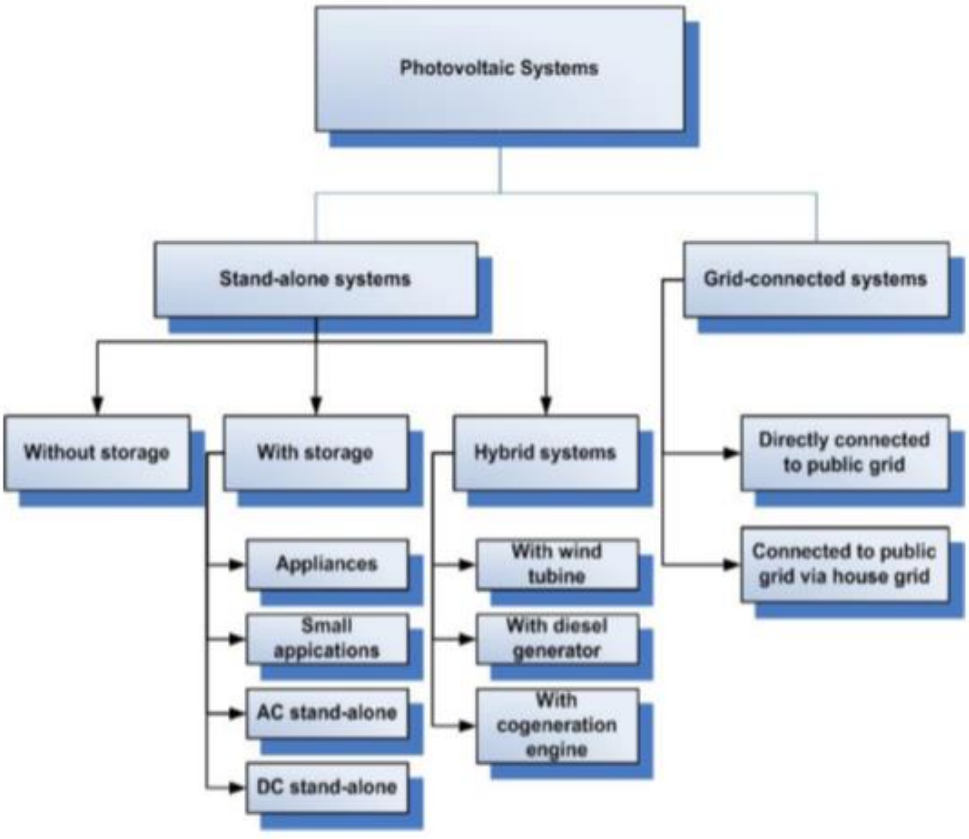

Figure 2.2: Classification of PV system (Gwinyai Dzimano, 2008).

2.1.3 Solar photovoltaic (PV) array

PV cell is the basic element of solar PV system. When many of these PV cells are connected together, they form solar modules. The interconnection of modules which in turn made up of many PV cells in series or parallel is a photovoltaic array. The PV cells exhibit nonlinear characteristics which can further be expanded in the form of arrays as per the power requirements. Figure 2.3 illustrates the hierarchical structure of the formation of solar PV array from the cells.

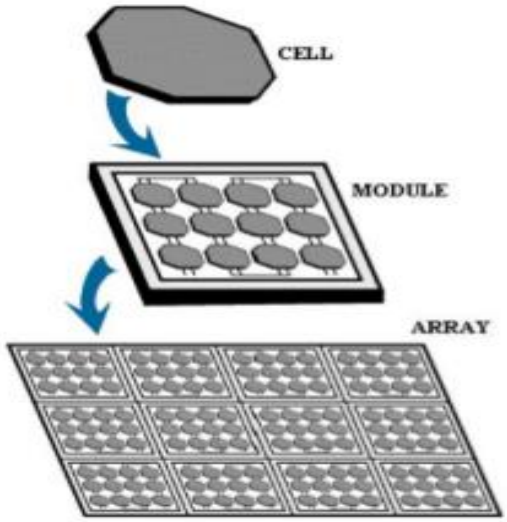

Figure 2.3: Illustration of PV hierarchy showing the formation of a PV array
(Mba, Chukwuneke, Achebe & Okolie, 2012)

2.1.4 Concept of solar radiation

Solar energy is the most abundant renewable resource. Photovoltaics generate electric power when illuminated by sunlight or artificial light. They directly convert the sun's energy into electricity which can be easily transported and converted to other forms for the benefit of society. In terms of power they come in various sizes from mW to MW ranges. The modular structure allows one to scale them depending on application. Practically, they may consist of one or more solar modules in combination with other balance of system components (BOS) covered by the National Electric Code (NEC). The balance of system components include mounting materials for the modules, wire and all wiring components, lightning protectors, grounding connections, power converters and battery storage (Gwinyai Dzimano, 2008).

Knowledge of the sun is very important in the optimization of photovoltaic systems (Markvart & Castaner, 2003). The electromagnetic waves emitted by the sun are referred to as solar radiation. The amount of sunlight received by any surface on earth will depend on several factors including; geographical location, time of the day, season, local landscape and local weather. The light's angle of incidence on a given surface will depend on the orientation since the Earth's surface is round and the intensity will depend on the distance that the light has to travel to reach the respective surface. The radiation received by a surface has two components – one is direct radiation which depends on the distance the rays travel (air mass) while the other component is called diffuse radiation as illustrated in figure 2.4. The range of wavelengths of light that reach the earth varies from 300nm to 400nm approximately (Castaner, 2002). This is significantly different from the spectrum outside the atmosphere, which closely resembles 'black body' radiation, since the atmosphere selectively absorbs certain wavelengths.

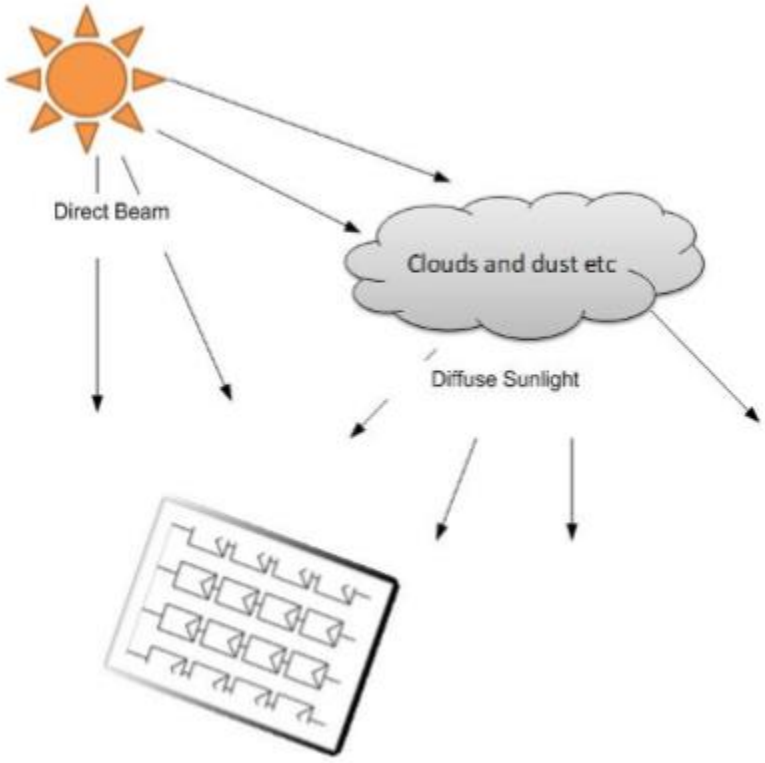

Figure 2.4: Diagram showing solar rays (Gwinyai Dzimano, 2008)

2.1.5 Working principle and mathematical representation of a PV system

Solar PV cells contain a semiconductor material such as silicon (Si), gallium arsenide (GaAs), copper indium diselenide (CIS), cadmium telluride (CdTe), and so on. These semiconductor materials are capable of capturing the energy from the sun and converting it into electricity. When photons emitted from the sun strikes a PV cell, a certain amount of energy is absorbed within the semiconductor material thereby creating an electric field across the layers and electron-hole pairs are formed. The bandgap energy causes the electrons to flow hence generating a current. The common denominator of PV cells is that a p-n junction, or the equivalent, such as a Schottky junction, is needed to enable the photovoltaic effect (Kreith & Goswami, 2007). Photons of light with energy higher than the band-gap energy of PV material can make electrons in the material break free from atoms that hold them and create hole-electron pairs (Akihiro, 2005; El-Ghonemy, 2012). The power produced by a single module is seldom enough for commercial use, so modules are connected to form array to supply the load. The connection of the modules in an array is same as that of cells in a module. Modules can also be connected in series to get an increased voltage or in parallel to get an increased current. The output of the PV cell varies with solar irradiation and with ambient temperature (Houssamo, Locment & Sechilariu, 2010; Villalva, Gazoli & Filho, 2009).

Since no cell is ideal, shunt and series resistances are added to the model. The intrinsic series resistance is R_s and the shunt resistance is R_p. Series resistance is very small and exists because of ohmic contact between metal and semiconductor internal resistance whereas shunt resistance is very large and corresponds to the surface quality along the periphery, noting that in ideal case R_s is zero (0) and R_p is infinity (∞). R_p appears in the denominator of the general equations meant for analysis and therefore neglected (Mboumboue et al., 2013). The equivalent circuit model of PV cell is shown in Figure 2.5.

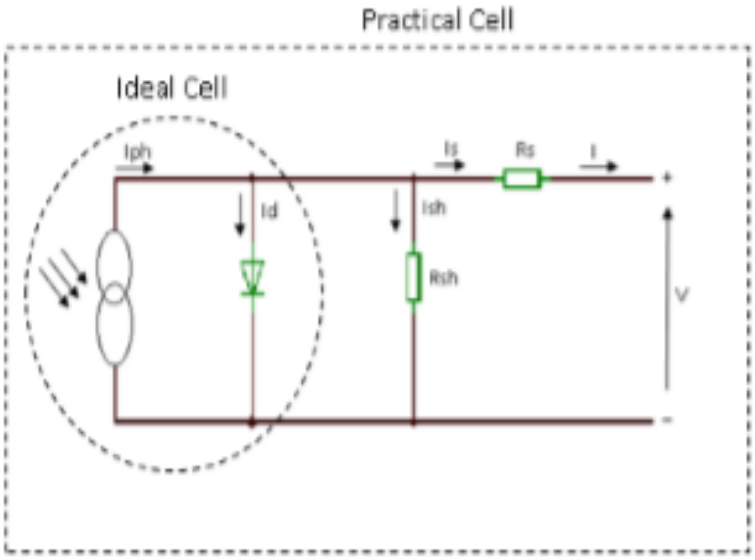

Figure 2.5: General configuration of a PV cell (Mboumboue & Njomo, 2013).

The general equation of a PV cell current I is given by,

$$\boldsymbol{I = I_L - \left[I_o e^{q\left(\frac{V+I\cdot R_s}{n\cdot k\cdot T_a}\right)} - 1\right] - \frac{V + I\cdot R_s}{R_p}} \ \textbf{(Mboumboue \& Njomo, 2013)}. \qquad \textbf{(2.1)}$$

Where I_L is the light generated current given by,

$$\boldsymbol{I_L = I_{sc} + K_i(T_a - T_r)\cdot\frac{\lambda}{1000}} \ \textbf{(Mboumboue \& Njomo, 2013)} \qquad \textbf{(2.2)}$$

I_o is the saturation current given by,

$$\boldsymbol{I_o = I_{rs}\left(\frac{T_a}{T_r}\right)^3 e^{\left[\frac{q\cdot E_{g0}}{n\cdot k}\left(\frac{1}{T_r}-\frac{1}{T_a}\right)\right]}} \ \textbf{(Mboumboue \& Njomo, 2013)} \qquad \textbf{(2.3)}$$

Reverse saturation current I_{rs} is given by

$$\boldsymbol{I_{rs} = \frac{I_{sc}}{e^{\left(\frac{q\cdot V_{oc}}{N_s\cdot k\cdot n\cdot T_a}\right)} - 1}} \ \textbf{(Mboumboue \& Njomo, 2013)} \qquad \textbf{(2.4)}$$

Where: $T_r = Module\ temperature\ (Kelvin)$

. $T_a = Ambient\ temperature\ (Kelvin)$

$I_{sc} = Short\ circuit\ current$

$\lambda = Solar\ irradiance\ (W/m^2)$

$V_{oc} = Open\ circuit\ voltage$

$q = Charge\ of\ an\ electron\ (1.622 \times 10^{-19} Coulumbs)$,

$n = Diode\ ideality\ factor\ (1 < n < 2)$

$E_{g0} = Bandgap\ energy\ of\ semiconductor\ (1.1eV)$

$k = Boltzmann's\ constant\ (1.3807 \times 10^{-23} Joules/Kelvin)$

$K_i = \text{Cell's short} - \text{circuit temperature coefficient}$

$N_s = Number\ of\ series\ cells\ (36)$

$N_p = Number\ of\ shunt\ cells\ (1)$

To make a PV module, the cells are connected in series and parallel as shown in Figure 2.6.

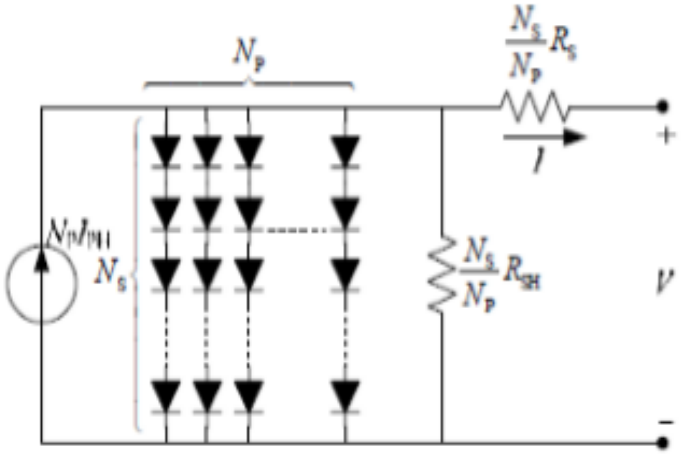

Figure 2.6: Equivalent circuit of a PV module

(Tsai, Tu & Su, 2008; Kachhiya, Lokhande & Patel, 2011).

Since the current passes through the series of cells (N_p), then the equation for the total module output current I_{PV} is given by

$$\boldsymbol{I_{PV} = N_p \cdot I_{ph} - N_p \cdot I_o \left\{ e^{\left[\frac{q\cdot(V_{PV}+I_{PV}\cdot R_s)}{N_s\cdot k\cdot n\cdot T_a}\right]} - 1 \right\}} - \frac{\boldsymbol{V_{PV} + I_{PV}\cdot R_s}}{\boldsymbol{R_p}} \quad (\textbf{Mboumboue \& Njomo, 2013}) \qquad (\boldsymbol{2.5})$$

To have a simplified model, since the shunt resistance is of higher value (that is, $R_p = \infty$) then equation 2.5 becomes,

$$\boldsymbol{I_{PV} = N_p \cdot I_{ph} - N_p \cdot I_o \left\{ e^{\left[\frac{q\cdot(V_{PV}+I_{PV}\cdot R_s)}{N_s\cdot k\cdot n\cdot T_a}\right]} - 1 \right\}} \ (\textbf{Mboumboue \& Njomo, 2013}) \qquad (\boldsymbol{2.6})$$

Where: $V_{PV} = Module\ voltage,$

$I_{ph} = I_L = Light\ generated\ current,$

$I_o = Saturation\ current$

2.2 Overview of boost converter as power electronic converter

The role of power electronic converters is to provide power to the user in a suitable form at high efficiency. Power electronic converters are needed in PV systems to convert DC voltage to the required values and to convert from DC to AC and vice versa (Esram & Chapman, 2007). In addition, they control the charging and discharging of batteries in systems where batteries are storage elements. Boost, Buck, and Buck-boost converters are the main MPPT topologies that have been used with solar cells to track the MPP (Kolsi, Samet & Amar, 2014). The Boost converter is more suitable for PV applications because it requires low inductance that removes the current ripples, and it has low switching losses (Tran, Nollet, Essounbouli & Hamzaoui, 2017). Furthermore, the Boost converter has a continuous current with less current stress during the converter operation compared with other topologies (Ahmed, Mousa & Orabi, 2010). The Boost converter is a simple power electronic converter which basically consists of a voltage source, an inductor, a power electronic switch and a diode. To smoothen the output, a filter capacitor is also used in the converter circuit. The function of the boost converter as shown in figure 2.7 is to step up DC voltage so that the desired level is achieved.

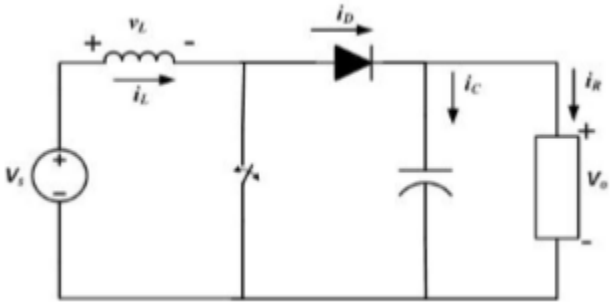

Figure 2.7: Boost converter circuit diagram

If the switch is turned on and off repeatedly at very high frequencies and assuming that in the steady state the output will basically be DC (large capacitor):

$$\boldsymbol{i_C = I_C = 0} \ \textbf{(Ahmed, Mousa \& Orabi, 2010)}. \qquad \textbf{(2.7a)}$$

$$\boldsymbol{i_L = I_L = I_R + I_{switch}} \ \textbf{(Ahmed, Mousa \& Orabi, 2010)}. \qquad (2.7b)$$

$$\boldsymbol{i_L = I_L = I_R + DI_L} \quad \textbf{(Ahmed, Mousa \& Orabi, 2010)}. \qquad (2.8)$$

$$\boldsymbol{I_L = \frac{V_o}{R(1-D)}} \quad \textbf{(Ahmed, Mousa \& Orabi, 2010)}. \qquad (2.9)$$

The DC component of voltage across the inductor has to be zero if losses are neglected. The average voltage across the inductor is given by:

$$v_L = \frac{1}{T}\left(\int v_{on}\,dt + \int v_{off}\,dt\right) = 0 \quad \text{(Ahmed, Mousa \& Orabi, 2010).} \tag{2.10}$$

$$v_L = \frac{1}{T}\left(\int V_s\,dt + \int (V_s - V_o)dt\right) = 0$$

$$v_L = \frac{1}{T}[(V_s DT - (V_s - V_o)(1-D)T] = 0$$

$$v_L = \frac{1}{T}[V_s - (1-D)V_o]T = 0$$

$$v_L = V_s - (1-D)V_o = 0$$

$$\frac{V_o}{V_s} = \frac{1}{1-D} \quad \text{(Ahmed, Mousa \& Orabi, 2010).} \tag{2.11}$$

The fraction to the right is always greater than one since the duty is always less than one thus the voltage is stepped up. The filter inductor that determines the boundary is given by equation (2.12)

$$\boldsymbol{L_{boundary} = \frac{(1-D)^2 DR}{2f}} \quad \textbf{(Esram et al., 2007).} \tag{2.12}$$

The boost converter will operate in the continuous conduction mode if the inductance is larger than this value. A much larger filter capacitance C is required as the current supplied to the output RC circuit is discontinuous (Esram et al., 2007). The limiting value is given by equation (2.13). The key design equations for a boost converter are given in (2.12) and (2.13).

$$\boldsymbol{C_{min} = \frac{DV_o}{V_r \mathrm{R} f}} \quad \textbf{(Esram et al., 2007).} \tag{2.13}$$

2.3 Review of maximum power point tracking (MPPT)

The photovoltaic module operates at the I-V characteristics determined by the load. The maximum power is generated by the solar module at a point of the I-V characteristic where the product of voltage and current is maximum. This point is known as the MPP. The role of the MPPT is to ensure that the PV module operates at its MPP, hence extracting the maximum available power. Since the power harvested from the photovoltaic module is different at different operating points it is important that the load is matched in such a way that maximum power is obtained from the photovoltaic module (Hussein, Muta, Hoshino & Osakada, 1995). There are numerous algorithms and a comparative study has been done on these algorithms by Hohm and

Ropp, (2000). Maximum power point tracking (MPPT) techniques are used in photovoltaic (PV) systems to maximize the PV array output power by tracking continuously the maximum power point (MPP) which depends on panel temperature and irradiance conditions (Femia, Petrone & Spagnuolo, 2005). If there is a good irradiance condition, the photovoltaic system can generate maximum power efficiently while an effective MPPT algorithm is used with the system. A lot of MPPT algorithms have been developed by researchers all over the world such as Differential method, Perturb and Observe (P & O), Incremental Conductance (Inc. Con.), Curve fitting, Open Circuit Voltage PV generator, Short circuit PV generator method. The efficiency of a PV plant is affected mainly by three factors: the efficiency of the PV module, efficiency of inverter (93-95%) and the efficiency of the Maximum Power Point Tracking (MPPT) algorithm (Sengar, 2014).

The maximum power supplied by the photovoltaic panels is oscillatory in nature. That is to say that it is not always stable and fixed in the same operating point. Such an instability is normally caused by variations in the weather conditions, such as solar irradiation, shadow, and temperature. This changes cause the PV array to have a non-linear I-V characteristic which affects the output power. There is a point on I-V, P-V characteristic curve of PV array called as Maximum Power Point (MPP), where the PV system produces its maximum output power. Location of MPP changes with change in environmental condition. The purpose of MPPT is to adjust the solar operating voltage close to MPP under changing environmental conditions. In order to continuously gather the maximum power from the PV array, they have to operate at their MPPT despite the inhomogeneous change in environmental conditions. The two most commonly used algorithms for PV applications are Perturb and Observe (P&O) and Incremental Conductance (Inc. Con.) as they have the advantage of an easy implementation (Sengar, 2014). To extract the maximum power, it is necessary to implement an MPPT algorithm that dynamically adjusts the extraction of the power. Convergence speed is one of the most important features among all different MPPT algorithms. Any improvement in the rise time of MPPT improves the reliability of the system and increases the power extraction and efficiency of the whole system.

2.3.1 Curve fitting method

Salas et al., 2006 in his work explained curve-fitting method to be an offline method where PV module characteristics, all data and manufacturing details are required. He further stated that in this method mathematical model and equations describing the output characteristics are pre-decided. The PV module characteristic equation, which represents the curve fitting method is as shown in equation (2.14). Once the coefficients a, b, c and d are determined by sampling m values of PV voltage V_{pv}, PV current I_{pv} and output power P_{pv} then the maximum power point voltage can be calculated from equation (2.15). Though the curve fitting method has advantage in its simplicity, it requires prior and accurate knowledge of physical parameters and also requires large memory as number of calculation is more and speed is less hence the need for an alternative method of control.

$$\boldsymbol{P_{pv} = aV_{pv}{}^{3} + bV_{pv}{}^{2} + cV_{pv} + d} \quad \textbf{(Salas et al., 2006)} \tag{2.14}$$

At maximum power point, $\frac{dP_{pv}}{dV_{pv}} = 0$

$$\boldsymbol{V_{mpp} = \frac{-b \pm \sqrt{b^2 - 3ac}}{3a}} \quad \textbf{(Salas et al., 2006)} \tag{2.15}$$

2.3.2 Differential method

The differential method is obtained by differentiating $P = VI$ to obtain,

$$\boldsymbol{\frac{dP_{pv}}{dt} = V\frac{dI_{pv}}{dt} + I\frac{dV_{pv}}{dt} = 0} \ \textbf{(Salas et al., 2006)} \tag{2.16}$$

In this method, equation (2.16) must be solved very fast in order to provide accurate operating point. The disadvantage of this method is that it requires more calculation time as after calculating equation (2.16) parameters, the sum is calculated and a comparison of this sum to an equal perturbation on the opposite side of the operating point. This is done repeatedly till final sum becomes zero if not then more calculations should be carried out (Salas et al., 2006).

2.3.3 Open-circuit voltage method

The flowchart shown in figure 2.8 illustrates how the open-circuit method can be implemented. Firstly, the PV array is temporarily isolated from MPPT then V_{oc} is measured. After that V_{mpp} is calculated according to equation (2.25) and the operating voltage is finally set to the maximum

voltage point. This process is repeated periodically. In this method the ratio of PV array's maximum power voltage (V_{mpp}) to its open circuit voltage (V_{oc}) is approximately constant as given by equation (2.17). The advantage of this method is that it is simple and cheap but it is difficult to choose an optimal value of constant k_1. Eltawil & Zhao (2013) and Salas et al., (2006) reported that the values of k_1 may range from 0.73 to 0.80 for Polycrystalline PV modules.

$$\frac{V_{mpp}}{V_{oc}} \cong k_1 < 1 \quad (\text{Salas et al., 2006}) \tag{2.17}$$

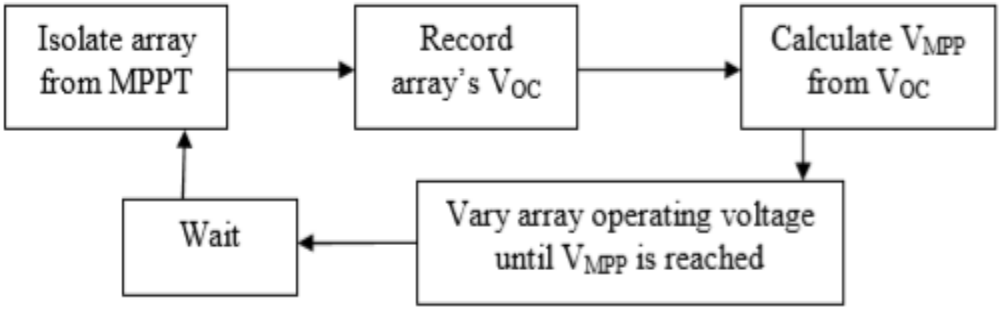

Figure 2.8: Open-circuit voltage method flowchart (Eltawil & Zhao, 2013)

2.3.4 Short-circuit method

Similar to the open-circuit voltage method which exhibits the linearity nature between V_{oc} and V_{mpp}, the current in MPP (I_{mpp}) is linearly proportional to short-circuit current (I_{sc}) as in equation (2.18). In his work, Salas (2006) suggested that the value of k_2 is considered to be around 0.85. Like the open-circuit method Short-circuit method is simple and cheap but the way of determining k_2 is more complicated than any of fixed value.

$$\frac{I_{mpp}}{I_{sc}} \cong k_2 < 1 \quad (\text{Salas et al., 2006}) \tag{2.18}$$

2.3.5 Hill climbing techniques

The two methods of hill climbing techniques are: perturbation and observation (P&O) and incremental conductance (Inc. Con.) methods. In the Hill Climbing Principle, Morales (2010) explained that the operating point of the PV module moves in the increasing direction of power.

2.3.5.1 Perturbation and observation (P&O) method

According to Salas et al., 2006, P&O is an iterative method which senses the panel operating voltage periodically and compares the PV output power with that of the previous power; the resulting change in power (ΔP_{pv}) is measured. If ΔP_{pv} is positive, the perturbation of the operating voltage should be in the same direction of the increment. However, if it is negative, the system operating point obtained moves away from the MPPT and the operating voltage should be in the opposite direction of the increment hence its perturbation reversed to move back towards the MPP. This process continues till $\frac{dP_{pv}}{dV_{pv}} = 0$ regardless of the irradiance and PV module's terminal voltage.

P&O algorithm is simple and does not require previous knowledge of the PV generator characteristics or the measurement of solar intensity and cell temperature and is easy to implement with analogue and digital circuits. It perturbs the operating point of the system causing the PV array terminal voltage to fluctuate around the MPP voltage even if the solar irradiance and the cell temperature are constants (Elgendy, Zahawi, & Atkinson, 2012). Moreover, it is the most widely used and workhorse MPPT algorithm because of its balance between performance and simplicity. However, it suffers from the lack of speed and adaptability which is necessary for tracking the fast transients under varying environmental conditions (Malek & Chen, 2014). It is simple and straight forward technique but degraded performance is achieved due to the trade-off between accuracy and speed upon selecting the step size (Elobaid, Abdelsalam & Zakzouk, 2012). A scheme of P&O algorithm is shown in the flow chart of Figure 2.9, according to which PV module output voltage V_{pv} and output current I_{pv} are sensed. Once the voltage and current are obtained then power $P_{PV}(k)$ is calculated and compared with the power measured at the previous sample $P_{PV}(k-1)$ in order to calculate ΔP. Then according to the sign of ΔP and ΔV, MPP is tracked accordingly. The limitation of P&O algorithm is that it reduces its MPPT efficiency. Another limitation of P&O is that it oscillates around the MPP, as this method becomes unstable with rapid change in atmospheric conditions such as irradiance and temperature. The oscillation can be minimized by reducing the perturbation step size. However, a smaller perturbation size slows down the MPPT. A solution to this conflicting

situation is to have a variable perturbation size that gets smaller towards the MPP (Esram & Chapman, 2007).

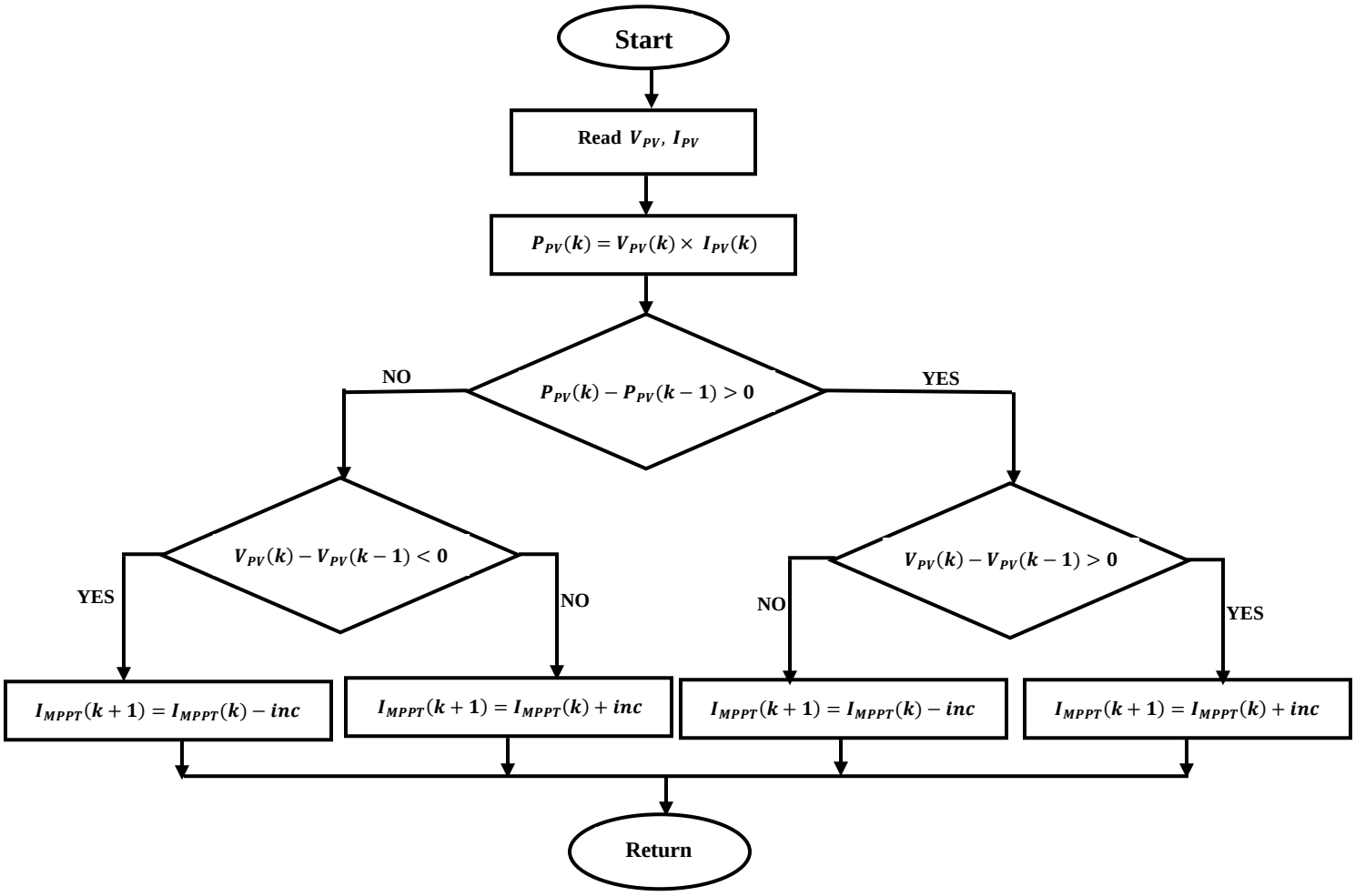

Figure 2.9: Flowchart of P&O algorithm (Manel & Hfaiedh, 2016)

2.3.5.2 Incremental conductance (Inc. Con.) method

The incremental conductance method is based on the principle that the slope of the PV array power curve is zero at the MPP, so that $\Delta P/\Delta V = 0$, with $P = VI$ the MPP can be tracked by comparing the instantaneous conductance I/V with the incremental conductance $\Delta I/\Delta V$. The algorithm increments or decrements the reference until the condition $\Delta I/\Delta V = -I/V$ is achieved. Once the maximum power is reached, the operation of the PV array is maintained at this point. It is an effective algorithm and requires high sampling rates and fast calculations of the power slope (Tapre & Deshbhratar, 2015). It offers different advantages which are good tracking efficiency and automatic adjustment of the module operating voltage with no oscillations. Also,

the response is improved and the control for the extracted power is optimized (Visweswara, 2014). The implementation of this algorithm in the control unit is difficult and expensive, but with recent developments in microcontrollers it became more cost effective (Mirbagheri, Mekhilef & Mirhassani, 2013). It lends itself well to digital signal processing (DSP) control, which can easily keep track of previous values of voltage and current (Esram & Chapman, 2007). Figure 2.10 shows the Inc. Con. algorithm.

The output power of PV module P_{pv} is given by equation (2.19).

$$\boldsymbol{P_{pv} = I_{pv}V_{pv}}\ \textbf{(Salas et al., 2006)} \qquad (\mathbf{2.19})$$

Differentiating (2.19) with respect to V_{pv} gives the basis of Inc. Con. algorithm as in equation (2.20),

$$\frac{\boldsymbol{dP_{pv}}}{\boldsymbol{dV_{pv}}} = \boldsymbol{I_{pv}} + \boldsymbol{V_{pv}}\frac{\boldsymbol{dI_{pv}}}{\boldsymbol{dV_{pv}}}\ \textbf{(Salas et al., 2006)} \qquad (\mathbf{2.20})$$

The Inc. Con. method is based on the fact that $\frac{dP_{pv}}{dV_{pv}} = 0$ or $\frac{dP_{pv}}{dV_{pv}} = -\frac{I}{V}$ at the MPP, $\frac{dI_{pv}}{dV_{pv}} < -\frac{I}{V}$ or $\frac{dP_{pv}}{dV_{pv}} < 0$ if the operating point is on the right of the P-V curve and $\frac{dI_{pv}}{dV_{pv}} > -\frac{I}{V}$ or $\frac{dP_{pv}}{dV_{pv}} > 0$ if the operating point is on the left of the P-V curve (Hohm & Ropp, 2003). A scheme of Inc. Con. algorithm is shown in the flow chart of Figure 2.10. In this algorithm, present and previous values of PV module voltage and current are sensed and are used to calculate the values of dI_{pv} and dV_{pv}. The advantage of the incremental conductance method, which is superior to those of the other MPPT algorithms, is that it can calculate and find the exact perturbation direction for the operating voltage of PV modules. By comparing the instantaneous panel conductance, $\frac{I_{pv}}{V_{pv}}$ with the incremental panel conductance, $\frac{dI_{pv}}{dV_{pv}}$, the Inc. Con. Method therefore solve the problem of the operating point oscillating around the MPP as observed in P&O method. The voltage of MPP is tracked to satisfy $\frac{dP_{pv}}{dV_{pv}} = 0$ (Bhatnagar & Nema, 2013). This method is also easy to implement, has high tracking speed and highly efficient (Bhatnagar & Nema, 2013) but the challenging issue associated with this method is that it requires complex control circuits (Salas et al., 2006).

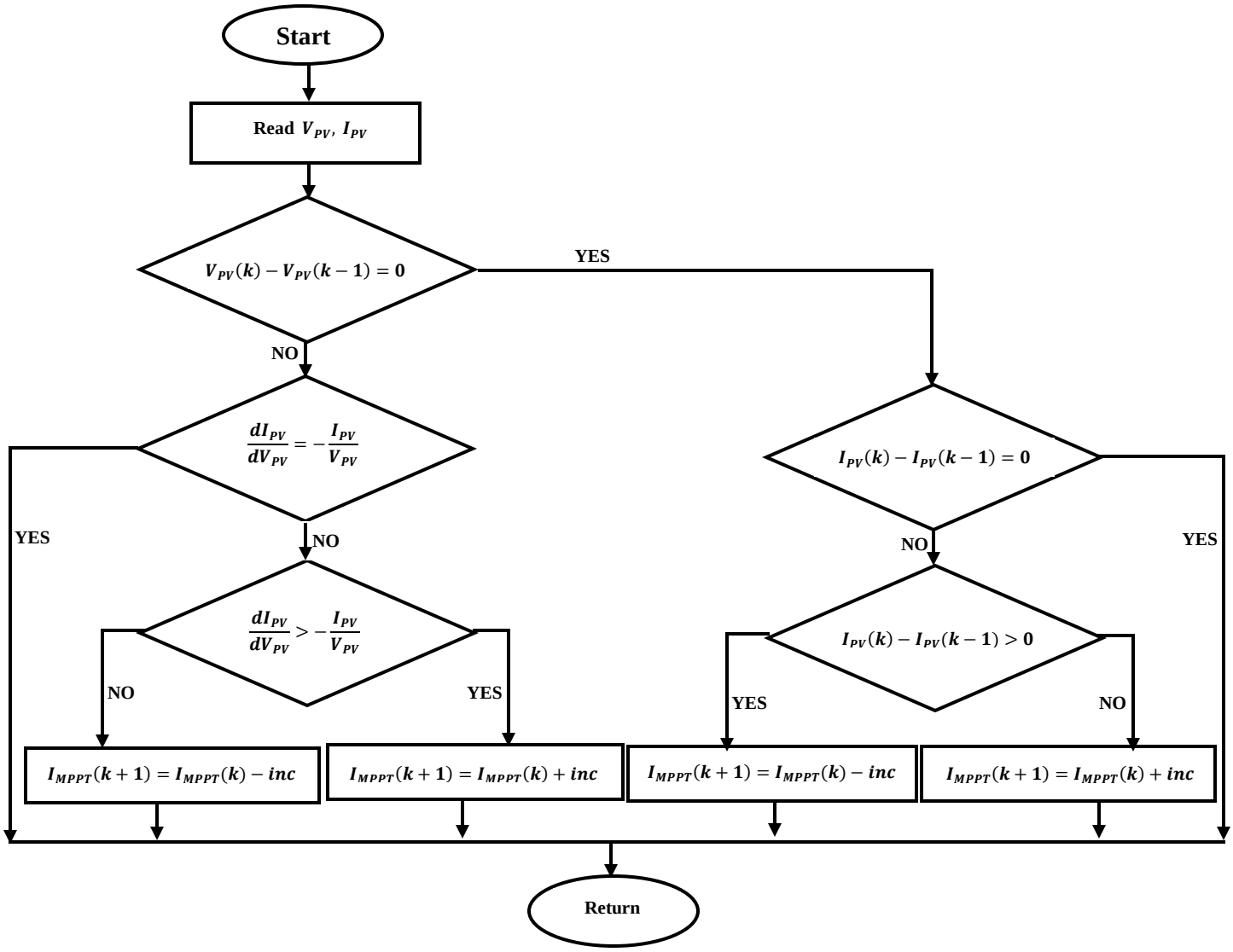

Figure 2.10: Flowchart of Inc. Con algorithm (Manel & Hfaiedh, 2016)

2.4 Concept of linear quadratic regulator (LQR)

The Linear Quadratic Regulator (LQR) is a standard optimal control technique whose design is aimed at minimizing or maximizing the required performance index (Kirk, 1998). A certain state trajectory is defined after applying the controller signal obtained from the optimal controller over a certain period of time along with an initial state for the system at t_0. The optimal control problem is defined by finding an optimal control u for the system given by

$$\dot{x} = f(x(t), u(t), t) \qquad (2.21)$$

which makes it follow an optimal trajectory x that minimizes or maximizes the targeted performance measure J given in Equation (2.22) where $\boldsymbol{h}$ and $\boldsymbol{g}$ are scalar functions.

$$\boldsymbol{J = h(x_{tf}, t_f) + \int_{t_0}^{t_f} g(x(t), u(t), t)dt} \quad \textbf{(Anderson \& Moore, 1989)}. \tag{2.22}$$

$$\begin{aligned} \boldsymbol{J} = \frac{\boldsymbol{1}}{\boldsymbol{2}}\boldsymbol{[z(t_f) - y(t_f)]^T F(t_f)[z(t_f) - y(t_f)]} \\ + \frac{\boldsymbol{1}}{\boldsymbol{2}}\int_{t_0}^{t_f} \{[\boldsymbol{z(t) - y(t)}]^{\boldsymbol{T}}\boldsymbol{Q}[\boldsymbol{z(t) - y(t)}] \\ + \boldsymbol{u^T(t)Ru(t)}\}\boldsymbol{dt} \quad \textbf{(Kirk, 1998)}. \end{aligned} \tag{2.23}$$

$z(t)$ represents the desired output vector and $y(t)$ represents the output vector. Q and R are the matrices that should be chosen in order to give the minimum value of the performance index (J). Q is the error weighted matrix, and it should be positive semidefinite. The more focus is required on minimizing a certain parameter, the larger the weight that should be attributed to its corresponding state variable in the Q matrix. R is the control weighted matrix and it should be positive definite (Kirk, 1998). At the final time (t_f), the terminal cost term $F(t_f)$ should be 0, therefore, the first term of equation (2.22) is cancelled to give equation (2.24). When the optimal values of Q and R matrices are substituted in the Riccati equation (Equation 2.25), it provides the optimal co-state matrix (P) (Anderson & Moore, 1989).

$$\boldsymbol{J = \int_{t_0}^{t_f} g(x(t), u(t), t)dt} \tag{2.24}$$

$$\boldsymbol{\dot{P}(t) = P(t)A(t) + A^T(t)P(t) + Q(t) - P(t)B(t)R^{-1}B^T(t)P(t)} \tag{2.25}$$

This co-state matrix (P) is substituted into the optimal controller $u(t)$ (Equation 2.26) in the form of state feedback gain (K) as follows,

$$\boldsymbol{u(t) = R^{-1}B^T(t)P(t)x(t) = -K(t)x(t)} \tag{2.26}$$

The optimal controller is implemented by feeding back these gains to their corresponding state variables to obtain the optimal response of the system. An optimal controller does not always exist for every system. In order to check if an optimal controller exists for the system under study, the controllability and observability matrices have to be obtained. If both matrices have ranks that are equal to the rank of the system state matrix A from the state space model of the

system, then an optimal controller can be designed for this system hence, the system is controllable and observable (Kirk, 1998). This is important to ensure that the inputs are accessible, thus, can be controlled, and the outputs are accessible, thus, can be observed and feedback to the system for the controller to operate properly. If the system is controllable and observable, and an optimal controller exists for the system, the main challenge remaining in LQR is a suitable choice of Q and R matrices that are chosen based on the user experience (Anderson & Moore, 1989).

2.5 Concept of model reference adaptive control (MRAC)

Adaptive control techniques allow the control of systems where certain system parameters are not known or change over time due to changing operating environment. One of the adaptive control techniques that can solve this problem is model reference adaptive control (MRAC), which involves a defined reference model whose dynamics in response to a reference input should be followed by the plant process. For the plant process with unknown parameters, a specific control law alters the reference input signal in order for the output signal of the plant to match the one of the reference model. MRAC is an adaptive strategy with some adjustable controller parameters and an adjusting mechanism to adjust them. Adaptive controller is very effective to handle the unknown parameter variations and environmental changes and consists of two loops – an outer (normal feedback) loop and an inner (parameter adjustment) loop. MRAC has the following components:

(i) **Reference Model:** The purpose of reference model in MRAC is to specify the ideal response of the adaptive control system to external command. It should reflect the performance specifications in control tasks. The ideal behavior specified by the reference model should be achievable for the adaptive control system (Pankaj, Shailendra & Nema, 2011). A critically damped system for instance, could be taken as a reference model.

(ii) **Controller:** It is usually parameterized by a number of adjustable parameters. The adjustable parameter may be represented by θ. The control law is linear in terms of the adjustable parameters (linear parameterization). Adaptive controller design normally requires linear parameterization in order to obtain adaptation mechanism with guaranteed stability and tracking convergence. The values of these control parameters are mainly

dependent on adaptation gain which in turn changes the control algorithm of adaptation mechanism (Pankaj et al., 2011).

(iii) **Adaptation Mechanism:** It is used to adjust the parameters in the control law. Adaptation law searches for the parameters such that the response of the plant which should be same as the reference model. It is designed to guarantee the stability of the control system as well as conversance of tracking error to zero. Mathematical techniques like MIT rule, Lyapunov theory and augmented error theory can be used to develop the adaptation mechanism (Pankaj et al., 2011).

2.6 Review of related literatures

Designing a suitable MPPT system for the purpose of achieving the best performance is one of the major challenging issues as it requires a sophisticated design. This is because solar energy fluctuates throughout the day. This fluctuation therefore affects the output power delivered to the load hence the need for power correction. In their work, Napole, Derbeli & Barambones, (2021) presented an analysis of a real PV system, the objective of which was to track the MPP for performance improvement. Since the PV used in the research provided a low output voltage a boost-converter with a non-linear control law was implemented to reach a suitable end-used voltage. Napole et al., (2021) in their research work therefore adopted a novel MPPT method based on a voltage reference estimator (VRE) combined with a fuzzy logic controller (FLC) in order to obtain the maximum power from the PV panel. This structure was implemented in a dSpace 1104 board for a commercial PV panel, PEIMAR SG340P. The scheme was compared with a conventional perturbation and observation (P&O) and with a sliding mode controller (SMC), where the outcomes demonstrated the superiority of the proposed advanced method. The results showed that the FLC has a slower correction, although the ripple amplitude is reduced significantly. Napole et al., (2021) also analyzed future trends for MPPT in PV systems which should be applicable as the objective of forthcoming investigations. Such trends include an analysis of Fuzzy Logic control type (FLC type-2) based on an uncertainty study, which can be contrasted with the present obtained results. Improved P&O algorithms can also be compared in order to search for better chattering management reduction.

MPPT method with conventional control is not optimal to resolve power inaccuracies in the system. In their research article, Prastyawan et al., (2021) developed a MPPT Full Bridge Converter Using Fuzzy Type-2 on DC Nano Grid System. The purpose was to track an MPP based on P-V characteristic curve since the PV output power changes with certain conditions such as temperature and irradiation, and as a result brings about unstable output power so that the accuracy of the power generated is not maximum. Implemented on MATLAB/Simulink software, simulation results in Model 1 show that the average power accuracy with Fuzzy Type-2 is 91.40% compared to Fuzzy Type-1 with an average power accuracy of 80.64%. In Model 2, Fuzzy Type-2 is 87.63% compared to Fuzzy Type-1 of 77.93%. MPPT method using fuzzy type-2 is better than using fuzzy type-1 in terms of power accuracy. Fuzzy Type-2 has a power tracking value closer to the MPP value at low, medium, to high levels of irradiation parameters, and is more stable to ripples and transients during conditions of decreasing irradiation.

Nisso, Raïdandi, Djongyang & Menga, (2018) modelled and analyzed boost converter in small-signals as applied to the wind energy conversion system using MATLAB/Simulink. For this purpose it has been shown that the problem of stabilizing a boost converter in small-signal situations using linear control laws is derived by the means of oriented circuit procedure. After establishing a small-signal circuit model for the boost regulator including state-feedback, conditions for the stability of circuit are studied. Thereafter, a linear analysis is performed in order to design the desired dynamics and robust behavior of the boost converter. The linear analysis assumed shows that only a state feedback gain matrix is necessary, provided that the coordinates of the equilibrium points are known. This operation is done by using the root locus method to choose the eigenvalue of this gain vector. Contrary to classical control methods of boost converter, the technique here reported guarantees small-signal stability of the boost converter. In their design, Nisso et al. guaranteed small-signal stability of a linearly controlled boost converter by means of a linear analysis. It is generally assumed that the obtained control input is applied to boost converter by using pulse-width modulation. Performance of the proposed pole placement method is evaluated by Simpower/MATLAB simulation at the equilibrium operating points chosen. To verify a feasibility of the proposed method, set parameters of the system is implemented. The control scheme is verified through MATLAB

simulation, which is present to verify the performance of proposed method and simulation results validate the analytical predictions.

Vyshnavi & Subramanian, (2015) developed an adaptive control architecture for tracking maximum power point in photovoltaic systems. To achieve their result, their thesis proposed a two-layer adaptive control architecture that can effectively handle the uncertainties and perturbations in the photovoltaic systems and the environment. According to their report, two control algorithms which are: ripple correlation control (RCC) and model reference adaptive control (MRAC), were decoupled to achieve the maximum power point tracking with shorter time constants and overall system stability. The RCC algorithm was used as the first control stage to compute the duty cycle, which serves as the input to the MRAC layer. To compensate for the under-damped characteristics of the power conversion system, the MRAC algorithm was incorporated as the second stage of the control. With this control technique, the Lyapunov approach was employed to derive an adaption law of the controller so that the MRAC system can eliminate the underdamped modes in power conversion hence an improved efficiency realized.

Khanna et al. (2014) in his report also proposed a similar control technique of employing adaptive control architecture for maximum power point tracking (MPPT) in photovoltaic systems so as to deliver the maximum available power to the load under changes in the solar insolation and ambient temperature. The aim of this technique according to their report was to reduce complexity in system control while effectively handling the uncertainties and perturbations in the photovoltaic systems and its environment. The control architecture consisted of the ripple correlation control (RCC) and the model reference adaptive control (MRAC). By decoupling these two control algorithms, the system achieves MPPT with overall system stability. The implication of the results obtained was that the proposed control algorithm enables the system to converge to the maximum power point in milliseconds.

Kollimallam & Mishra, (2014) proposed a novel adaptive P&O MPPT algorithm to extract the maximum power from photovoltaic (PV) panel under sudden changes in the irradiance considering sudden changes in the irradiance. The method employed was short-circuit current-based adaptive perturb and observe algorithm which consists of two control schemes, namely,

current perturbation algorithm and adaptive control algorithm. The function of the current perturbation algorithm was to ensure that the PV panel operates at maximum power point while the adaptive control algorithm identifies the operating limit violation and ensures that a new operating point nearer to maximum power point is set. To realize this algorithm, a boost converter was used. To validate the results obtained from the proposed algorithm, experimental results were obtained by developing a hardware prototype for sudden changes in the irradiance was carried out, and the results were compared with a conventional algorithm. A faster response was obtained from the proposed algorithm for sudden changes in the irradiance contrary to the conventional algorithm.

Anbarasi & Kanthalakshmi (2016) developed a linear quadratic regulator (LQR) based maximum power point tracking method for a standalone solar photovoltaic system. Simulations for constant as well as changing environmental conditions were carried out in MATLAB/Simulink environment. According to their report the tracking performance of the LQR method was compared with that of the conventional Perturb and Observe (P&O) method in MATLAB/Simulink environment. Through real time implementation using dSPACE controller the result was validated and LQR method was found to perform better than the conventional P&O method because of its capability to effectively track MPP. The tracking speed was discovered as 0.04s, which is the time taken to reach MPP by LQR, while it was 0.165s for P&O based MPPT. By dividing energy generated by the PV module by the theoretical maximum energy the tracking efficiency was determined as 96.93% and 91.83% for LQR and P&O, respectively (Anbarasi & Kanthalakshmi, 2016).

Safari & Mekhilef, (2011) presented simulation and hardware implementation of incremental conductance (Inc. Cond.) maximum power point tracking (MPPT) used in solar array power systems with direct control method. They employed a fixed-step-size incremental conductance MPPT with direct control method, and consequently, the necessity of another control loop was eliminated. The proposed system was different from the existing one it has the ability to eliminate the proportional–integral control loop and investigate the effect of simplifying the control circuit. The analysis of the work done by Safari & Mekhilef, (2011) showed that the resultant system was capable of tracking MPPs accurately and rapidly without steady-state

oscillation, and also, its dynamic performance was satisfactory. MATLAB and Simulink were employed for simulation studies, and Code Composer Studio v3.1 was used to program a TMS320F2812 digital signal processor. The proposed system was developed and tested successfully on a photovoltaic solar panel in the laboratory. The results acquired during the simulations and hardware experiments, confirmed that, with a well-designed system including a proper converter and selecting an efficient and proven algorithm, the implementation of MPPT is simple and can be easily constructed to achieve an acceptable efficiency level of the PV modules. Experimental results indicate the feasibility and improved functionality of the system. The results also indicated that the proposed control system was capable of tracking the PV array maximum power and thus improves the efficiency of the PV system and reduces power loss and system cost.

In the work of Femia, Petrone, Spagnuolo & Vitelli, (2005), the aim was to optimize perturb and observe maximum power point tracking method. The main advantage which makes perturb and observe algorithm the most commonly used method is low-cost implementations. However, at steady state, the operating point oscillates around the MPP which in turn lead to some amount of available energy being wasted. Moreover, P&O algorithm can as well be confused during those time intervals characterized by rapidly changing atmospheric conditions. In order to limit the negative effects associated to the above drawbacks, the P&O MPPT parameters must be customized to the dynamic behavior of the specific converter adopted (Femia et al., 2005). To do this, the theoretical analysis allowing the optimal choice of such parameters was also carried out by Femia et al., (2005) and the results of experimental measurements obtained were found out to be in agreement with the predictions of theoretical analysis. The results obtained by means of such an approach clearly showed that in the design of efficient MPPT regulators the easiness and flexibility of P&O MPPT control technique can be exploited by optimizing it according to the specific system's dynamic characteristics (Femia et al., 2005).

Due to several challenges associated with the application of P&O MPPT technique in maximum power point tracking which include such challenges as sustained oscillation around the MPP, fast tracking versus oscillation tradeoffs, and user predefined constants Abdelsalam, Massoud, Ahmed & Enjeti, (2011) in their work, presented a modified P&O MPPT technique, applicable

for PV systems. The technique was observed to achieve the tasks which are: adaptive tracking and no steady-state oscillations around the MPP; and there was no need for predefined system-dependent constants, hence provides a generic design core. To validate the results obtained, Abdelsalam et al., (2011) presented practical results for experimental implementation of the proposed technique. It has been demonstrated that high-performance steady-state operation can be achieved with no oscillations around the MPP using the proposed technique. A comparison between the proposed technique and other adaptive P&O techniques has been carried out. Finally, an experimental setup has been held to demonstrate the capabilities of the proposed technique. Practical results for high- and low-irradiance conditions validate the proposed technique's effectiveness by comparing its performance to the fixed perturb technique.

In their paper, Welch & Venayagamoorthy, (2007) proposed an application of optimal energy control scheme for a grid independent photovoltaic (PV) solar system which consists of a PV array, battery energy storage, and time varying loads (a small critical load and a larger variable noncritical load). In the optimal controller design their focus was based on a class of Adaptive Critic Designs (ACDs) called the Action Dependent Heuristic Dynamic Programming (ADHDP) (Welch & Venayagamoorthy, 2007). Three different US cities were considered as a case study and the results show that the ADHDP based optimal control scheme outperforms the conventional PV-priority control scheme in maintaining the stated objectives almost all the time (Welch & Venayagamoorthy, 2007).

Ngan & Tan (2011) also discussed two categories of MPPT algorithms, namely indirect and direct methods. In addition to that, the review of MPPT algorithms as well as their respective advantages and disadvantages were presented. Ngan & Tan (2011) also performed simulations of PV modules using Perturb and Observe algorithm and Fuzzy Logic controller (FLC) and compared the simulation results produced by the two algorithms with the expected results generated by Solarex MSX60 PV modules. The P&O algorithm was observed as the simplest method, which resulted in low cost of installation and it may be competitive with other MPPT algorithms (Ngan & Tan, 2011). According to Ngan & Tan, fuzzy logic control method provided a simpler way to arrive at a definite conclusion, but it should be noted that it highly depends on the user's knowledge of the process operation for the FLC parameter setting (Ngan & Tan,

2011). The two researchers concluded that the conventional MPPT algorithms are not capable of solving the problems of multiple peaks that are established in the P-V characteristic curves of the PV systems due to partial shaded conditions and therefore recommended that further research should be done to extract maximum power effectively from the PV systems under non-uniform insolation.

Zhang (2012) suggested the use of adaptive control for solar energy based DC microgrid system development. From his point of view, during the upgrading of current electric power grid, it is expected to develop smarter, more robust and more reliable power systems integrated with distributed generations. To realize these objectives, Zhang opined that the traditional control techniques are no longer effective in either stabilizing systems or delivering optimal and robust performances. Therefore, development of advanced control methods has received increasing attention in power engineering (Zhang, 2012). The work of Zhang (2012) addresses two specific problems in the control of solar panel based microgrid systems. First, a new control scheme is proposed for the microgrid systems to achieve optimal energy conversion ratio in the solar panels. The control system can optimize the efficiency of the maximum power point tracking (MPPT) algorithm by implementing two layers of adaptive control. Such hierarchical control architecture has greatly improved the system performance, which is validated through both mathematical analysis and computer simulation. Second, in the development of the microgrid transmission system, the issues related to the tele-communication delay and constant power load (CPL)'s negative incremental impedance are investigated. A reference model based method is proposed for pole and zero placements that address the challenges of the time delay and CPL in closed-loop control. The effectiveness of the proposed modeling and control design methods are demonstrated in a simulation testbed. Practical aspects of the proposed methods for general microgrid systems are also discussed Zhang (2012).

The results presented by Zhang (2012) shows the effectiveness of using adaptive control in improving the energy conversion efficiency in the MPPT and therefore the voltage output shows smoother convergence curve in the transient dynamics of the system. The MPPT algorithm's realization is based on the foundation that two control schemes can be decoupled together. And the full state feedback control and model matching control techniques are trying to mitigate the

effect by redistribute the locations of the poles and minimal phase zeros in the system and therefore the stability of the system can be assured. Moreover, better transient response can be improved. As we are pacing with the progress of technology revolution where we will expect more and more distributed variable renewable generators or energy sources in the field. Many realistic issues cannot be encountered through the analysis and they are more likely to encounter through the experiment or real life. We may not expect the time delay issue by just doing the simulation as there are always some assumptions that require us to simplify the problem or which are even beyond our consideration. This work comprehensively illustrates the essential contribution by developing control techniques by using modern control design techniques. These methods are more versatile and effective to deal with the situations in practice (Decker & Loftis, 1997). Due to the fact that adaptive control is rather so complicated to realize the computation there is need to simplify the control implementation, depending on the size of the system. Moreover, as we have tasted the flavor of the adaptive control in addressing different types of problems and how robust it is when we are no longer to require the wholesome information of the system. Zhang (2012) proposed the development of the model reference adaptive control to address the constant power load stability issue in sense of global.

Sometimes conventional feedback controllers may not perform well online because of the variation in process dynamics due to nonlinear actuators, changes in environmental conditions and variation in the character of the disturbances. To overcome the above problem, Jain & Dr. Nigam (2013) presented the design of a controller for a second order system with Model Reference Adaptive Control (MRAC) scheme using the MIT rule for adaptive mechanism. In this rule, a cost function is defined as a function of error between the outputs of the plant and the reference model, and controller parameters are adjusted in such a way so that this cost function is minimized. The designed controller gives satisfactory results, but is very sensitive to the changes in the amplitude of reference signal. It follows from the simulation work carried out in this paper that adaptive system becomes unstable if the value of adaptation gain or the amplitude of reference signal is sufficiently large. This paper also deals with the use of MIT rule along with the normalized algorithm to handle the variations in the reference signal, and this adaptation law is referred as modified MIT rule. The performances of the proposed control algorithms are evaluated and shown by means of simulation on MATLAB and Simulink. The results obtained

from the application of MIT scheme for different values of adaptation gain were compared. It has been observed that the response of the system improves with the increment in adaptation gain but beyond a certain limit $(0.5 < \gamma < 5)$ the performance of the system becomes very poor. In this paper, the MIT rule is applied in many different cases. The selection of adaptation gain is very important and depends on the signal levels. The Normalized algorithm, used in this paper, is less sensitive even for very large and very small amplitudes of reference input. Therefore, it is shown in this paper that for suitable values of adaptation gain, the MIT rule with normalization can make the plant to follow the model as accurately as possible (Jain & Nigam, 2013).

Karanjkar, Chatterji & Kumar, (2014) also proposed linear quadratic regulator (LQR) approach for maximum power point tracking for a solar photo-voltaic system. They carried out real time simulations on MATLAB^{TM}/dSPACE^{TM} platform for solar photovoltaic system with buck converter and compared the performance with the existing methods such as perturb and observe, incremental conductance, fuzzy logic, neural network. The experimental results showed the superiority of the LQR method for tracking maximum power point under rapidly varying solar radiations with an efficiency of 77.60 – 79.39% for P&O, 85.63 – 88.88% for fuzzy logic and 90.87 – 94.78% for LQR. Karanjkar et al, (2014) also recommended that although the LQR approach needs three sensors, it does not require calculation of PV power as in the case of other conventional methods. The absence of parameter tuning capability also makes this approach non-ideal in a situation where the parameters deviate away from the original design it was meant to serve.

In view of the foregoing reviewed literatures, several methods for controlling solar photovoltaic energy system have been reported. These methods are used to establish the algorithm for maximum power point tracking and each of them has advantages and limitations over the other methods, and varies in terms of system complexity, tracking speed, sensor requirement, and cost hence the need for further research to find out an efficient method that can yield an optimal control. Linear quadratic regulator (LQR) is one of the optimal control methods which is widely developed for its usage in many applications and is a fixed gain optimal control technique. However, it has no ability to adapt to parametric uncertainties which may have occurred due to changes in environmental conditions. Also, model reference adaptive control can also be used to

enable the system adapt to the parametric uncertainties when there is variation in environmental conditions but adaptive control alone is not ideal because fast adaptation can lead to undesirable oscillations and instability. To enhance tracking performance and robustness to failures and parametric uncertainties, the combination of a fixed gain and an adaptive controller to obtain an efficient control optimization and adaptability will not be a bad idea. The main contribution in this research work is therefore to analyze a standalone PV control system consisting of boost converter that can track MPP using a two-level control approach.

2.7 Summary of the research gap

Author(s)	Task	Method	Result	Limitation
Napole, Derbeli & Barambones, (2021)	Fuzzy Logic Approach for Maximum Power Point Tracking Implemented in a Real Time Photovoltaic System.	Real time experiment based on voltage reference estimator (VRE) combined with Fuzzy logic control (FLC).	An improved tracking with respect to the conventional P&O method.	Slowness in power correction. Fuzzy rules are predefined based on PV specifications.
Prastyawan, Efendi & Murdianto, (2021)	MPPT Full Bridge Converter Using Fuzzy Type-2 on DC Nano Grid System.	Implemented on MATLAB/Simulink software using two models.	Improved efficiency was observed in Fuzzy Type-2. Model 1 Fuzzy Type-2 (91.40%); Fuzzy Type-1 (80.64%). Model 2 Fuzzy Type-2 (87.63%); Fuzzy Type-1 (77.93%).	System implementation can be undesirably complex.

Anbarasi & Kanthalakshmi, (2016)	Development of LQR-based maximum power point tracking method for standalone photovoltaic system with an experimental validation.	The LQR method was used and simulation was done with MATLAB/Simulink environment.	LQR method showed an improved performance when compared with that of the conventional (P&O) method. Tracking speed LQR (0.04s); P&O (0.165s) Tracking efficiency LQR (96.93%); P&O (91.83%)	No adaptive features.
Vyshnavi & Subramanian, (2015).	Developed model reference adaptive control for maximum power point tracking in PV systems	They adopted a two-level control algorithms which are: ripple correlation control (RCC) and model reference adaptive control (MRAC) with Lyapunov approach.	An improved performance achieved with shorter time constants and overall system stability.	High gain can cause instability.
Khanna, Zhang, Stanchina, Reed & Mao, (2014)	Maximum Power Point Tracking Using Model Reference Adaptive Control	Two-level control consisting of ripple correlation control (RCC) and the model reference adaptive control (MRAC).	The implication of the results obtained was that the proposed control algorithm enables the system to converge to the maximum power point in milliseconds.	A large magnitude of control gain may lead to oscillations at the operating point.
Karanjkar, Chatterji & Kumar (2014).	Design and Implementation of a Linear Quadratic Regulator Based Maximum Power Point Tracker for Solar Photo-Voltaic System.	Real time experiment and simulation carried out.	Comparison showed a better efficiency than others. **P&O:** 77.60 – 79.39% **Fuzzy Logic:** 85.63 – 88.88% **LQR:** 90.87 – 94.78%	Parameter tuning is essential.

CHAPTER THREE

MATERIALS AND METHODS

3.1 Materials

The following tools and equipment were used during the course of this work:

(i) MATLAB/Simulink software application – MATLAB version 2019

(ii) Solar photovoltaic (PV) data sheet – Mitsubishi Electric Photovoltaic Module (Specification sheet) found online at https://www.studylib.net/doc/18057350/mlu-specification-sheet-250-255w.

(iii) Internet

(iv) LQR and MRAC mathematical tools

3.2 Methods

The control method used in this work was incorporated linear quadratic regulator (LQR) and model reference adaptive control (MRAC). In this method, the two control schemes were merged to investigate the control performance, with respect to LQR-only and MRAC-only.

3.2.1 Description of the proposed method

The method employed in this work was LQR and MRAC. The purpose is to control the amount of power from the solar photovoltaic system hence tracking maximum power sufficient for driving the loads connected to the system. The function of the LQR controller is to ensure that optimal power is delivered to the load through the converter by maintaining a fixed gain. The optimal control problem is defined by finding an optimal control u for the system given by

$$\dot{\boldsymbol{x}}(\boldsymbol{t}) = \boldsymbol{A}\boldsymbol{x}(\boldsymbol{t}) + \boldsymbol{B}\boldsymbol{u}(\boldsymbol{t}) \quad (\textbf{Kirk}, \textbf{1998}). \qquad (\textbf{3.1})$$

Hence the use of LQR technique is to minimize or maximize the required performance index J defined by,

$$\boldsymbol{J} = \int_{\boldsymbol{0}}^{\boldsymbol{t}} (\boldsymbol{x}^{\boldsymbol{T}}\boldsymbol{Q}\boldsymbol{x} + \boldsymbol{u}^{\boldsymbol{T}}\boldsymbol{R}\boldsymbol{u})\boldsymbol{dt} \quad (\textbf{Kirk}, \textbf{1998}). \qquad (\textbf{3.2})$$

$where$ Q and R are the weighting matrices that should be chosen in order to give the minimum value of the performance index (J). To achieve the required objectives, LQR control method therefore applies the following steps:

(i) **Selecting the state and control penalty matrices, Q and R respectively:** The main challenge in LQR is a suitable choice of Q and R matrices. The choice could be made based on the user experience (Anderson & Moore, 1989).

(ii) **Solving the Algebraic Riccatti equation:** When the optimal values of Q and R matrices are substituted in the Algebraic Riccati equation (3.3), then the $\boldsymbol{P}$ matrix is obtained either by algebraic computation or MATLAB code.

$$\dot{\boldsymbol{P}} = \boldsymbol{PA} + \boldsymbol{A^T P} + \boldsymbol{Q} - \boldsymbol{PBR^{-1}B^T P} = \boldsymbol{0} \quad (\textbf{Anderson \& Moore, 1989}) \qquad (\boldsymbol{3.3})$$

(iii) **Obtaining the feedback gain:** Once the matrix $\boldsymbol{P}$ is determined then the feedback gain defined by equation (3.4) can be obtained.

$$\boldsymbol{K} = \boldsymbol{R^{-1}B^T P}\, \boldsymbol{u(t)} \quad (\textbf{Anderson \& Moore, 1989}) \qquad (\boldsymbol{3.4})$$

Hence, the optimal controller $u(t)$ in terms of the state feedback gain (K) is obtained as,

$$\boldsymbol{u} = \boldsymbol{R^{-1}B^T P}\, \boldsymbol{x(t)} = -\boldsymbol{Kx(t)} \quad (\textbf{Anderson \& Moore, 1989}) \qquad (\boldsymbol{3.5})$$

On the other hand, adaptive control mechanism will ensure that the controller parameters are adjusted with respect to changes in environmental conditions so as to generate the suitable control law capable of driving the plant to meet the required power demand. Since a large gain may cause instability in the system as the parameters vary then the LQR will help to maintain a fixed optimal gain. The model reference will be set in form of a critically damped system and the output of the plant, y_p will have to follow the output of the reference model, y_m. The system compares the plant's output with the output of the reference model and generates an error signal which is used by adaptation mechanism to update the controller parameters for effective power optimization. The block diagram of the proposed control architecture is as shown in figure 3.1. To realize the objective of this work, four steps were taken into consideration to derive the adaptation law for controller parameters in MRAC:

(i) Choosing the controller structure;

(ii) Finding state-space expressions for the controlled plant and the reference model;

(iii) Constructing error equations; and

(iv) Deriving an adaptation law for MRAC using the Lyapunov method.

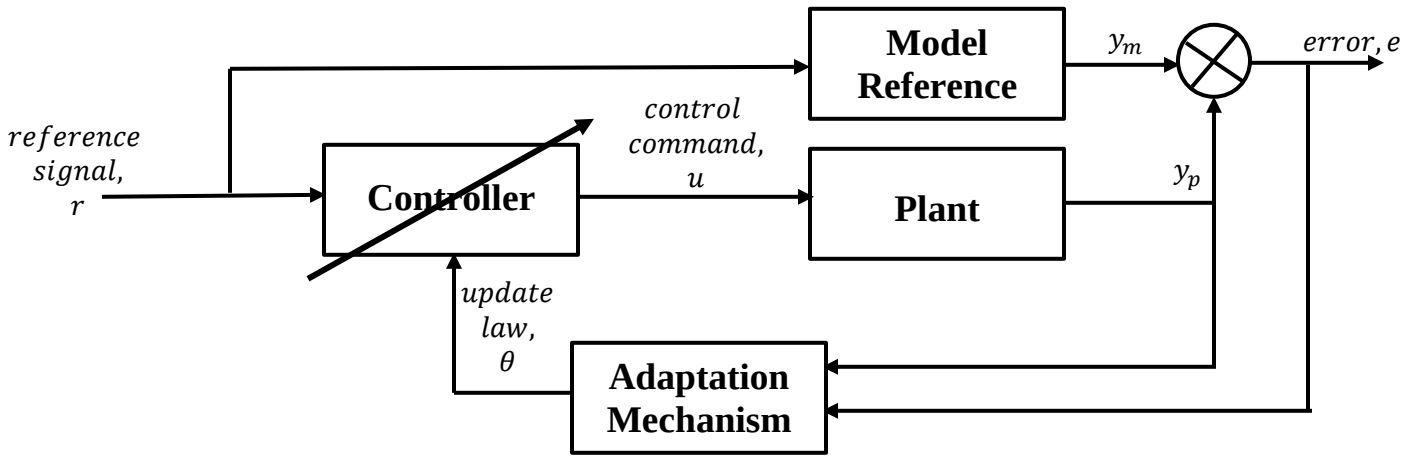

Figure 3.1: Generic block diagram of the proposed control architecture

3.2.2 System description

PV system consists of PV module, power converter, the MPPT controller to track maximum power and a load. The controller has an inbuilt algorithm that ensures the extraction of maximum power from PV module at any environmental conditions. This work is focused on tracking the maximum power through the application of LQR and MRAC designed to generate duty cycle d which when effected on the controller can effectively allow the panel impedance to match with source impedance thereby extracting maximum power. The complete block diagram of standalone photovoltaic system with the MPPT controller is depicted in Figure 3.2. The use of DC-DC converter enables the source and load impedances to be matched hence maximum power is allowed to be transferred from source to load. Boost converter is selected for this work because it is capable of increasing the module voltage to the level required by the load. In the view of power conservation, the load current is always lesser than the source current. The converter has a source, inductor, capacitor switch, and a load. To boost up the output voltage, the inductor is placed at the front of switching network.

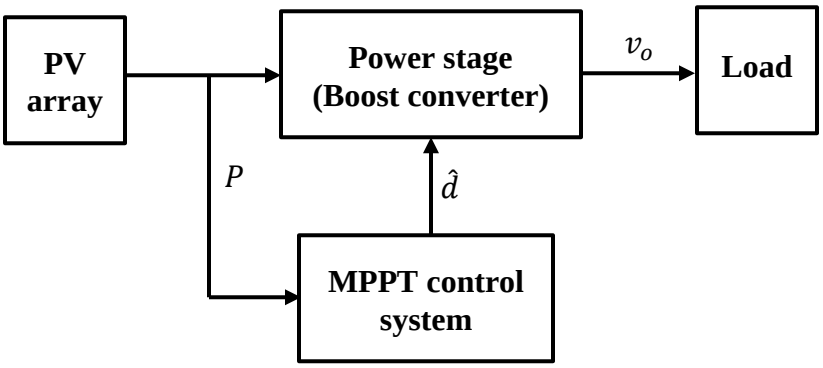

Figure 3.2: Block diagram of PV system with the power system and MPPT controller

3.2.3 Data validation

The data used for this work was obtained from Mitsubishi electric photovoltaic module specification sheet. The model name of the solar PV module used for this work was $PV - MLU255HC$ and it has a power rating of $255W$. To validate the data in the manufacturer's specification sheet as shown in Appendix I, MATLAB/Simulink was used to simulate the module. Based on the mathematical equations (2.1 – 2.6), which characterize the photovoltaic module, the behavior of the proposed PV model $PV - MLU255HC$ was implemented in MATLAB environment using Simulink models. The Simulink models were created from the module equations that represent Saturation current, reverse saturation current, shunt current and photo-current as in equations (3.6 – 3.9). (Refer to Appendix II for the Simulink models).

$$\textbf{Photocurrent: } I_L = I_{sc} + K_i(T_a - T_r) \cdot \frac{\lambda}{1000} \quad (\textbf{Mboumboue \& Njomo, 2013}) \tag{3.6}$$

$$\textbf{Saturation current: } I_o = I_{rs}\left(\frac{T_a}{T_r}\right)^3 e^{\left[\frac{qE_{g0}}{nk}\left(\frac{1}{T_r}-\frac{1}{T_a}\right)\right]} (\textbf{Mboumboue \& Njomo, 2013}) \tag{3.7}$$

$$\textbf{Reverse saturation current: } I_{rs} = \frac{I_{sc}}{e^{\left(\frac{qV_{oc}}{N_s knT_a}\right)} - 1} \quad (\textbf{Mboumboue \& Njomo, 2013}) \tag{3.8}$$

PV current:

$$I_{PV} = N_p I_{ph} - N_p I_o \left\{ e^{\left[\frac{q(V_{PV}+I_{PV}R_s)}{N_s knT_a}\right]} - 1 \right\} - \frac{V_{PV}+I_{PV}R_s}{R_p} (\textbf{Mboumboue \& Njomo, 2013}) \tag{3.9}$$

The models which were originally created separately were then interconnected to form a whole as shown in Figure 3.3(a). To simplify the model, Figure 3.3(b) was obtained by creating a subsystem to measure the output of the system.

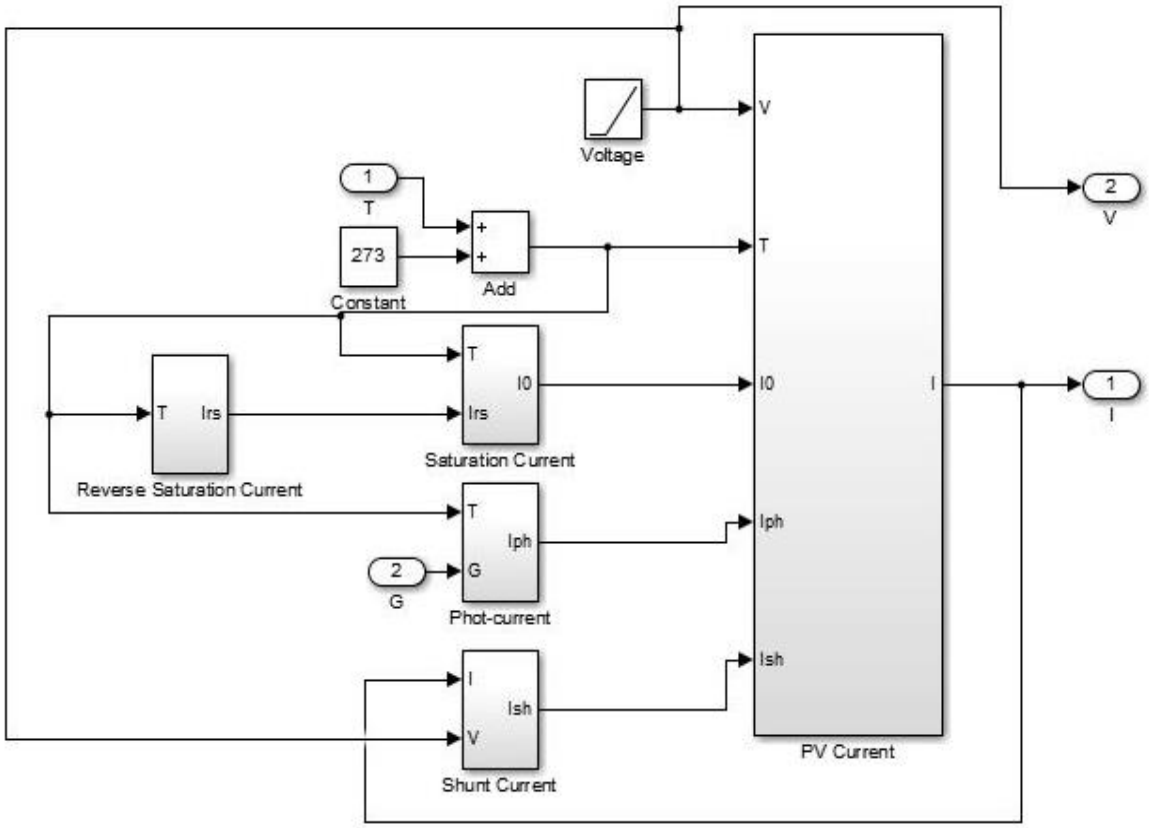

(a)

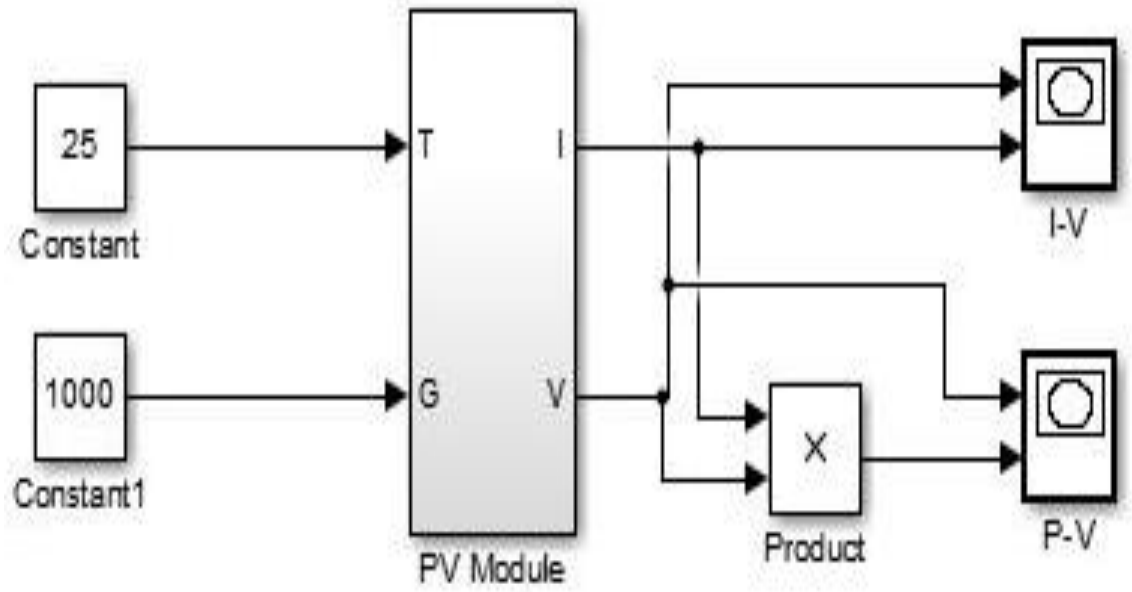

(b)

Figure 3.3: Simulink model of a PV module: (a) Subsystems interconnection (b) Output measurement at STC

The simulation of the model resulted in three classic parameters that are very important on the PV characteristics which are: short-circuit current (I_{sc}), open-circuit voltage (V_{oc}) and the maximum power point ($P_{mp} = V_{mp}I_{mp}$). With these parameters three remarkable points were defined as $(0,\ I_{sc})$, $(V_{mp},\ I_{mp})$ and $(V_{oc},\ 0)$. The coordinate $(V_{mp},\ I_{mp})$ is the points at which the power delivered by a PV cell attains a maximum value. The Power-Voltage (P-V) and the Current-Voltage (I-V) characteristic curves of the module at Standard Test Conditions (STC) of $1000W/m^2$ solar irradiance and a temperature of $25°C$ are shown in Figure 3.4. According to the XY plot shown in Figure 3.4(a) the maximum current (V_{mp}) obtained was 8A while Figure 3.4(b), showed the maximum voltage (V_{mp}) of about 31V and a maximum power output of approximately 250W as expected. These values affirmed the rated values of the PV module as recorded on data sheet (as in Appendix I).

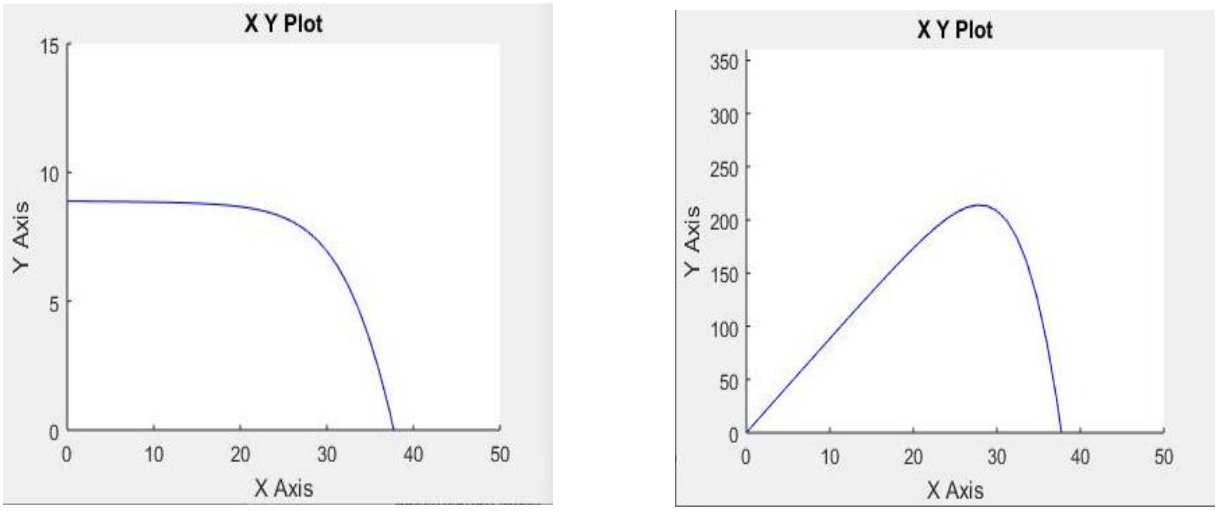

(a) (b)

Figure 3.4: (a) Solar I-V curve illustrating the I-V characteristic at STC

(b) Solar P-V curve illustrating the maximum power attained at STC

3.2.4 Boost converter design

The design of the power converter (boost) was first obtained. Modelling is particularly required to understand how variations in the parameters such as input voltage, duty cycle, and load

current have affected the output voltage. The boost converter circuit shown in Figure 3.5 therefore made the modelling process easy. For proper design of the converter circuit, the following assumptions were made:

(i) The components are ideal and lossless.

(ii) The time period is T of which switch is closed and opened for periods DT and $(1-D)T$, respectively, and operates in Continuous Conduction Mode.

(iii) The capacitor is selected such that the output voltage is constant.

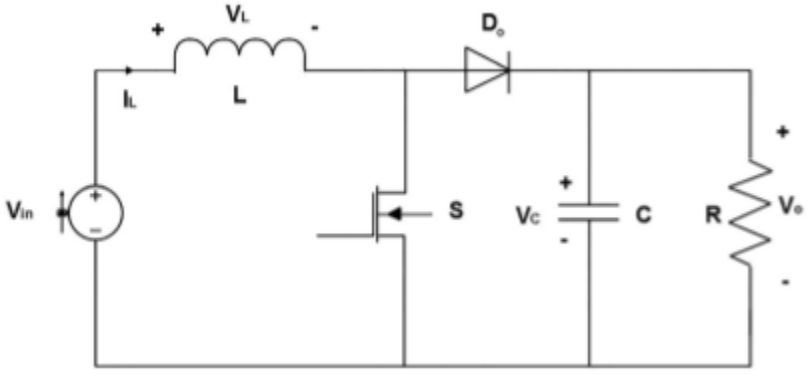

Figure 3.5: General configuration of a boost converter (Nisso, et. al, (2018))

The converter was modelled by utilizing two switch modes – the on-state and the off-state. The state variables chosen are output voltage $v_c = v_o$ and inductor current i_L, and the expressions during turn on and turn off processes are written as

Case 1: ON-MODE $(0 \leq t < DT)$

$$L\frac{di_L}{dt} = v_{in} \tag{3.10a}$$

$$C\frac{dv_o}{dt} = -\frac{v_o}{R_L} \tag{3.10b}$$

Case 2: OFF-MODE $(DT \leq t < T)$

$$L\frac{di_L}{dt} = v_{in} - v_o \tag{3.11a}$$

$$C\frac{dv_o}{dt} = i_L - \frac{v_o}{R_L} \tag{3.11b}$$

To link the modelled equations shown in the two cases, equations obtained by on-state switch mode should be multiplied by the duty ratio D while that obtained by off-state switch mode

should be multiplied by $(1-D)$ hence, from the first state equations (3.10a) and (3.11a), and second state equations (3.10b) and (3.11b) we have that

$$L\frac{di_L}{dt} = Dv_{in} + (1-D)(v_{in} - v_o) \tag{3.12a}$$

$$C\frac{dv_o}{dt} = -D\frac{v_o}{R_L} + (1-D)(i_L - \frac{v_o}{R_L}) \tag{3.12b}$$

$$L\frac{di_L}{dt} = v_{in} - (1-D)v_o \tag{3.13a}$$

$$C\frac{dv_o}{dt} = (1-D)i_L - \frac{v_o}{R_L} \tag{3.13b}$$

Linearizing equation (3.13) about the equilibrium point ($\hat{\imath}_L$, $\hat{v}_o$) would give the steady state operating point of the system as in equation (3.14). This can be obtained by setting the derivatives of equation (3.13) to zero.

$$\hat{v}_o = \frac{V_{in}}{(1-D)} \tag{3.14a}$$

$$\hat{\imath}_L = \frac{V_{in}}{R_L(1-D)^2} \tag{3.14b}$$

The small signal modelling of the power converter can be done by setting $i_L = (I_L + \hat{\imath}_L)$, $v_{in} = (V_{in} + \hat{v}_{in})$, $v_o = (V_o + \hat{v}_o)$ and $D = \left(d + \hat{d}\right)$ in equation (3.13), to give the linearized state model of the system given by

$$L\frac{d\hat{\imath}_L}{dt} = \hat{v}_{in} - (1-d)\hat{v}_o + V_o\hat{d} \tag{3.15a}$$

$$C\frac{d\hat{v}_o}{dt} = (1-d)\hat{\imath}_L - \frac{\hat{v}_o}{R_L} - \hat{\imath}_L\hat{d} \tag{3.15b}$$

By letting $\hat{\imath}_L = x_1$, $\hat{v}_o = x_2$, the state space dynamic equation for the system and the output equation using equations in are represented by the two equations in (3.16) respectively.

$$\begin{cases} \begin{bmatrix} \dot{x}_1 \\ \dot{x}_2 \end{bmatrix} = \begin{bmatrix} 0 & -\frac{1}{L}(1-d) \\ \frac{1}{C}(1-d) & -\frac{1}{CR_L} \end{bmatrix} \begin{bmatrix} x_1 \\ x_2 \end{bmatrix} + \begin{bmatrix} \frac{V_o}{L} \\ -\frac{I_L}{C} \end{bmatrix} \hat{d} + \begin{bmatrix} \frac{1}{L} \\ 0 \end{bmatrix} \hat{v}_{in} \\ y = x_2 = [0 \quad 1] \begin{bmatrix} x_1 \\ x_2 \end{bmatrix} \end{cases} \tag{3.16}$$

$$\begin{cases} \begin{bmatrix} \dot{x}_1 \\ \dot{x}_2 \end{bmatrix} = \begin{bmatrix} 0 & -\frac{1}{L}(1-d) \\ \frac{1}{C}(1-d) & -\frac{1}{CR_L} \end{bmatrix} \begin{bmatrix} x_1 \\ x_2 \end{bmatrix} + \begin{bmatrix} \frac{V_o}{L} & \frac{1}{L} \\ -\frac{I_L}{C} & 0 \end{bmatrix} \begin{bmatrix} \hat{d} \\ \hat{v}_{in} \end{bmatrix} \\ y = x_2 = [0 \quad 1] \begin{bmatrix} x_1 \\ x_2 \end{bmatrix} \end{cases} \tag{3.17}$$

Design Specification for boost converter

The power from the PV module P_{PV} as indicated by the PV characteristics shown in Figure 3.4(b) is approximately $248W$, which corresponds to the range of maximum power P_{max} shown on the Mitsubishi data sheet (Refer to Appendix I). This is the power generated by the solar PV module at STC through the simulation of the Simulink models. Taking into consideration the steady state operating point $(7.8A, 80V)$ derived in equation (3.9), then the corresponding load resistance could be determined as,

$$P_{max} = \frac{{V_o}^2}{R_L}$$

$$R_L = \frac{{V_o}^2}{P_{max}} = \frac{80^2}{255} = 25\Omega$$

The value of the output voltage is the steady state voltage. At this state the duty ratio is determined according to equation (2.19) as,

$$D = 1 - \frac{V_{in}}{V_o} = 1 - \frac{31.2}{80} = 0.6$$

The steady state inductor current is obtained as follows:

$$I_L = \frac{V_{in}}{R_L(1-D)^2} = \frac{31.2}{25(0.4)^2} = 7.8A$$

Selection of the inductance and filtering capacitance

To ascertain the choice of the filtering inductance and the output filtering capacitance, equations (2.12) and (2.13) apply. To compute these parameters, it was taken into consideration that the converter could be switched on and off at very high frequencies in the range $10kHz - 100MHz$ Gwinyai (2008), hence the choice of the switching frequency $f = 20kHz$. The limiting inductance of the circuit is determined as,

$$L > \frac{(1-D)^2 DR}{2f} = \frac{0.16 \times 0.6 \times 25}{2 \times 20 \times 10^3} = 60\mu H = L_b \qquad (3.18)$$

The design of the boost converter should be such that the filter inductor L is greater than L_b so that the converter will operate in continuous conduction mode. The choice of a much larger filtering capacitance greater than the limiting capacitance C_{min} could be used so that the current supplied to the output RC circuit does not go into a discontinuous conduction mode.

$$C > \frac{DV_o}{V_r \mathrm{R} f} = \frac{0.6 \times 80}{0.02 \times 25 \times 20 \times 10^3} = 4.8mF = C_{min} \qquad (3.19)$$

To validate the inductance and capacitance selected for the design of the boost converter, the graphs of inductance and capacitance were plotted against varying values of duty cycle as shown in Figure 3.6(a) and Figure 3.6(b) respectively by using appropriate MATLAB code as in Appendix IV. From the graph, it is clear that the values of the inductance and capacitance are in agreement with the computed values above. Since the maximum value of the inductance reached was $0.93 \times 10^{-4} H$ (Refer to Figure 3.6(a)) then the value of inductance selected for the design was $0.1mH$ and the value of capacitance selected was $5.0mF$, since the maximum value of the capacitance was obtained at the duty cycle of 0.6 as $4.8mF$.

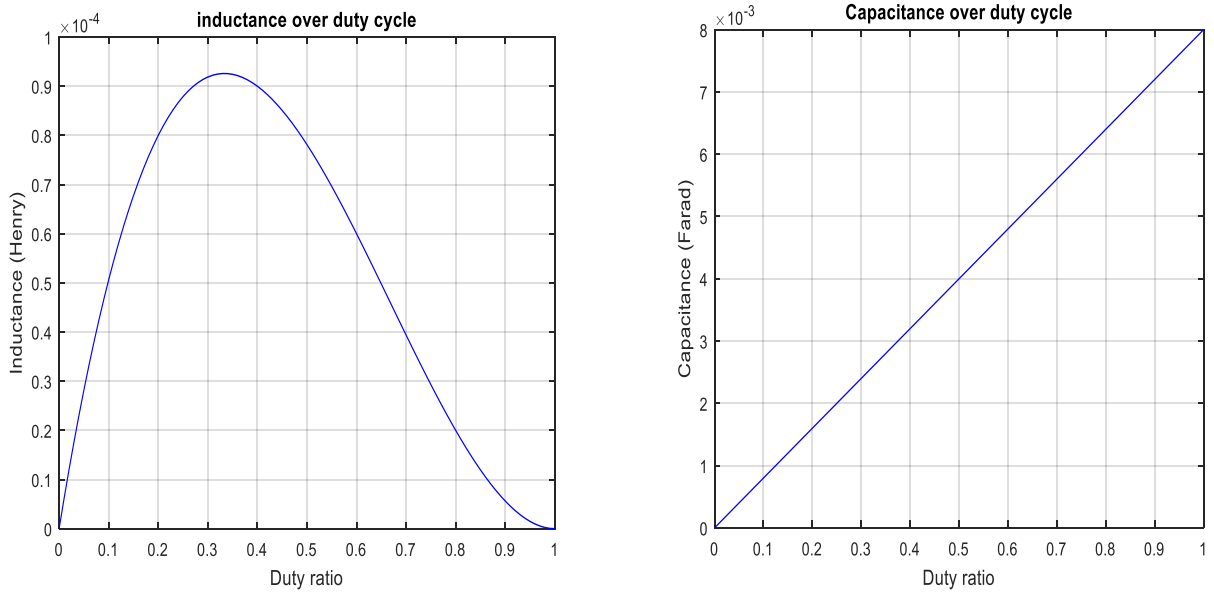

(a) **(b)**

Figure 3.6: Graphical illustration of inductance and capacitance against duty cycle
(a) Inductance over duty cycle (b) Capacitance over duty cycle

The summary of the design specification for the boost converter is as shown in Table 3.1.

Table 3.1: Summary of the boost converter design specification

Description of component	**Rating**
Input voltage (V_{in})	$31.2V$
Output capacitance (C)	$5.0mF$
Load resistance (R_L)	25.0Ω
Inductance (L)	$0.1mH$
Nominal duty ratio (D)	0.6
Switching frequency	$20kHz$

By inputting the values of the parameters in equation (3.17), the equation becomes,

$$\begin{cases} \begin{bmatrix} \dot{x}_1 \\ \dot{x}_2 \end{bmatrix} = \begin{bmatrix} \mathbf{0} & \mathbf{-4\times10^3} \\ \mathbf{80} & \mathbf{-8} \end{bmatrix} \begin{bmatrix} x_1 \\ x_2 \end{bmatrix} + \begin{bmatrix} \mathbf{8\times10^5} & \mathbf{10\times10^3} \\ \mathbf{-1.56\times10^3} & \mathbf{0} \end{bmatrix} \begin{bmatrix} \hat{d} \\ \hat{v}_{in} \end{bmatrix} \\ y = x_2 = [0 \quad 1] \begin{bmatrix} x_1 \\ x_2 \end{bmatrix} \end{cases} \qquad (3.20)$$

Where the constants, $\bar{A} = \begin{bmatrix} 0 & -4\times10^3 \\ 80 & -8 \end{bmatrix}$, $\bar{B} = \begin{bmatrix} 10\times10^3 \\ 0 \end{bmatrix}$, $\bar{C} = [0 \quad 1]$ and $\bar{D} = 0$

3.2.5 LQR control system design

The main aim of LQR as an optimal state feedback controller is to minimize the quadratic cost function, $J = \int_0^\infty [x^T(t)Qx(t) + u^T(t)Ru(t)]\,dt$ to provide an optimal response. To achieve this, three steps need to be considered as a design procedure for finding the optimal gain K which are:

Step I: Selecting the state and control penalty matrices, Q and R respectively.

The control law promises to maintain the output as close as possible to the desired value with minimum effort. Q and R are the weighting matrices. Q is a symmetric positive semi definite matrix whereas R is a positive number. Generally, Q is varied while R is fixed and are designed based on the closed loop performance specifications specified by the user. In this work, to select the state and control penalty matrices Q and R respectively, Q_{22} component was set to a specified value while all other component values were set to zero. The value of Q_{22} component was varied while R was kept constant. The initial value of Q was determined by the MATLAB code $Q = \mathrm{C}' * \mathrm{C}$, which algebraically represented by

$$Q = C^T \mathrm{C} = \begin{bmatrix} 0 \\ 1 \end{bmatrix} [0 \quad 1] = \begin{bmatrix} 0 & 0 \\ 0 & 1 \end{bmatrix}$$

The $\boldsymbol{Q_{22}}$ value was repeatedly increased and decreased using the code until the minimal error was obtained. By varying the $\boldsymbol{Q_{22}}$ value the corresponding step responses for each value of Q_{22} were plotted as shown in Figure 3.6 and the performance of the system was studied from the plotted graph and recorded as shown in Table 3.2. The value that yielded the minimal error between the output signal and the reference was selected though settling time and overshoot were not also neglected in the selection criteria. Hence, Q_{22} was found to be 0.8, with 0.0062s settling time and 15% overshoot. Therefore, the state penalty matrix and the control penalty matrix were recorded as

$$Q = \begin{bmatrix} 0 & 0 \\ 0 & 0.8 \end{bmatrix} \ and \ R = 1$$

Table 3.2: Summary of the performance characteristics with respect to varying values of $\boldsymbol{Q_{22}}$

Values of $\boldsymbol{Q_{22}}$	**Settling time (secs.)**	**Rise time (secs.)**	**Overshoot**
0.5	0.0100	0.0024	0.45
0.8	0.0062	0.0023	0.15
1.0	0.0061	0.0022	0.05
5.0	0.0042	0.0019	-0.55

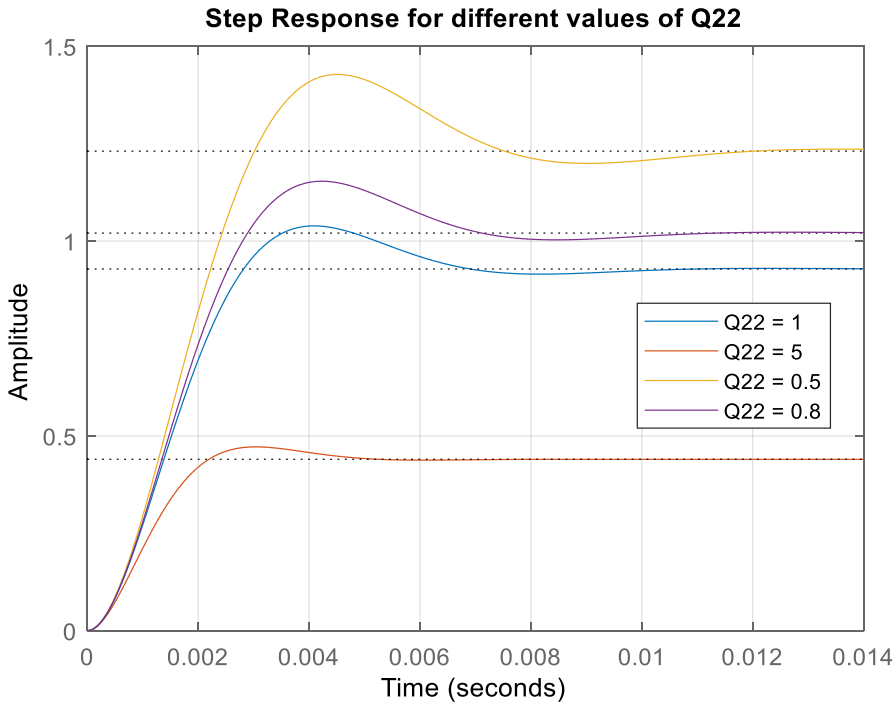

Figure 3.7: Time response for varying values of Q_{22}

Step II: Solving the Algebraic Riccatti equation.

The Riccatti coefficient matrix P was obtained by carefully solving the Algebraic Riccatti equation in equation (3.21) by using the MATLAB code $[K, P, E] = lqr(A, B, Q, R)$.

$$\boldsymbol{PA + A^T P - PBR^{-1}B^T P + Q = 0} \qquad (\mathbf{3.21})$$

The Riccatti coefficient P obtained was recorded as,

$$P = \begin{bmatrix} 0.0000 & 0.0001 \\ 0.0001 & 0.0012 \end{bmatrix}$$

Step III: Obtaining the gain using $K = R^{-1}B^T P$.

The feedback control law which minimizes the cost function is given by

$$\boldsymbol{u = -Kx} \qquad (\mathbf{3.22})$$

Where K the optimal gain matrix given by

$$\boldsymbol{K = R^{-1}B^{T}P} \qquad (\mathbf{3.23})$$

The MATLAB code $[K, P, E] = lqr(A, B, Q, R)$ used in step II also gave the result for the optimal gain K and the closed-loop eigenvalues E as,

$$K = [0.0955 \quad 0.5702] \; and \; E = -481.6 \pm j742.9$$

The closed-loop eigenvalues shows the control stability since the real part of the eigenvalues are negative. From the results obtained, the closed loop system was computed as,

$$\begin{cases} \begin{bmatrix} \dot{x}_1 \\ \dot{x}_2 \end{bmatrix} = \begin{bmatrix} -955.2 & -9702.4 \\ 80 & -8 \end{bmatrix} \begin{bmatrix} x_1 \\ x_2 \end{bmatrix} + \begin{bmatrix} 10000 \\ 0 \end{bmatrix} u \\ y = x_2 = [0 \quad 1] \begin{bmatrix} x_1 \\ x_2 \end{bmatrix} \end{cases} \qquad (\mathbf{3.24})$$

$Where$:

$$A_{cl} = A - BK = \begin{bmatrix} -955.2 & -9702.4 \\ 80 & -8 \end{bmatrix}; \quad B_{cl} = \begin{bmatrix} 10000 \\ 0 \end{bmatrix}; \quad C_{cl} = [0 \quad 1] \quad and \quad D_{cl} = 0$$

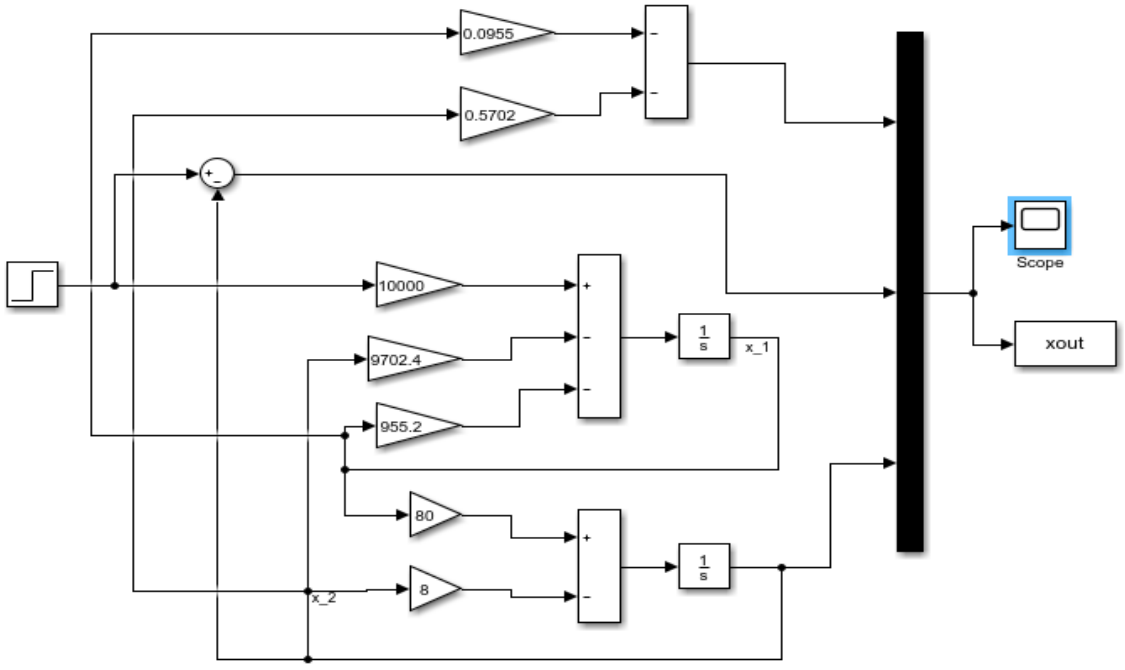

Figure 3.8: LQR Simulink model

3.2.6 MRAC control system design

The MRAC system design took four steps to accomplish as explained in the following subsections. The steps range from expression of the controlled plant and reference model, determination of control law and adaptation parameters, error Analysis to derivation of the update (adaptation) law.

Step I: Expression of the control plant and reference model

The process dynamics, $Y_p(s)$and the reference model, $Y_m(s)$ are given in equation (3.25) respectively,

$$\boldsymbol{Y_p(s) = \frac{k_p}{s^2 + a_p s + b_p} U(s)} \ \textbf{(Pankaj et al., 2011)}. \qquad \textbf{(3.25a)}$$

$$\boldsymbol{Y_m(s) = \frac{k_m}{s^2 + a_m s + b_m} R(s)} \ \textbf{(Pankaj et al., 2011)}. \qquad \textbf{(3.25b)}$$

In time domain, equation becomes,

$$\boldsymbol{\ddot{y}_p = -a_p \dot{y}_p - a_p y_p + b_p u} \qquad \textbf{(3.26a)}$$

$$\boldsymbol{\ddot{y}_m = -a_m \dot{y}_m - a_m y_m + b_p r} \qquad \textbf{(3.26b)}$$

Hence, the state space equations for the system was derived as,

$$\begin{bmatrix} \dot{y}_{p1} \\ \dot{y}_{p2} \end{bmatrix} = \begin{bmatrix} 0 & 1 \\ -b_p & -a_p \end{bmatrix} \begin{bmatrix} y_{p1} \\ y_{p2} \end{bmatrix} + \begin{bmatrix} 0 \\ k_p \end{bmatrix} u \qquad \textbf{(3.27a)}$$

$$\begin{bmatrix} \dot{y}_{m1} \\ \dot{y}_{m2} \end{bmatrix} = \begin{bmatrix} 0 & 1 \\ -b_m & -a_m \end{bmatrix} \begin{bmatrix} y_{m1} \\ y_{m2} \end{bmatrix} + \begin{bmatrix} 0 \\ k_m \end{bmatrix} r \qquad \textbf{(3.27b)}$$

Equation (3.27) can be represented in general form as,

$$\boldsymbol{\dot{y}_p = -A_p y_p + B_p u} \qquad \textbf{(3.28a)}$$

$$\boldsymbol{\dot{y}_m = -A_m y_m + B_m r} \qquad \textbf{(3.28b)}$$

$$Where: \quad A_p = \begin{bmatrix} 0 & -1 \\ b_p & a_p \end{bmatrix}; \quad A_m = \begin{bmatrix} 0 & -1 \\ b_m & a_m \end{bmatrix}, B_p = \begin{bmatrix} 0 \\ k_p \end{bmatrix} \text{ and } B_m = \begin{bmatrix} 0 \\ k_m \end{bmatrix}$$

Step II: Determination of control law and adaptation parameters

The control law is given by

$$\boldsymbol{u = r\theta_1 - y_p\theta_2} \ \textbf{(Pankaj et al., 2011)} \qquad \textbf{(3.29)}$$

Substituting for u in equation (3.28a), we have that

$$\dot{y}_p = -(A_p + B_p\theta_2)y_p + B_p\theta_1 r \quad (3.30)$$

For the process dynamics to match the reference model, θ_1 and θ_2 need to be obtained by comparing equation (3.28b) with (3.30). Hence, we have

$$\theta_1 = \frac{B_m}{B_p} \quad \text{and} \quad \theta_2 = \frac{A_m - A_p}{B_p} \quad (3.31)$$

Step III: Error Analysis

Error equation is given by

$$e = y_p - y_m \quad (\textbf{Pankaj et al., 2011}). \quad (3.32a)$$

$$\dot{e} = \dot{y}_p - \dot{y}_m \quad (\textbf{Pankaj et al., 2011}). \quad (3.32b)$$

$$\dot{e} = -A_p y_p + B_p u - (-A_m y_m + B_m r) \quad (3.32c)$$

$$\dot{e} = -A_p y_p + B_p u + A_m y_m - B_m r + A_m y_p - A_m y_p \quad (3.32d)$$

$$\dot{e} = -A_m(y_p - y_m) + (A_m - A_p)y_p - B_m r + B_p r\theta_1 - B_p y_p \theta_2 \quad (3.32e)$$

$$\dot{e} = -A_m(y_m - y_p) - (B_p\theta_2 + A_p - A_m)y_p + (B_p\theta_1 - B_m)r \quad (3.33)$$

Step IV: Derivation of the update (adaptation) law

The Lyapunov function was therefore applied at this stage to determine the update law. The Lyapunov function was obtained as

$$V(e, \theta_1, \theta_2) = \frac{1}{2}\Gamma e^2 + \frac{1}{2B_p}(B_p\theta_1 - B_m)^2 + \frac{1}{2B_p}(B_p\theta_2 + A_p - A_m)^2 \quad (3.34)$$

The derivative of V with respect to time gives

$$\dot{V}(e, \theta_1, \theta_2) = \Gamma e\dot{e} + (B_p\theta_1 - B_m)\dot{\theta}_1 + (B_p\theta_2 + A_p - A_m)\dot{\theta}_2 \quad (3.35a)$$

$$\dot{V}(e, \theta_1, \theta_2) = -\Gamma A_m e(y_p - y_m) - \Gamma e(B_p\theta_2 + A_p - A_m)y_p + \Gamma e(B_p\theta_1 - B_m)r + (B_p\theta_1 - B_m)\dot{\theta}_1 + (B_p\theta_2 + A_p - A_m)\dot{\theta}_2 \quad (3.35b)$$

$$\dot{V}(e, \theta_1, \theta_2) = -\Gamma A_m e^2 + (\Gamma e r + \dot{\theta}_1)(B_p\theta_1 - B_m) + (-\Gamma e y_p + \dot{\theta}_2)(B_p\theta_2 + A_p - A_m) \quad (3.36)$$

Therefore, the update law

$$\dot{\theta}_1 = -\Gamma e r \quad (3.37a)$$

$$\dot{\theta}_2 = \Gamma e y_p \quad (3.37b)$$

Design of reference model for MRAC-only and LQR-MRAC case

By transforming the state space equation (3.20) to its corresponding transfer function using $G(s) = C(sI - A)^{-1}B_1 + D$ or MATLAB code $[num, den] = ss2tf(A, B, C, D)$, the plant's equation was obtained as,

$$\boldsymbol{G(s) = \frac{(8 \times 10^5)}{s^2 + 8s + (3.2 \times 10^5)}} \tag{3.38}$$

The design of the reference model for the MRAC system was done by considering the characteristic equation of the plant, that is, equation (3.38) given as,

$$\boldsymbol{s^2 + 8s + 320000 = 0} \tag{3.39a}$$

By comparing equation (3.38) with the second order canonical form of characteristic equation given as,

$$\boldsymbol{s^2 + 2\xi\omega_n s + {\omega_n}^2 = 0} \tag{3.39b}$$

Where $\boldsymbol{\xi}$ is the damping ratio and $\boldsymbol{\omega_n}$ is the natural frequency

Then,

$$\boldsymbol{{\omega_n}^2 = 320000 \Longrightarrow \omega_n = 565.69 rad/s} \tag{3.40}$$

$$\boldsymbol{2\xi\omega_n = 8 \Longrightarrow \xi\omega_n = 4 \Longrightarrow \xi = \frac{4}{\omega_n} = \frac{4}{565.69} = 0.007} \tag{3.41}$$

The damping ratio of 0.007 showed an under-damped system. For such a system to adapt to environmental uncertainties, a reference model system was designed by assuming a critically damped system such that $\xi = 1$, hence the natural frequency was obtained as,

$$2\omega_n = 8 \Longrightarrow \omega_n = 4$$

The choice of the k_m value was made by varying the numerator of the transfer function upon simulation on Simulink. The value of k_m which yielded the response with minimal oscillations was 20. This value must be chosen such that $k_m \geq {w_n}^2 = 16$. From the result, the reference model system was determined as,

$$\boldsymbol{G(s) = \frac{20}{s^2 + 8s + 16}} \tag{3.42}$$

In the case of an incorporated LQR-MRAC system, the design of the MRAC system was done by using the LQR controlled closed loop system shown in equation (3.24) hence the eigenvalues of the state matrix, A_{cl} which shows the solution of the characteristic equation were determined as,

$$\boldsymbol{E = -481.6 \pm j742.9} \qquad (\boldsymbol{3.43a})$$

Recall that by solving the second order characteristic equation shown in equation (3.24) the solution becomes,

$$\boldsymbol{s = -\xi\omega_n \pm j\omega_n\sqrt{1-\xi^2}} \qquad (\boldsymbol{3.43b})$$

By comparing equation (3.43a) with (3.43b), it was determined that

$$\boldsymbol{\xi\omega_n = 481.6} \qquad (\boldsymbol{3.44a})$$

$$\boldsymbol{\omega_n\sqrt{1-\xi^2} = 742.9} \qquad (\boldsymbol{3.44b})$$

The two equations were solved simultaneously to obtain ξ and ω_n thus:

$$\boldsymbol{{\omega_n}^2(1-\xi^2) = 551900.41 \Longrightarrow {\omega_n}^2 - (\xi\omega_n)^2 = 551900.41} \qquad (\boldsymbol{3.44c})$$

$$\boldsymbol{{\omega_n}^2 - (481.6)^2 = 551900.41} \qquad (\boldsymbol{3.44d})$$

$$\boldsymbol{{\omega_n}^2 = 551900.41 + 231938.56 = 783838.97 \Longrightarrow \omega_n = 885.3 rad/s} \qquad (\boldsymbol{3.44e})$$

$$\boldsymbol{\xi = \frac{481.6}{\omega_n} = \frac{481.6}{885.3} = 0.5} \qquad (\boldsymbol{3.44f})$$

The damping ratio ξ of 0.5 shows an underdamped system, hence a critically damped system was designed as a reference model. From equation (3.44a), if $\xi = 1$ then $\omega_n = 481.6 rad/s$, hence ${\omega_n}^2 = 231938.56 rad^2/s^2$ and $2\xi\omega_n = 963.2 rad/s$. The value of $k_m = 240000$ was chosen for the reference model after series of tests by simulation such that the value of $k_m \geq {w_n}^2$ hence the system transfer function was obtained as,

$$\boldsymbol{G(s) = \frac{240000}{s^2 + 963.2s + 231938.56}} \qquad (\boldsymbol{3.45})$$

Following the MRAC design above, the Simulink models for both MRAC-only and incorporated LQR-MRAC schemes were developed as shown in Figure 3.9, 3.10, 3.11 and 3.12. The models were used to obtain the step response of the system for different gain values.

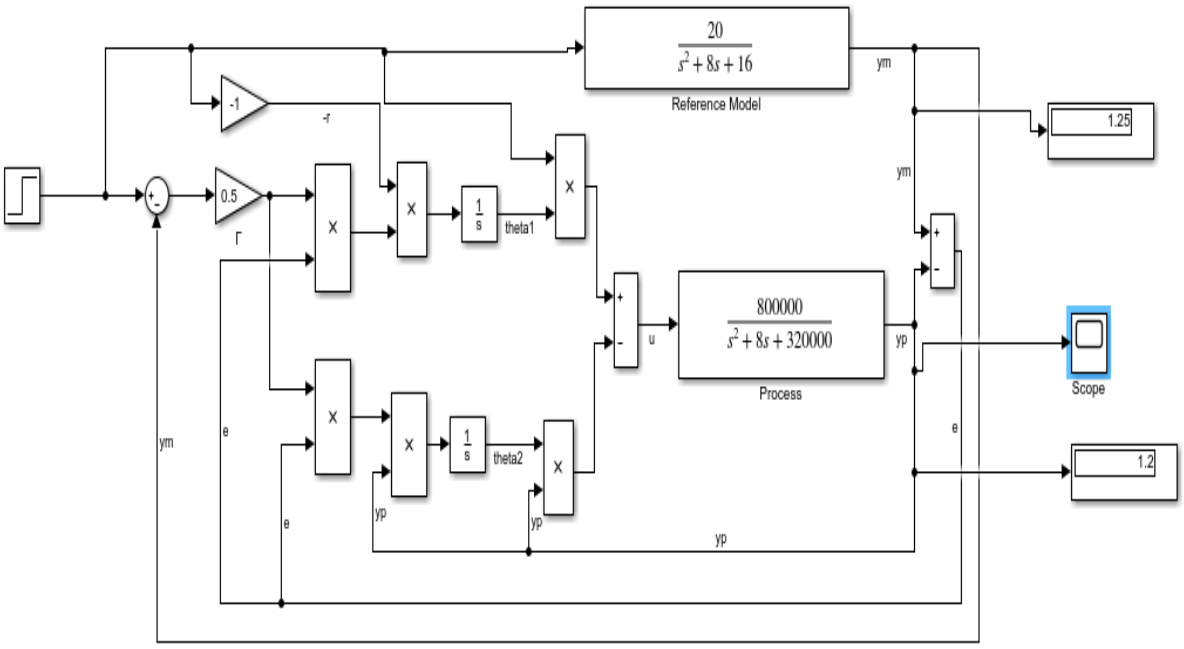

Figure 3.9: Simulink model of MRAC-only control scheme

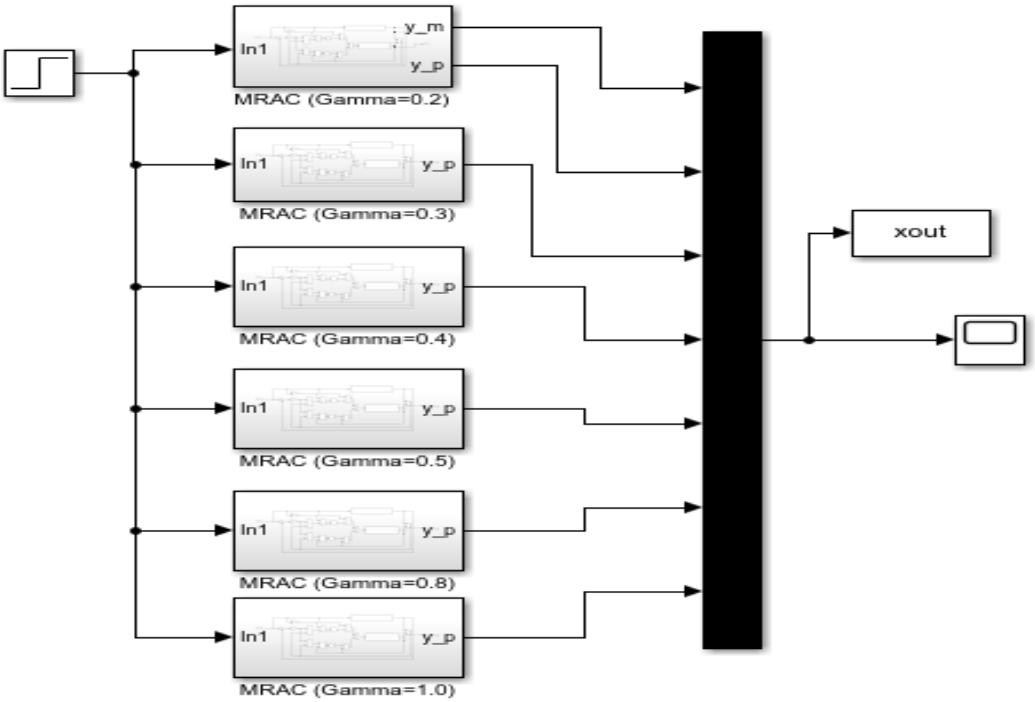

Figure 3.10: MRAC-only subsystem for different gain values

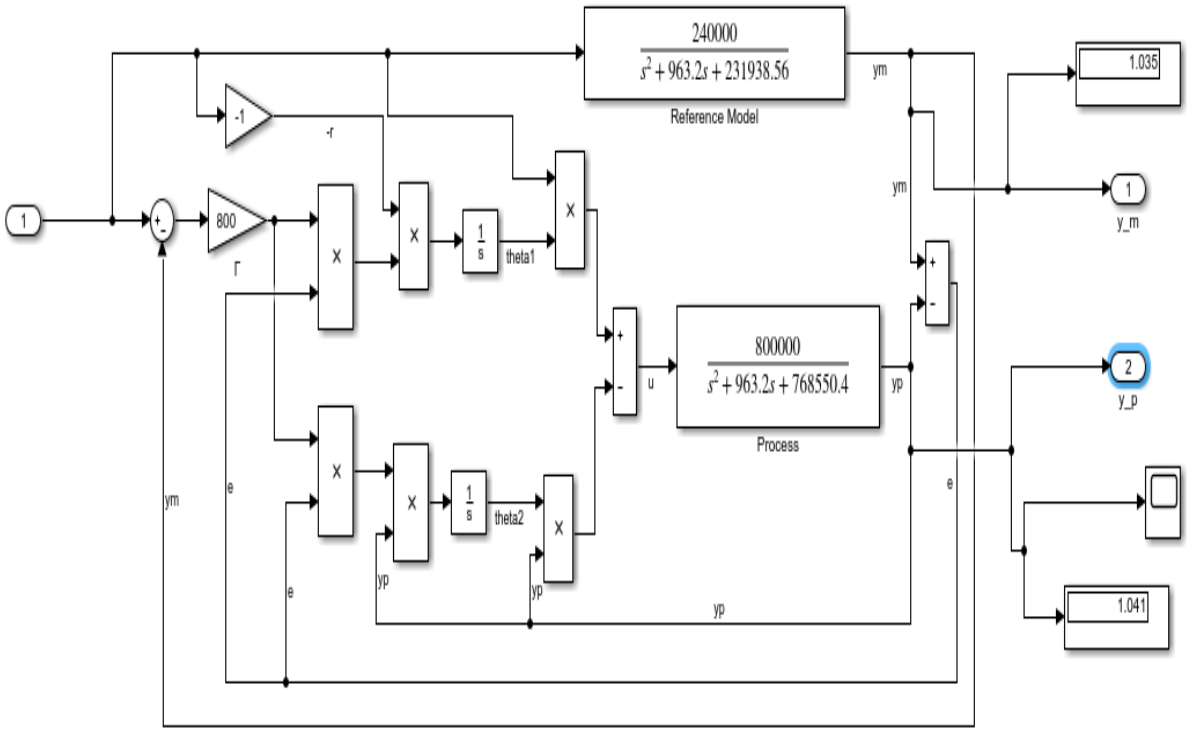

Figure 3.11: Simulink model of LQR-MRAC control

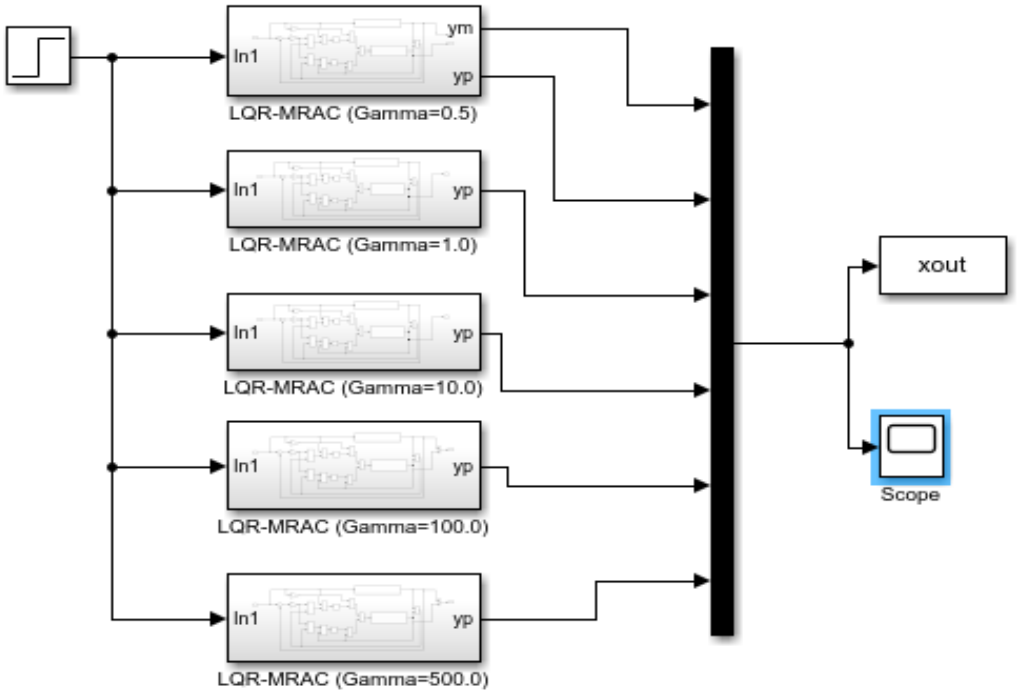

Figure 3.12: LQR-MRAC control subsystem for different gain values

3.2.7 Measured performance characteristics

The performance of each of the control schemes was studied by inspecting the response of the system upon simulation. Such performance characteristics studied which were critical to the comparison of the schemes applied were tracking efficiency, maximum overshoot, tracking or convergence speed, etc. The qualitative method which involves taking into consideration the steady state response of the system upon simulation was employed to assess the efficiency of the control methods under study. In this method, the steady state error of each control scheme was taken and then used to compute the corresponding tracking efficiency.

The LQR case

Considering the steady state value of the output signal for LQR scheme upon simulation (that is 1.02), the output voltage could be determined as,

$$V_o = 80 - (80 \times 0.02) = 78.4V$$

This voltage value therefore yielded the power output computed thus:

$$P_o = V_o I_R = V_o I_L(1 - D) = 78.4 \times 7.8 \times 0.4 = 244.6W$$

With values of the input power (that is, $255W$), which was extracted from the data sheet *(Appendix 1)*, the efficiency was determined thus:

$$\eta_{LQR} = \frac{244.6W}{255W} \times 100 = 95.92\%$$

The MRAC case

In this case, the steady state was observed to be 1.25 hence the value of the output voltage becomes

$$V_o = 80 - (80 \times 0.25) = 60V$$

The output power was computed thus:

$$P_o = V_o I_R = V_o I_L(1 - D) = 60 \times 7.8 \times 0.4 = 187.2W$$

The input power, $P_{in} = 1.25 \times 255 = 318.75W$

Hence, the efficiency becomes:

$$\eta_{MRAC} = \frac{187.2W}{255W} \times 100 = 73.41\%$$

The Incorporated LQR-MRAC case

In this case, the steady state was observed to be 1.035

This value indicates that the output voltage falls within the range,

$$V_o = 80 - (80 \times 0.035) = 77.2V$$

The limits of the power output were computed thus:

$$P_o = V_o I_R = V_o I_L (1 - D) = 77.2 \times 7.8 \times 0.4 = 240.86W$$

Hence, the efficiency becomes:

$$\eta_{LQR-MRAC} = \frac{258.3W}{255W} \times 100 = 94.45\%$$

No-controller case

In this case, the steady state was 0.75. This value indicates that the output voltage

$$V_o = (80 - (80 \times 0.75)V = 20V$$

The power output was computed thus:

$$P_o = V_o I_R = V_{omin} I_L (1 - D) = 20 \times 7.8 \times 0.4 = 62.4W$$

Hence, the efficiency becomes:

$$\eta_{No-controller} = \frac{62.4W}{255W} \times 100 = 24.5\%$$

The tracking efficiency was determined to be 24.5%.

3.2.8 Determination of the duty cycle

Recall that it was established in equation (2.19) that

$$\frac{V_o}{V_{in}} = \frac{1}{1 - d}$$

Hence, to ensure efficient control the duty cycle for each control scheme was determined by

$$d = 1 - \frac{V_{in}\eta}{V_o}$$

$Where$:

$$V_{in} = Input\ voltage = 31.2V$$

$$V_o = Desired\ output\ voltage = 80V$$

$$\eta = Control\ efficiency$$

$$d = 1 - \frac{31.2\eta}{80} = 1 - 0.39\eta$$

By inputting the values of η for each control schemes as previously determined as η_{LQR}, η_{MRAC}, $\eta_{LQR-MRAC}$, and $\eta_{No-controller}$ which are 95.92%, 73.41%, 94.45% and 24.5% respectively, the following values were obtained for the duty cycles.

Table 3.3: Duty cycle for each control scheme

Control scheme	**Efficiency (η)**	**Duty cycle (d)**
LQR	0.9592	0.626
MRAC	0.7341	0.714
LQR-MRAC	0.9445	0.632
No-controller	0.2450	0.904

CHAPTER FOUR

RESULTS AND DISCUSSION

4.1 Results

No-controller system performance

The time response of the open-loop system in Figure 4.1 shows an oscillation about a fixed value. Figure 4.2 also shows a closed-loop system with no controller and it shows the reduction in the oscillation that occurred in the open-loop system but with a great amount of error measured from the desired value hence, the need for the integration of a controller to the system for optimal control.

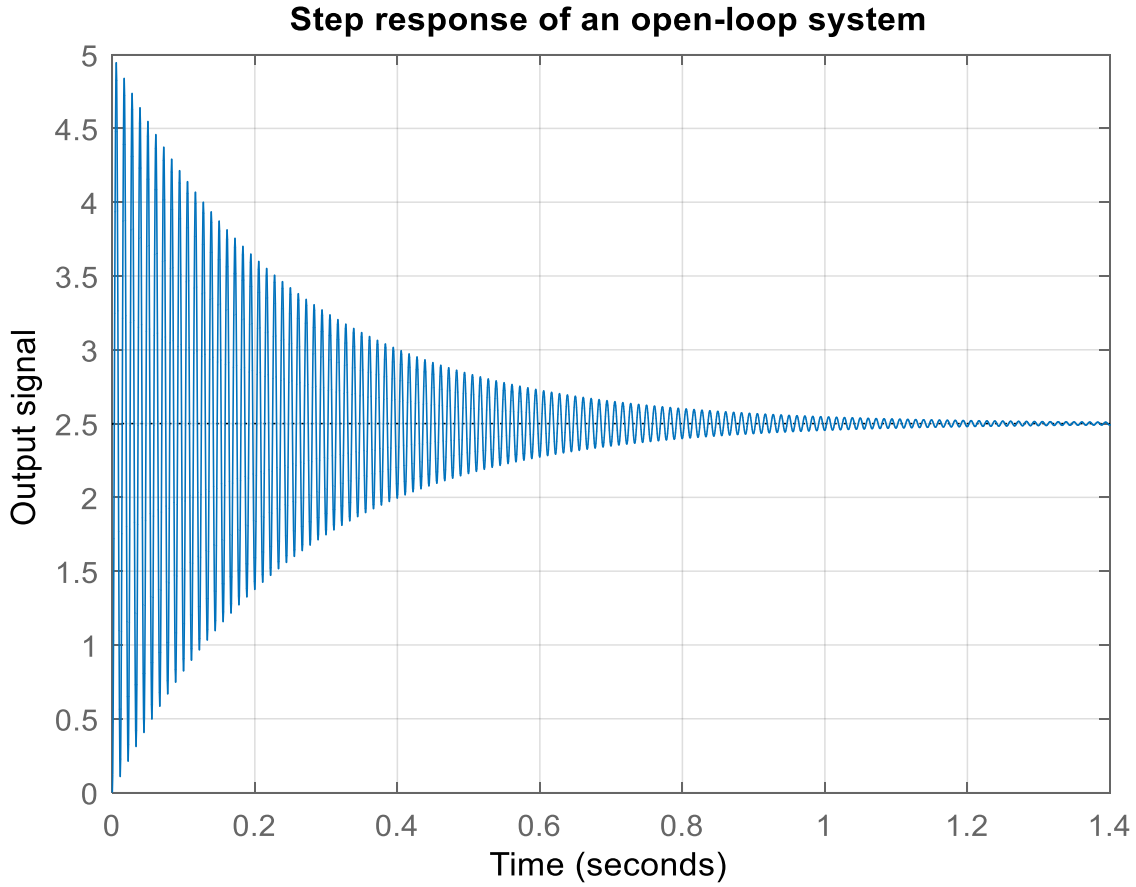

Figure 4.1: Time response of an open-loop system

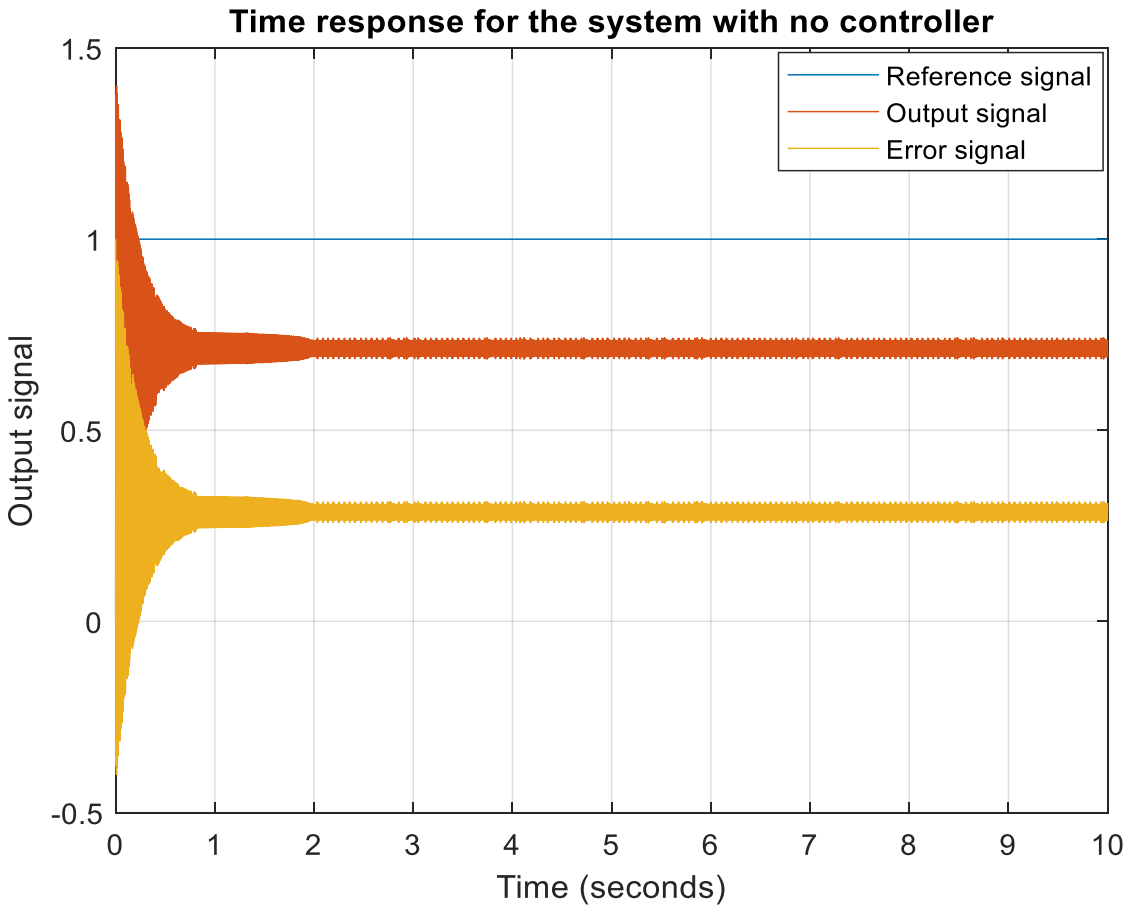

Figure 4.2: Time response of a closed-loop system without controller

Results for LQR control

The time response of the system using LQR control technique, the corresponding error and the control signals of the system were simulated as shown in Figure 4.3. Table 4.1 also summarizes the measured performance results for LQR control scheme upon simulation.

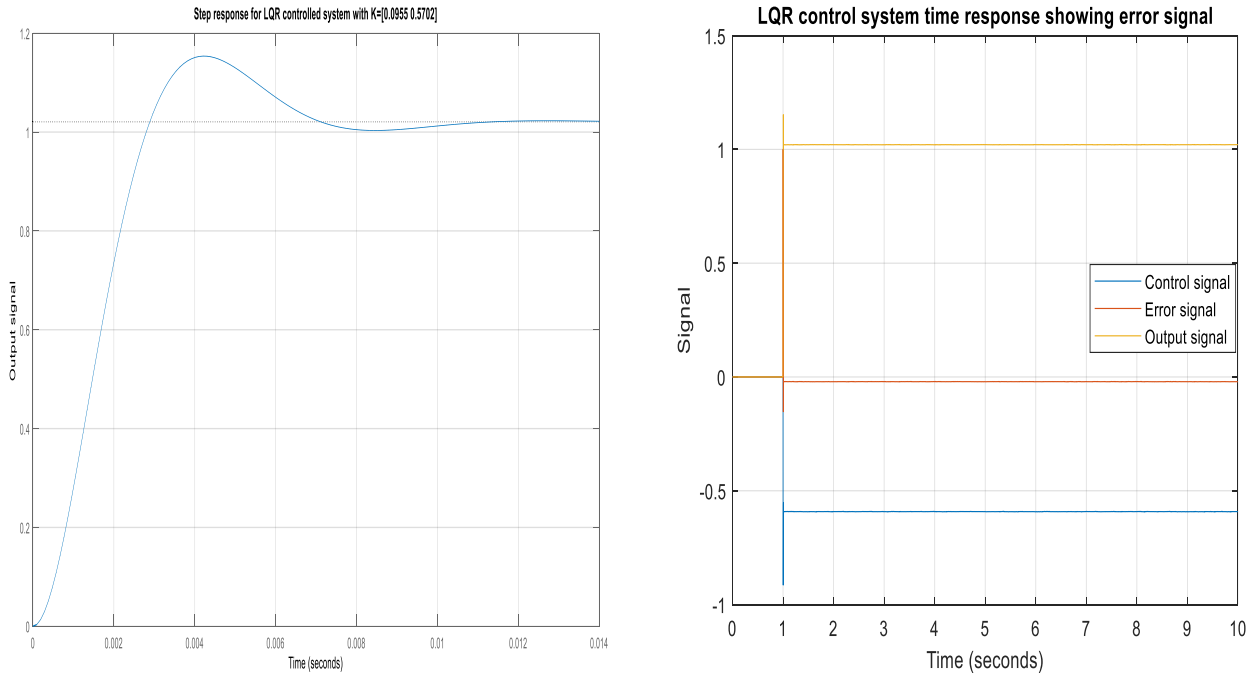

Figure 4.3: Time response using LQR control

Table 4.1: Summary of the performance characteristics for LQR scheme

Parameter	Value
Overshoot	13%
Settling time	5.98ms
Rise time	1.95ms
Steady state	1.02
Peak amplitude	1.15
Peak time	4.21ms

4.3 Results for MRAC control

Figure 4.4(a) shows simulation results for the time response for the system at different gain values using LQR-MRAC control while Figure 4.4(b) and (c) shows the error between the process and reference model at different gain values and control signal respectively. The parameters estimation for the system were also simulated as shown in Figure 4.5. Table 4.2 summarizes the performance results of the system measured at different adaptation gains upon simulation.

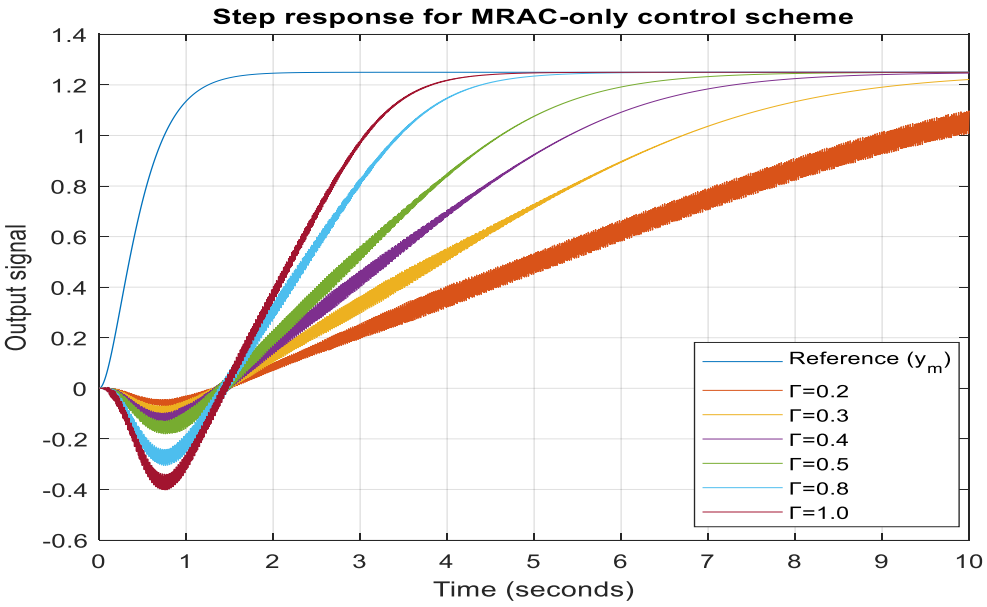

(a)

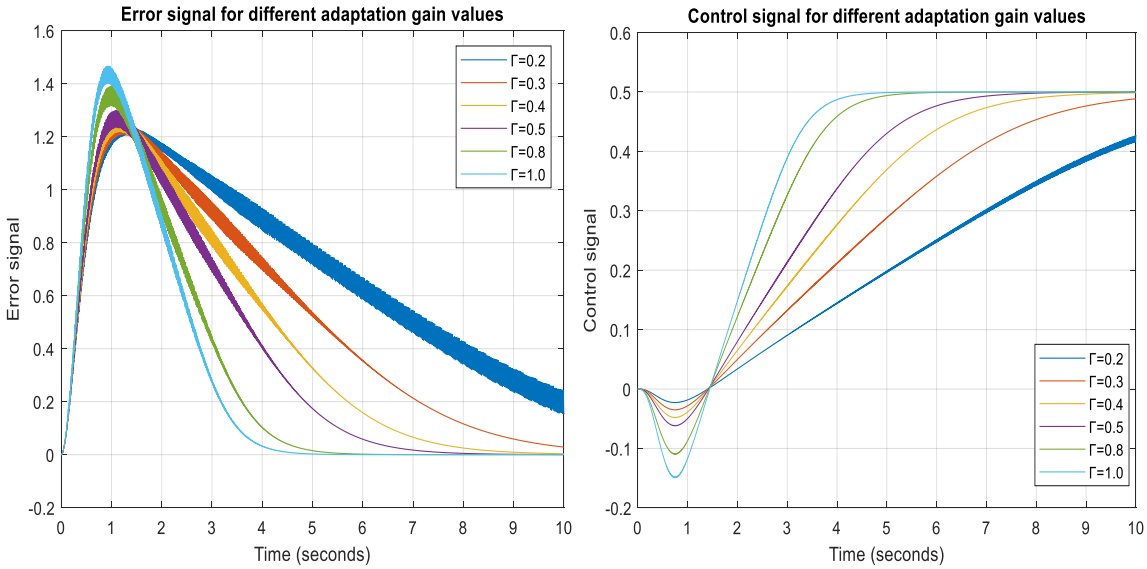

(b) **(c)**

Figure 4.4: Time response curve for different gain values using MRAC control (a) Output signal (b) Output error measurement (c) Control signal

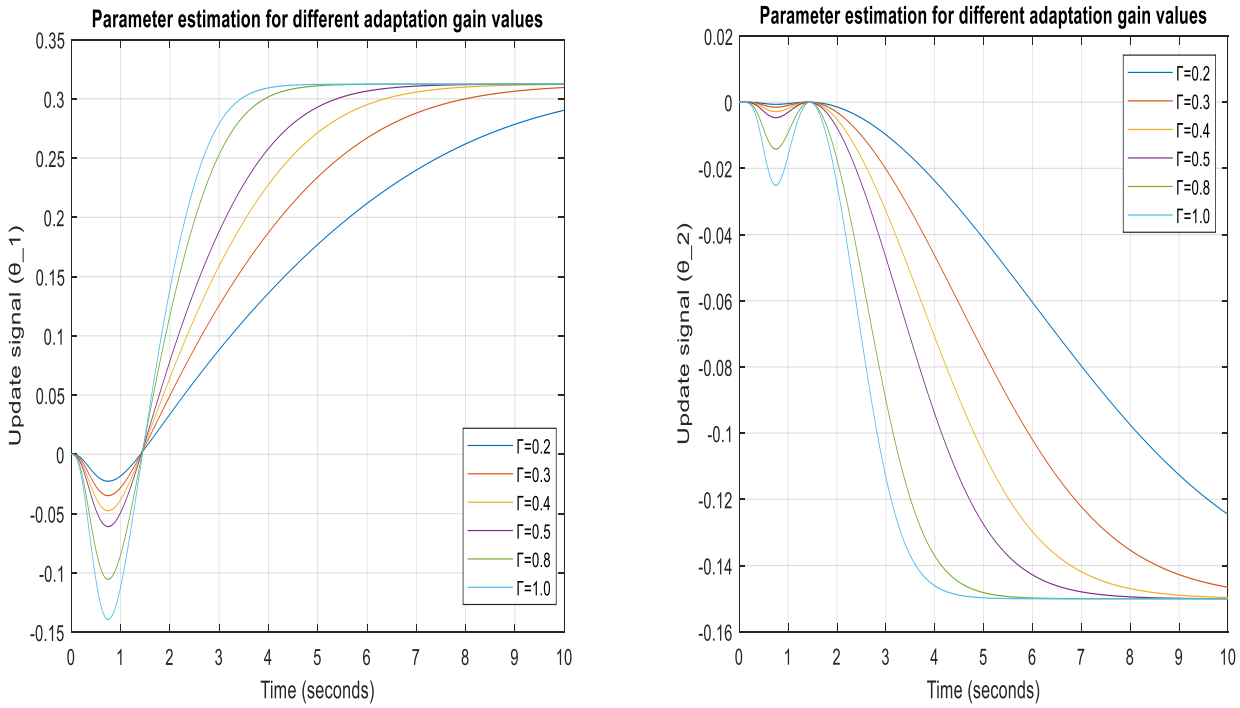

(a) **(b)**

Figure 4.5: Parameter estimation for different gain values (a) Update law $[\theta_1]$ (b) Update law $[\theta_2]$

Table 4.2 System performance as per different adaptation gains for MRAC scheme

Adaptation Gain	$\boldsymbol{\theta_1}$	$\boldsymbol{\theta_2}$	**Rise time (s)**	**Overshoot (%)**	**Steady state**
0.005	0.032	-0.0002139	3.083	-96.5	0.008861
0.05	0.117	-0.01745	2.662	-78.0	0.2806
0.1	0.2028	-0.05511	4.704	-71.6	0.6232
0.2	0.2903	-0.1245	5.964	4.9	1.093
0.3	0.3097	-0.1463	5.475	21.5	1.227
0.4	0.3121	-0.1497	4.506	24.0	1.247
0.5	0.3124	-0.15	3.666	20.4	1.25
0.6	0.3124	-0.1501	2.855	23.9	1.25
0.7	0.3124	-0.1501	2.74	25.0	1.25
0.8	0.3124	-0.15	2.133	25.0	1.25
0.9	0.3124	-0.1501	1.899	25.2	1.25
1.0	0.3124	-0.1501	2.049	24.2	1.25
1.5	0.3124	-0.1501	1.173	24.6	1.254
1.8	0.3123	-0.1501	1.476	24.0	1.243
1.9	0.3134	-0.1492	1.323	20.7	1.192

4.4 Incorporated LQR-MRAC results

The final stage of this work involved the incorporation of both the LQR and MRAC system to study its performance. Upon the simulation of the integrated LQR-MRAC scheme at different adaptation gain values using MATLAB/Simulink environment, the system response, its error signal and control signal were as shown in Figure 4.6. The parameter estimation of the system were also simulated as shown in Figures 4.7. Table 4.3 also summarizes the performance characteristics of the system measured at different adaptation gains in the course of the simulation.

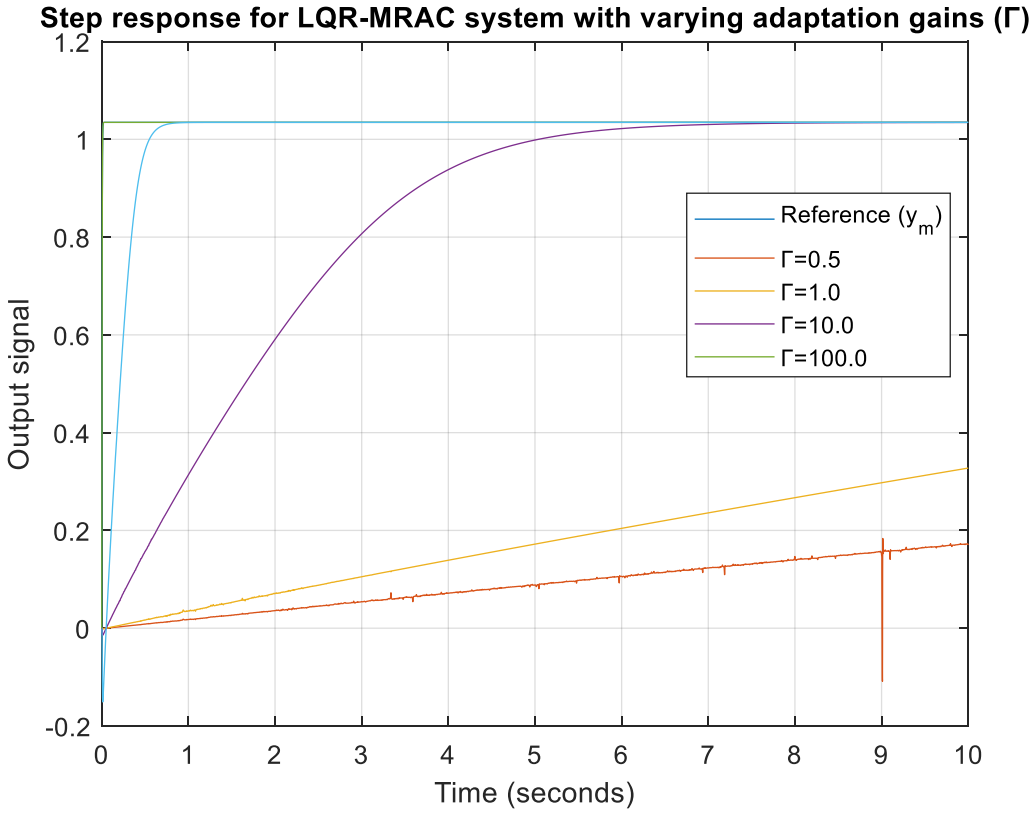

Figure 4.6a: Time response illustrating the output signal for different gain values using LQR-MRAC control

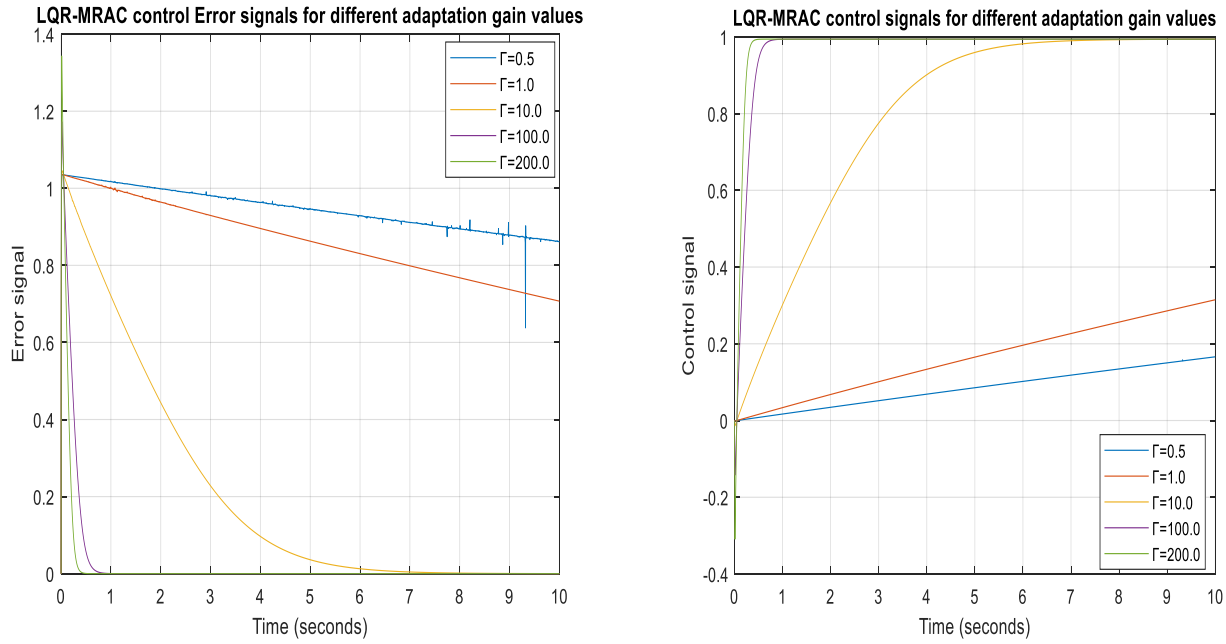

(i) **(ii)**

Figure 4.6b: Time response for different gain values using LQR-MRAC control (i) Output error (ii) Control signal

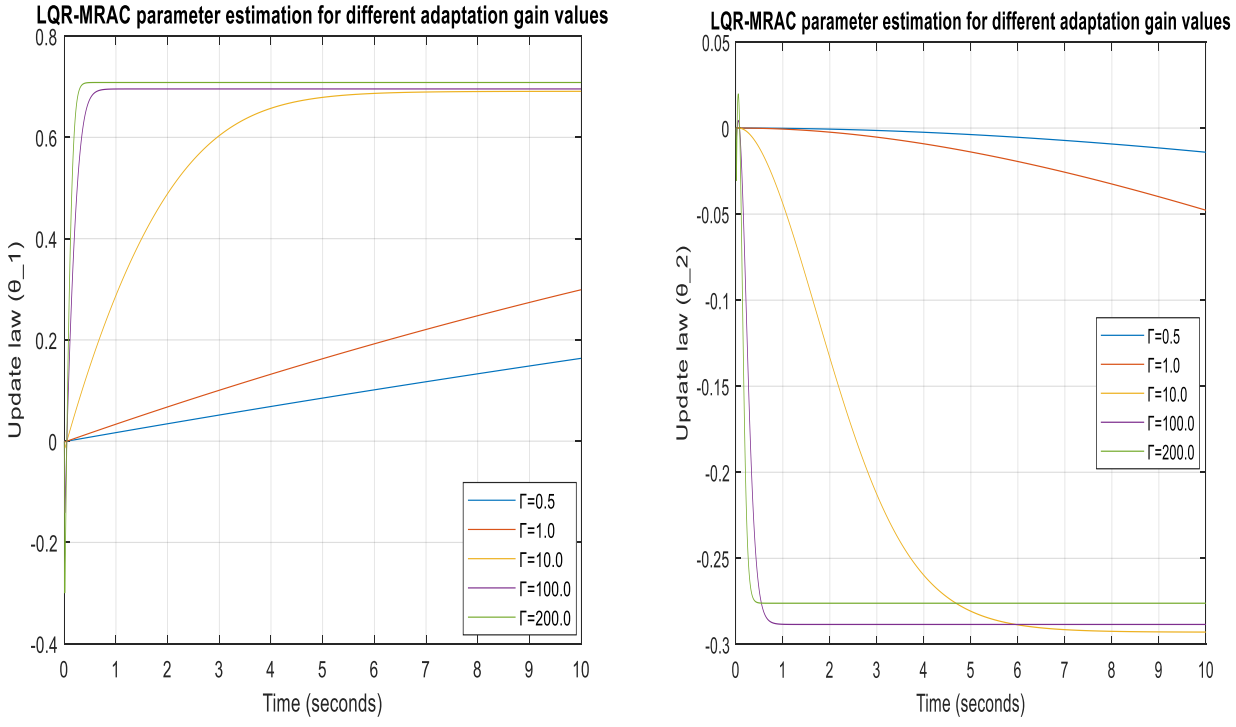

(a) **(b)**

Figure 4.7: Parameter estimation for different gain values (a) Update law $[\theta_1]$ (b) Update law $[\theta_2]$

Table 4.3: System performance as per different adaptation gains for LQR-MRAC

Adaptation Gain	θ_1	θ_2	Rise time (secs.)	Steady state
0.005	0.001788	-0.000001674	2.220	0.001696
0.05	0.01773	-0.0001638	2.743	0.01838
0.1	0.03515	-0.0006431	2.289	0.03646
0.5	0.1636	-0.01404	5.377	0.1726
1	0.2991	-0.04773	0.0019	0.3276
2	0.495	-0.1373	6.143	0.6011
3	0.6061	-0.2152	7.719	0.813
4	0.6583	-0.2609	7.260	0.9407
5	0.6792	-0.2811	6.534	0.9995
10	0.691	-0.2928	3.537	1.035
25	0.6914	-0.2925	1.409	1.035
50	0.6924	-0.2915	0.707	1.035
100	0.6957	-0.2884	0.354	1.035
200	0.7084	-0.2761	0.178	1.035
400	0.7728	-0.2138	0.098	1.035
500	0.8417	-0.1472	0.1004	1.035
800	1.351	-0.3446	0.000881	1.035
900	0.9401	-0.05219	0.000156	1.035
950	199.8	194.9	0.000038	0.7267

4.5 Results validation for different control schemes

The simulation results for the control schemes studied were compared to observe the performance of one scheme over the other. This comparison was carried out by varying the gain values of each of the control system using MATLAB/Simulink model/codes for the system. As shown in Figure 4.8(a)-(g), the LQR technique only operated when original optimal gain designed for the system does not change. In the case of MRAC technique, the system only operated at low adaptation gain of less than 2.0. On the other hand, the integrated MRAC-LQR control method yielded a better response in terms stability and convergence speed, even when the adaptation gain is increased to a higher value compared to using MRAC scheme only. Such advantages may be attributed to the LQR, which helped to maintain the optimal gain of the system while MRAC scheme compensates for the varying adaptation gains, which may occur as a result of the uncertainties in the environmental conditions. It is also worthy to note that without

a controller then optimal control would not be ensured as the error between the set point and the output would be so high, and oscillations may also occur. The performance of the different control schemes studied is also summarized in Table 4.4. The performance of the MRAC-LQR, MRAC-only, LQR-only and No-controller systems were compared as shown in Figures 4.8 by simulating the Simulink models in Figures 3.8, 3.9, 3.10, 3.11 and 3.12. Note that y_p is the process dynamics, y_m is the model reference and Γ is the adaptation gain.

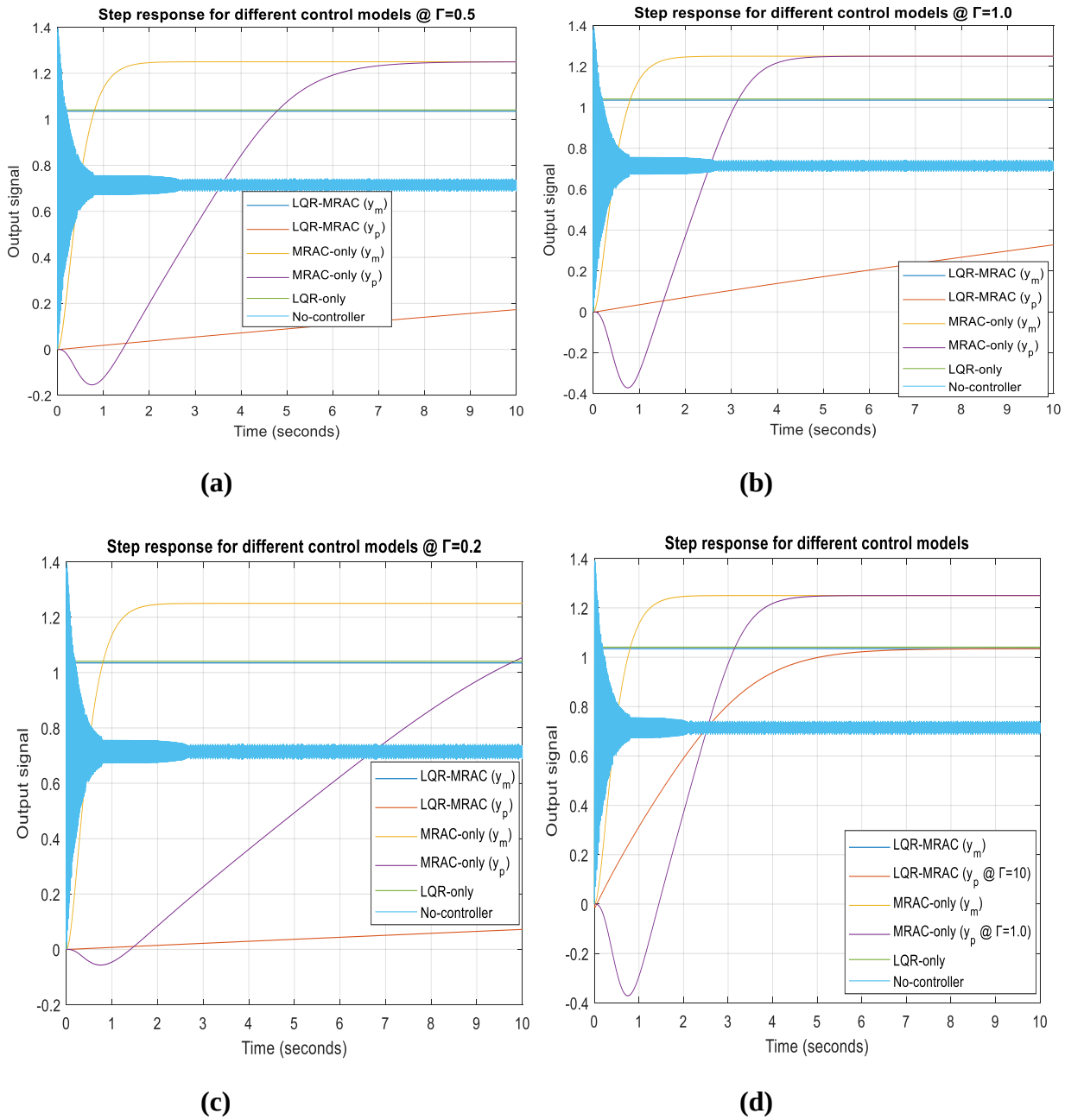

Figure 4.8(i): Time response illustrating the performance for different control schemes (a)-(d)

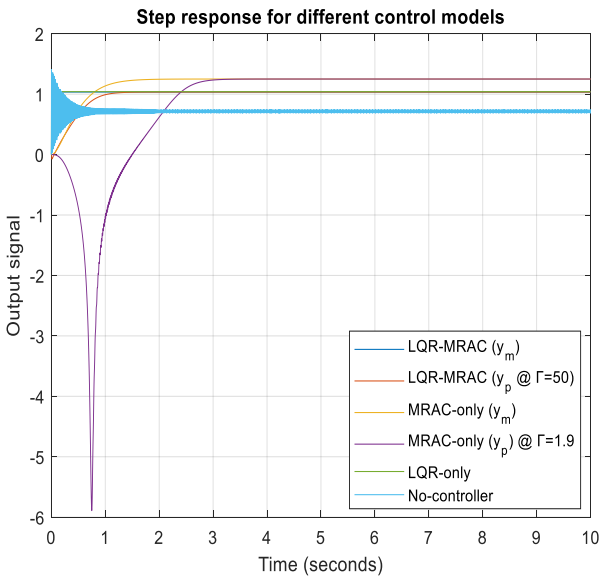

(e)

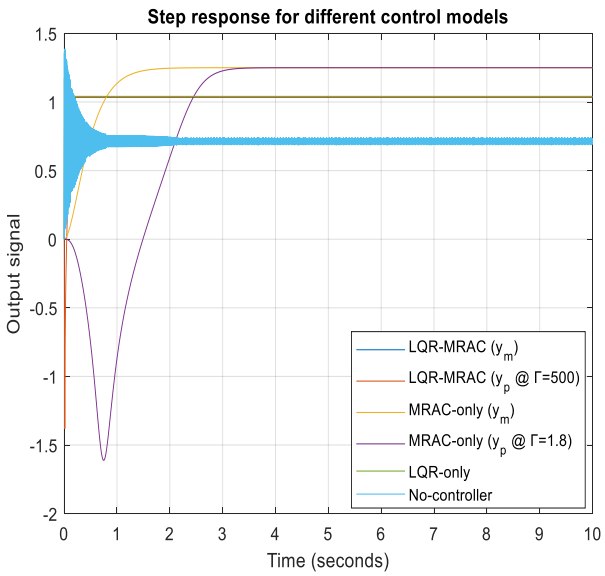

(f)

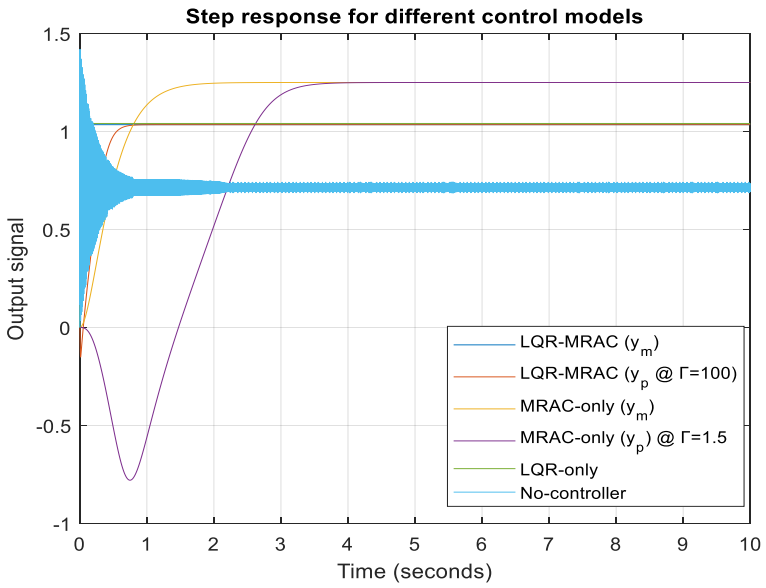

(g)

Figure 4.8(ii): Time response illustrating the performance for different control schemes (e)-(g)

Table 4.4: Different control schemes and performance characteristics

Control type	Overshoot (%)	Rise time (ms)	Tracking efficiency (%)	Adaptation gain	Duty cycle
No controller	-56.103	0.848	24.50		0.904
LQR-only	13.000	1.950	95.92	Fixed gain (No adaptation)	0.626
MRAC-only	15.698	1323	73.41	$0.1 < \Gamma < 2$	0.714
MRAC-LQR	28.182	0.156	94.45	$0.2 < \Gamma < 900$	0.632

4.2 Discussion

The purpose of this analysis was to investigate the control performance of the solar photovoltaic system using the control techniques such as LQR, MRAC, incorporated LQR-MRAC, etc. To carry out the work, MITSUBISHI electric photovoltaic module specification sheet was used to obtain the required data for the analysis hence, the application of the model $PV - MLU255HC$. To verify the power rating as in the data sheet, the Simulink model of the system was first implemented as shown in Figure 3.3. The I-V and the P-V curves resulting from the model affirmed the power rating in the range $255 \pm 3\%$ as indicated in the data sheet *(Appendix I)*.

With the application of a boost converter circuit with a switching frequency of $20kHz$, the system transfer function was designed using the specification in Table 3.1. The system was then controlled by first applying the LQR method through which the control penalty matrix $R = 1$ was kept constant while varying the state penalty matrix element Q_{22}. The $Q_{22} = 0.8$, which yielded the minimal error between the reference and the output signals, was selected hence, the optimal gain $K = [0.0955 \quad 0.5702]$ was obtained. From the simulation results, the LQR method took about 1.95ms to converge to the maximum power point (MPP) and yielded a tracking efficiency of 95.92% as shown in Table 4.4 which is in agreement with the range of efficiency postulated by Anbarasi & Kanthalakshmi, (2016) and Karanjkar, et al. (2014).in their work.

Upon the completion of the LQR stage, the following stage was the control design using MRAC method. In this stage, it was expected that the plant's output signal adapts to the changing condition hence the design of the reference model. For the system to track the reference model

signal the control law $u = r\theta_1 - y_p\theta_2$ was obtained. The simulation results as depicted in Figure 4.4 shows that the adaptation gain must be kept small to avoid oscillations of the system just as pointed out in a research work by Jain & Nigam (2013). It was also observed that with this control method, the system was able to track the MPP at average rise time of 1.323s as suggested by Khanna, *et al*. (2014). This control scheme rather gives a tracking efficiency of 73.41%, which is lower compared to the LQR scheme.

The integration of both LQR and MRAC control schemes gives the final control stage of this research work. It should be noted that in the MRAC stage, a critically damped second order system was used to design the reference model while the system was underdamped with a damping ratio $\boldsymbol{\xi = 0.56}$. As shown in the simulation results of Figure 4.6, this control scheme accepts a higher value of adaptation gain compared to the system with MRAC-only scheme and the oscillations which occur as a result of higher adaptation gain in MRAC-only scheme was eliminated. However, MRAC-LQR control scheme caused the system to converge at maximum power point at an average rise time of 0.156ms, which is faster compared to the corresponding MRAC-only and LQR-only schemes. Moreover, the tracking efficiency of the MRAC-LQR control scheme was found to be 94.45% with adaptation gain varying between $0.2 < \Gamma < 900$.

From the comparison results shown in Figure 4.8(a)-(g), the system would perform poorly without a controller. However, the performance of the system is dependent on the type of control scheme employed. It is obvious that LQR would give an optimal control just as expected but it lacks the adjustable mechanism to compensate for the changing conditions that may occur in the system hence the need for adaptive control technique. As depicted in the figures, MRAC scheme has adaptive control features that makes the system adjust itself when there are environmental uncertainties. At small adaptation gain value, this control system would work perfectly well but with high value of gain values the system would cease to operate as required. However, the use of LQR in combination with the MRAC technique seemed great as the system was able to accept a higher value of adaptation gain. In this case, it should be observed that since LQR is a fixed gain control technique which allows the system to operate based on the original optimal gain designed for the system hence, the system output converges at the steady state value of the

reference signal just like the LQR scheme and with the aid of the MRAC scheme, the system has the functional mechanism which gives it the necessary adjustment when need arises.

CHAPTER FIVE

CONCLUSION AND RECOMMENDATION

5.1 Conclusion

Photovoltaics (PV) is one of the renewable energy applications developed to track solar energy and convert it into electrical energy. The output power produced by the PV system is dependent on the irradiation and temperature conditions hence, due to such conditions Maximum Power Point (MPP) of the P-V characteristic curve changes regularly, which causes unstable output power so that the accuracy of the power delivered at the output is not maximum. For this reason, different control strategies have been adopted by researchers to ensure that optimal output power is ensured.

The idea behind this analysis was therefore to investigate the behavior of solar photovoltaic energy system with respect to such control schemes as LQR, MRAC and integrated MRAC-LQR. With the aid of a model ($PV - MLU255HC$) data extracted from MITSUBISHI electric photovoltaic module specification sheet (as shown in Appendix I), the system to be controlled was designed using a boost converter with an assumed switching frequency of $20kHz$.

The designed system was first controlled by designing a fixed gain optimal control scheme called Linear Quadratic Regulator (LQR) hence the optimal gain $K = [0.0955 \quad 0.5702]$ was obtained by selecting an appropriate state and control matrices, and solving the Algebraic Riccatti equation $PA + A^TP - PBR^{-1}B^TP + Q = 0$ using the MATLAB code lqr(A,B,Q,R). It was discovered that this method showed an appreciable control with a tracking efficiency of 95.92% and a duty cycle of approximately 0.6, though it lacks the ability to adjust itself to compensate for any uncertainties that may occur in the system. For this reason, it became necessary to proffer a solution by designing an adjustable mechanism hence, the need for model reference adaptive control (MRAC).

Model Reference Adaptive Control (MRAC) was employed to obtain the adaptive features hence enabling the system to follow the reference model incorporated into the system in case of

environmental uncertainties like varying temperatures and irradiations. The adaptation mechanism would ensure that on changing conditions of the system parameters, the output power still maintain the optimal power by minimizing the error between the plant and reference model. However, this control strategy only accepts small adaptation gain in the range $0.1 < \Gamma < 2$ which is better compared to the LQR, which only operate on a fixed optimal gain of which it was originally designed hence LQR system would not function optimally if there is a deviation from the original design but MRAC would still function if the value of the adaptation gain obtained as a result of the changes is not high. MRAC system showed a duty cycle of about 0.7 and less efficiency (73.41%) than LQR system. Such features as non-acceptance of high gain values and less efficient control brought the need for incorporation of the two systems.

The main target of this work was to investigate the solar PV system with LQR-MRAC incorporated system. From the analysis, it was observed that incorporating these two control schemes would be a very good idea in the control of solar PV system, as it accepts a higher adaptation gain of range $0.2 < \Gamma < 900$, which is not possible in MRAC system as well as LQR system. The system also showed an approximate duty cycle of 0.6 as well as an efficiency of 94.45% which is almost the same as that of LQR system. Owing to the unique features such as appreciable control efficiency and rise time as well as operating at higher adaptation gain unlike the LQR-only and MRAC-only counterparts, then the proposed method (incorporated LQR-MRAC) may be adopted as best over the former. Practically speaking, integration of the incorporated LQR-MRAC control technique in solar PV energy system would yield an improved working performance of the system.

5.2 Recommendation

The incorporated LQR- MRAC technique is recommended over other schemes such as LQR-only and MRAC-only for the control of solar PV energy system considering its appreciable tracking efficiency and its ability to operate even at high adaptation gains. The control engineers and designers as well as power system engineers are hereby encouraged to adopt the technique of combining both the LQR and MRAC for controlling such a system. It should be noted that the analysis in this work was carried out using Standard Test Condition (STC) of $1000W/m^2$ solar irradiance and a temperature of $25°C$ hence, such analysis for varying temperature and

irradiance is also necessary. Finally, practical implementation would also help to reveal the cost as well as the complexity of the incorporated LQR-MRAC system.

5.3 Contribution to knowledge

This thesis has been to incorporate the two systems of control schemes for the purpose of improved control of solar PV system. It also established that the use of LQR-MRAC techniques to control solar PV energy system is better in terms of stability at higher adaptation gain values compared to MRAC-only scheme.

REFERENCES

Abdelsalam, A. K., Massoud, A. M., Ahmed, S. and Enjeti, P. N. (2011). "High-Performance Adaptive Perturb and Observe MPPT Technique for Photovoltaic-Based Microgrids." IEEE Transactions on Power Electronics. Vol. 26, No. 4, pp. 1010 – 1021.

Ahmed, M. E., Mousa, M. and Orabi, M. (2010). "Development of high gain and efficiency photovoltaic system using multilevel boost converter topology." International Proceedings of the 2nd International Symposium on Power Electronics for Distributed Generation Systems, Hefei, China, 16–18 June 2010; pp. 898–903.

Akihiro, O. (2005) "Design and simulation of photovoltaic water pumping system." A thesis presented to the Faculty of California Polytechnic State University, San Luis Obispo. pp. 5 – 36.

Anbarasi, M. and Kanthalakshmi, S. (2016). "Linear quadratic optimal control of solar photovoltaic system: An experimental validation." *Journal of Renewable and Sustainable Energy*. Vol. 8. http://dx.doi.org/10.1063/1.4966229.

Anderson, B. D. and Moore, J. B. (1989). "Optimal Control Linear Quadratic Methods." New Jersey: Prentice Hall.

Astrom, K. J. (1983). "Theory and applications of adaptive control survey." Automatica. Vol. 19, No. 5, pp. 471– 486.

Azadeh Safari and Saad Mekhilef, (2011). "Simulation and Hardware Implementation of Incremental Conductance MPPT with Direct Control Method Using Cuk Converter." IEEE Transactions on Industrial Electronics. Vol. 58, No. 4, pp. 1154 – 1161.

Bhatnagar, P. and Nema, R. K. (2013). "Maximum power point tracking control techniques: State-of-the-art in photovoltaic applications." ELSEVIER Renewable and Sustainable Energy Reviews. Vol. 23, pp. 224-241.

Brundtland, G. (1987). "Notre avenir à tous." Rapport Brundtland, Oxford University press.

Brunton, S. L., Rowley, C. W., Kulkarni, S. R. and Clarkson, C. (2010). "Maximum power point tracking for photovoltaic optimization using ripple-based extremum seeking control." IEEE Trans. Power Electronics. Vol. 25, No.10, pp. 2531–2540.

Casadei, D., Grandi, G. and Rossi, C. (2006). “Single-phase single-stage photovoltaic generation system based on a ripple correlation control maximum power point tracking.” IEEE Transactions on Energy Conversion. Vol. 21, No. 2, pp. 562–568.

Castaner, L. (2002). Modelling Photovoltaic Systems Using PSpice. CRC Press.

Decker, D. K. and Loftis (Jr), C. B., (1997). “Method of checking solar panel characteristics in an operating solar electrical system.” ed: Google Patents.

Dolara, A., Faranda, R. and Leva, S. (2009). “Energy comparison of seven MPPT techniques for PV systems.” *Journal of Electromagnetic Analysis and Applications*. Vol. 1, No. 3, pp.152–162.

Elgendy, M. A., Zahawi, B. and Atkinson, D. J. (2012). “Assessment of perturb and observe MPPT algorithm implementation techniques for PV pumping applications.” IEEE Transactions on Sustainable Energy. Vol.3, No.1, pp. 21–33.

El-Ghonemy, A. M. K. (2012). Photovoltaic Solar Energy: Review, *International Journal of Scientific & Engineering Research.* Vol. 3, Issue 11, ISSN 2229-5518.

Elobaid, L. M., Abdelsalam, A. K. and Zakzouk, E. E. (2012). “Artificial neural network based maximum power point tracking technique for PV systems.” International Proceedings of the 38th Annual Conference on IEEE Industrial Electronics Society (IECON ’12), Montreal, Canada, pp.937–942.

Eltawil, Mohamed A. and Zhao, Zhengming (2013). “MPPT techniques for photovoltaic applications.” ELSEVIER Renewable and Sustainable Energy Reviews. Vol. 25, pp. 793-813.

Esram, T. and Chapman, P. L. (2007). “Comparison of photovoltaic array maximum power point tracking techniques,” IEEE Transactions on Energy Conversion. Vol. 22, No. 2, pp. 439–449.

Femia, N., Petrone, G., Spagnuolo, G. and Vitelli, M. (2005). “Optimization of perturb and observe maximum power point tracking method.” IEEE Transactions on Power Electronics. Vol. 20, No. 4, pp. 963–973.

Ghaffar, A. A. and Richardson, T. (2015). “Model Reference Adaptive Control and LQR Control for Quadrotor with Parametric Uncertainties.” *International Journal of Mechanical and Mechatronics Engineering.* World Academy of Science, Engineering and Technology. Vol. 9, No. 2.

Goldemberg, J. (2000). Rural Energy in Developing Countries World Energy Assessment: Energy and the Challenges of Sustainability. World Bank, New York.

Gwinyai, B. S. Dzimano (2008). "Modeling of Photovoltaic Systems." A Thesis Presented in Partial Fulfillment of the Requirements for the Degree Master of Science in the Graduate School of the Ohio State University.

Hang, C. C., and Parks, P. (1973). "Comparative studies of model reference adaptive control systems." Automatic Control, IEEE Transactions on Sustainable Energy. Vol. 18, No. 5, pp. 419–428.

Hohm, D. and Ropp, M. (2000). "Comparative study of maximum power point tracking algorithms using an experimental, programmable, maximum power point tracking test bed." Photovoltaic Specialists Conference. Conference Record of the Twenty-Eighth IEEE, pp. 1699–1702.

Hohm, D. P. and Ropp, M. E. (2003). "Comparative Study of Maximum Power Point Tracking Algorithms." Progress in Photovoltaics: Research and Applications. Vol. 11, pp. 47-62.

Houssamo, I., Locment, F. and Sechilariu, M., (2010). "Maximum power tracking for photovoltaic power system: development and experimental comparison of two algorithms." Renewable Energy Vol. 35, pp. 2381–2387.

Hussein, K., Muta, I., Hoshino, T. and Osakada, M. (1995). "Maximum photovoltaic power tracking: an algorithm for rapidly changing atmospheric conditions," Generation, Transmission and Distribution, IEE Proceedings. Vol. 142, pp. 59–64.

International Energy Agency (2001). "Trends in photovoltaic applications." Survey report of selected IEA countries between 1992 and 2000.

Jain, P. and Nigam, M. J. (2013). "Design of a Model Reference Adaptive Controller Using Modified MIT Rule for a Second Order System." Advance in Electronic and Electric Engineering. ISSN 2231-1297, Vol. 3, No. 4, pp. 477-484 © Research India Publications http://www.ripublication.com/aeee.htm.

Jainand, S. and Agarwal, V. (2004). "A new algorithm for rapid tracking of approximate maximum power point in photovoltaic systems," IEEE Power Electron. Vol. 2, no. 1, pp. 16–19.

Kachhiya, K., Lokhande, M. and Patel, M., (2011). "MATLAB/Simulink Model of Solar PV Module and MPPT Algorithm‖." National Conference on Recent Trends in Engineering & Technology. B. V. M. Engineering College, V. V. Nagar, Gujarat India, pp. 1-5, 13-14.

Karanjkar, D. S., Chatterji, S. and Kumar, A. (2014). "Design and Implementation of a Linear Quadratic Regulator Based Maximum Power Point Tracker for Solar Photo-Voltaic System." *International Journal of Hybrid Information Technology*. Vol.7, No.1, pp. 167-182. http://dx.doi.org/10.14257/ijhit.2014.7.1.14. ISSN: 1738-9968 IJHIT Copyright ⓒ 2014 SERSC.

Khanna, R., Zhang, Q., Stanchina, W. E., Reed, G. F. and Mao, Z. (2014). "Maximum Power Point Tracking Using Model Reference Adaptive Control." IEEE Transactions on Power Electronics. Vol. 29, No. 3, pp. 1490 – 1499.

Kirk, D. (1998). "Optimal Control Theory an Introduction." Mineola NY: Dover Publications.

Kollimallam, S. K. and Mishra, M. K., (2014). "A Novel Adaptive P&O MPPT Algorithm Considering Sudden Changes in the Irradiance." IEEE Transactions on Energy Conversion. pp. 1 – 9. http://www.ieee.org/publications/standards/publications/rights/index.html.

Kolsi, S., Samet, H., Amar, M. B. (2014). "Design Analysis of DC-DC Converters Connected to a Photovoltaic Generator and Controlled by MPPT for Optimal Energy Transfer throughout a Clear Day." *Journal of Power Energy Engineering.* Vol. 2, No. 27.

Kreith, F. and Goswami, D. Y. (2007). "Handbook of Energy Efficiency and Renewable Energy." CRC Press.

Kumar, H. and Tripathi, R. K. (2012). "Simulation of variable incremental conductance method with direct control method using boost converter." International Proceedings of the Students Conference on Engineering and Systems (SCES '12), pp. 1–5, Allahabad, India.

Landau, I. (1974). "A survey of model reference adaptive techniques theory and applications." Automatica. Vol. 10, No. 4, pp. 353–379.

Malek, H. and Chen, Y. (2014). "BICO MPPT: a faster maximum power point tracker and its application for photovoltaic panels," *International Journal of Photoenergy*, Vol. 2014, Article ID 586503, 9 pages.

Manel, H. and Hfaiedh, M. (2016). "Comparison of Different MPPT Algorithms with a Proposed One Using a Power Estimator for Grid Connected PV Systems." *International Journal of*

Photoenergy. Hindawi Publishing Corporation. Volume 2016, Article ID 1728398, 10 pages http://dx.doi.org/10.1155/2016/1728398.

Markvart, T. and Castaner, L. (2003). "Practical Handbook of Photovoltaics, Fundamentals and Applications." Elsevier.

Masoum, M. A. S., Dehbonei, H. and Fuchs, E. F. (2002). "Theoretical and experimental analyses of photovoltaic systems with voltage and current-based maximum power-point tracking." IEEE Trans. Energy Conversion. Vol. 17, No. 4, pp. 514–522.

Mastromauro, R. A., Liserre, M., Kerekes, T. and Dell'Aquila, A. (2009). "A single phase voltage-controlled grid-connected photovoltaic system with power quality conditioner functionality." IEEE Trans. Ind. Electron. Vol. 56, No. 11, pp. 4436–4444.

Mba, E. F., Chukwuneke, J. L., Achebe, C. H., Okolie, P. C., (2012). "Modeling and Simulation of a Photovoltaic Powered Vapour Compression Refrigeration System." *Journal of Information Engineering and Applications.* ISSN 2224-5782 (print) ISSN 22250506 (online). Vol 2, No.10.

Mboumboue, E. and Njomo, D. (2013). "Mathematical Modeling and Digital Simulation of PV Solar Panel using MATLAB Software." *International Journal of Emerging Technology and Advanced Engineering*. Vol. 3, Issue 9, pp. 24 – 32. Website: www.ijetae.com (ISSN 2250-2459, ISO 9001:2008 Certified Journal)

Messenger, R. and Ventre, G. (2003). "Photovoltaic Systems Engineering." Second Edition. Wiley.

Messenger, R. and Ventre, J. (2005). "Photovoltaic Systems Engineering." Second Edition, CRC PRESS.

Miller, D. E. (2003). "A new approach to model reference adaptive control." IEEE Transaction on Automatic Control. Vol. 48, No. 5, pp. 743–757.

Mirbagheri, S. Z., Mekhilef, S. and Mirhassani, S. M. (2013). "MPPT with Incremental Conductance method using conventional interleaved boost converter." Energy Procedia. Vol.42, pp.24–32.

Mitsubishi Photovoltaic Module specification sheet (MLU): 250-255W [online], https://www.studylib.net/doc/18057350/mlu-specification-sheet-250-255w.

Morales, David Sanz (2010). “Maximum Power Point Tracking Algorithms for Photovoltaic Applications.” Thesis submitted for examination for the degree of Master of Science in Technology, Aalto University.

Napole, C., Derbeli, M. and Barambones, O. (2021). Fuzzy Logic Approach for Maximum Power Point Tracking Implemented in a Real Time Photovoltaic System. *Journal of Applied Sciences.* Vol. 11, No. 5927 pp. 1 – 18. https://doi.org/10.3390/app11135927; https://www.mdpi.com/journal/applsci.

Ngan, M. S. and Tan, C. W. (2011). “A Study of maximum power point tracking algorithms for stand-alone photovoltaic systems.” IEEE Applied Power Electronics Colloquium (IAPEC), pp. 22 – 27.

Nisso, N., Raïdandi, D., Djongyang, N. and Menga, F. D. (2018). “Modeling and analysis of boost converter in small-signals applied to the wind energy conversion system using MATLAB/Simulink.” Revue des Energies Renouvelables. Vol. 21 No.4, pp. 635 – 649.

Nkue et Njomo (2009). “Analyse du système énergétique camerounais dans une perspective de développement soutenable,” Revue de l‘énergie. Vol. 588, pp. 102-116, Mars-Avril.

Pankaj S., Shailendra J. and Nema, R. K. (2011). Effect of Adaptation Gain in Model Reference Adaptive Controlled Second Order System. ETASR - Engineering, Technology & Applied Science Research. Vol. 1, No.3, pp. 70-75.

Philipson, L. (2000). “Distributed and dispersed generation: addressing the spectrum of consumer needs.” Power Engineering Society Summer Meeting. IEEE, Vol. 3, pp. 1663–1665.

Prastyawan, A., Efendi, M. and Murdianto, F. (2021). “MPPT Full Bridge Converter Using Fuzzy Type-2 on DC Nano Grid System.” *Journal on Advanced Research in Electrical Engineering.* Vol. 5, No. 2, pp. 120 – 127.

Reisi, A. R., Moradi, M. H. and Jamasb, S. (2013). “Classification and comparison of maximum power point tracking techniques for photovoltaic system: a review.” Renewable and Sustainable Energy Reviews. Vol. 19, pp. 433–443.

Salas, V., Olıas, E., Barrado, A., Lazaro, A. (2006). “Review of the maximum power point tracking algorithms for stand-alone photovoltaic systems.” ELSEVIER Solar Energy Materials & Solar Cells, Vol. 90, pp. 1555– 1578.

Sastry, S. and Bodson, M. (2011). "Adaptive Control: Stability, Convergence and Robustness." New York: Dover Publications.

Sengar S. (2014). "Maximum Power Point Tracking Algorithms for Photovoltaic System: A Review." International Review of Applied Engineering Research. ISSN 2248-9967. Vol. 4, No. 2, pp. 147-154 © Research India Publications http://www.ripublication.com/iraer.htm.

Tapre, R. G. and Deshbhratar, R. G. (2015). "Comparative study and simulation of different maximum power point tracking (MPPT) techniques in a solar power generation." *International Journal on Recent and Innovation Trends in Computing and Communication.* Vol.3, pp.143–148.

Tran, C. H., Nollet, F., Essounbouli, N. and Hamzaoui, A. (2017). "Modeling and Simulation of Stand Alone Photovoltaic System using Three Level Boost Converter." International Proceedings of the 2017 International Renewable and Sustainable Energy Conference (IRSEC), Tangier, Morocco, 4–7; pp. 1–6.

Tsai, H., Tu, C. and Su, Y. (2008). "Development of Generalized Photovoltaic Model Using MATLAB/SIMULINK." Proceedings of the World Congress on Engineering and Computer Science, WCECS 2008, San Francisco USA, pp. 1-6.

Veerachary, M. Senjyu, T. and Uezato, K. (2003). "Neural-network-based maximum-power-point tracking of coupled-inductor interleaved-boost converter-supplied PV system using fuzzy controller." IEEE Transactions on Industrial Electronics. Vol. 50, No. 4, pp. 749–758.

Villalva, M. G., Gazoli, J. R. and Filho, E. R. (2009). "Comprehensive approach to modelling and simulation of photovoltaic arrays." IEEE Transactions on Power Electronics 5: 1198-08.

Visweswara, K. (2014). "An investigation of incremental conductance based maximum power point tracking for photovoltaic system," Energy Procedia. Vol. 54, pp.11–20.

Vyshnavi, N. and Subramanian, K. (2015). "Model reference adaptive control for maximum power point tracking in PV systems." IJARIIE - ISSN(O) – 2395-4396. Vol-1 Issue-5, pp. 556 – 568. www.ijariie.com.

Welch, R. L. and Venayagamoorthy, G. K. (2007). "Optimal control of a photovoltaic solar energy system with adaptive critics." Proceedings of International Joint Conference on Neural Networks. Institute of Electrical and Electronics Engineers (IEEE).

Whitaker, H. P., Yamron, J. and Kezer, A. (1958). “Design of model-reference adaptive control systems for aircraft.” Massachusetts Institute of Technology, Instrumentation Laboratory.

Yucelen, T. and Calise, A. J. (2011). “Derivative-free model reference adaptive control.” *Journal of Guidance, Control, and Dynamics.* Vol. 34, No. 4, pp. 933–950.

Zhang, Q. (2012). Adaptive Control for Solar Energy Based DC Microgrid System Development.

APPENDICES

APPENDIX I

MITSUBISHI ELECTRIC PHOTOVOLTAIC MODULE
(Specification Sheet)

Manufacturer	**MITSUBISHI ELECTRIC**	
Model name	$PV-MLU255HC$	$PV-MLU250HC$
Cell type	Monocrystalline Silicon ($78mm \times 156mm$)	
Number of cells	120 $cells$	
Maximum power rating (P_{max})	255 Wp	250 Wp
Warranted minimum P_{max}	247.4 Wp	242.5 Wp
PV USA test condition rating (PTC)	230.5 Wp	225.8 Wp
Open circuit voltage (V_{oc})	37.8 V	37.6 V
Short circuit current	8.89A	8.79 A
Maximum power voltage (V_{mp})	31.2 V	31.0 V
Maximum power current (I_{mp})	8.18 A	8.08 A
Module efficiency	15.4%	15.2%
Aperture efficiency	16.7%	16.4%
Tolerance of maximum power rating	$\pm$3%	
Static load test passed	5,400Pa	
Number of bus bars per cell	4 $bus\ bars$	
Normal operating cell temperature (NOCT)	45.7℃	
Maximum system voltage	DC 600V $DC\ 600V$	
Fuse rating	15A	
Dimensions	64.0 × 40.1 × 1.81 inch (1625 × 1019 × 46mm)	
Weight	44 lbs (20 kg)	
Number of modules per pallet	20	
Number of modules per container (40ft. container)	560	
Output terminal	$(+)$ 800mm $(-)$ 1250 $with\ MC\ connector$ (PV-KTB4/6 II-UR, PV-KST4/6 II-UR)	
Certifications	IEC 61215 2nd Edition, UL 1703	
Fire rating	Class C	

The following constant values were used to obtain the PV characteristic curves shown in Figure 3.2.

DESCRIPTION	CONSTANT VALUE
Cell's short-circuit temperature coefficient, (k_i)	$0.0032A/K$
Electron charge (q)	$1.602 \times 10^{-19}C$
Boltzmann's constant, (K)	$1.3807 \times 10^{-23}J/K$
Ideality factor of the junction (n)	1.3
Bandgap energy at $T = 0K$ (E_{g0})	$1.1eV$
Absolute temperature T_n	$298K$
Series resistance, (R_s)	0.221Ω
Shunt resistance, (R_{sh})	415.405Ω
Open-circuit voltage, (V_{oc})	$37.8V$
Short-circuit current (I_{sc})	$8.89A$
Number of cells connected in series, (N_s)	120

APPENDIX II

THE DEVELOPED SIMULINK MODELS

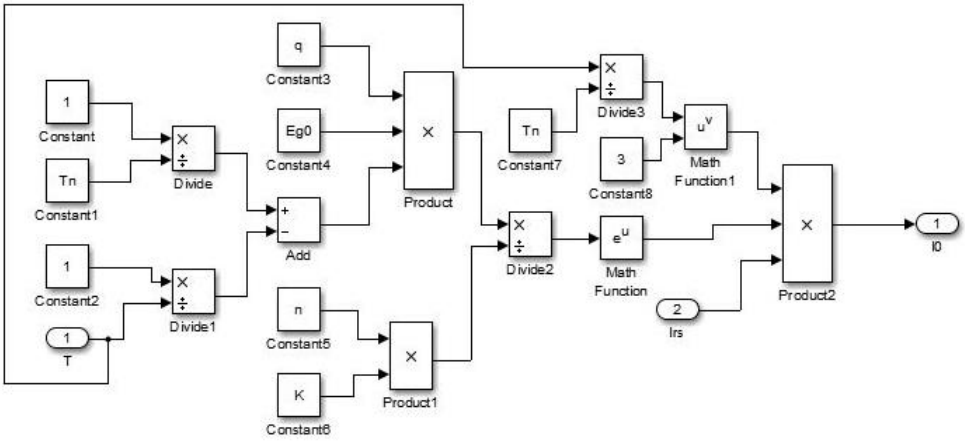

Saturation current:

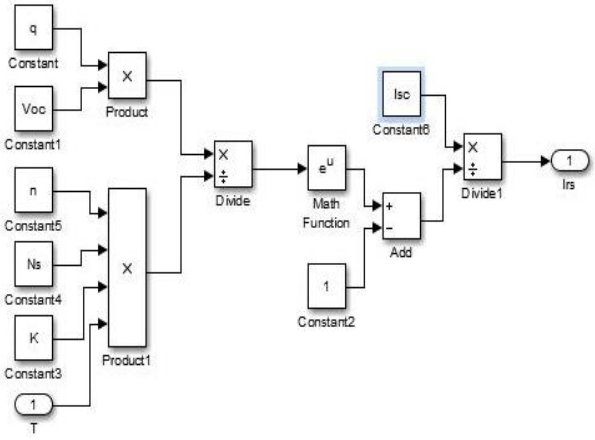

Reverse saturation current

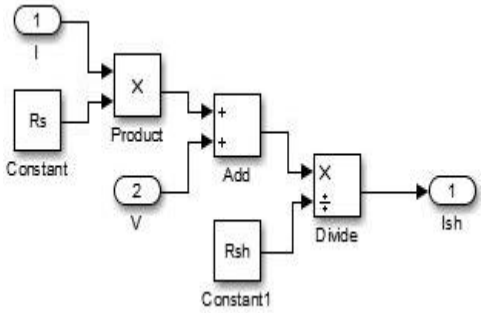

Shunt current

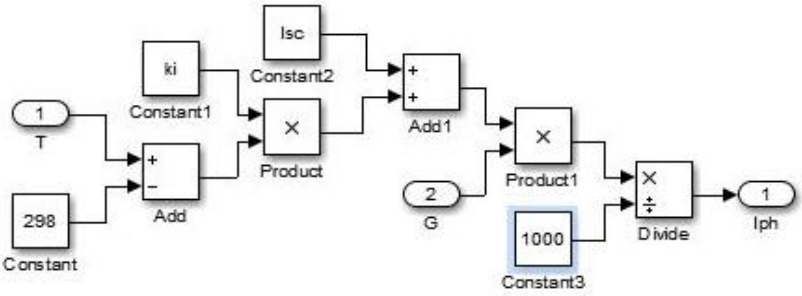

Photo-current

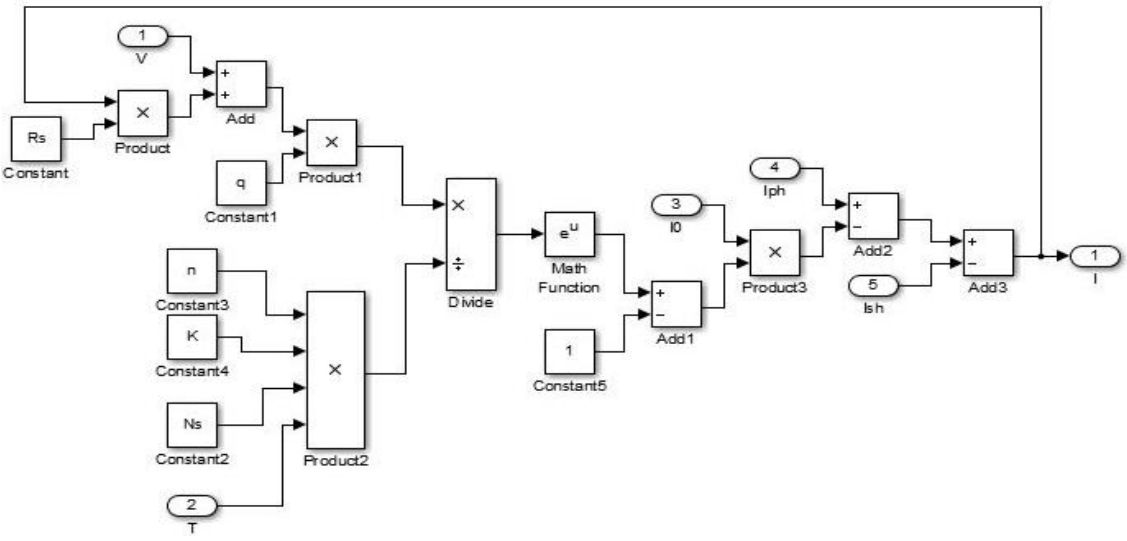

PV current: $I_{PV} = N_p I_{ph} - N_p I_o \left\{ e^{\left[\frac{q(V_{PV}+I_{PV}R_S)}{N_S k n T a}\right]} - 1 \right\} - \frac{V_{PV}+I_{PV}R_S}{R_p}$

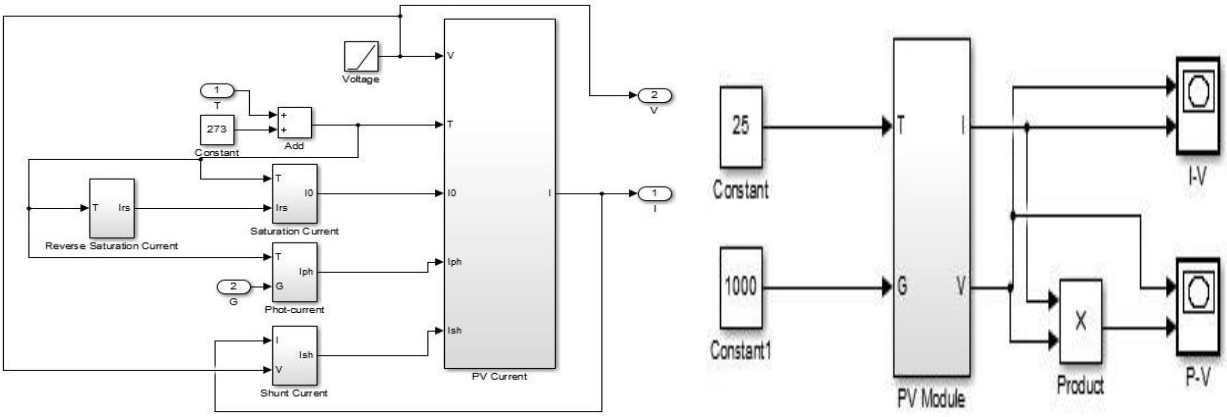

PV module subsystems interconnections

APPENDIX III

FULL DERIVATION OF TRANSFER FUNCTION OF THE PLANT

The transfer function model was obtained by

$$G(s) = C(sI - A)^{-1}B_1 + D$$

$$where; \qquad A = \begin{bmatrix} 0 & -\frac{1}{L}(1-D) \\ \frac{1}{C}(1-D) & -\frac{1}{CR_L} \end{bmatrix}; \qquad B_1 = \begin{bmatrix} \frac{1}{L} \\ 0 \end{bmatrix}, \qquad C = [0 \quad 1] \; and \quad D = 0$$

$$G(s) = [0 \quad 1]\left\{ \begin{bmatrix} s & 0 \\ 0 & s \end{bmatrix} - \begin{bmatrix} 0 & -\frac{1}{L}(1-D) \\ \frac{1}{C}(1-D) & -\frac{1}{CR_L} \end{bmatrix} \right\}^{-1} \begin{bmatrix} \frac{1}{L} \\ 0 \end{bmatrix}$$

$$G(s) = [0 \quad 1]\begin{bmatrix} s & \frac{1}{L}(1-D) \\ -\frac{1}{C}(1-D) & \left(s + \frac{1}{CR_L}\right) \end{bmatrix}^{-1} \begin{bmatrix} \frac{1}{L} \\ 0 \end{bmatrix}$$

$$G(s) = \left(\frac{LCR_L}{LCR_Ls^2 + Ls + R_L(1-D)^2}\right)[0 \quad 1]\begin{bmatrix} \left(s + \frac{1}{CR_L}\right) & -\frac{1}{L}(1-D) \\ \frac{1}{C}(1-D) & s \end{bmatrix}\begin{bmatrix} \frac{1}{L} \\ 0 \end{bmatrix}$$

$$G(s) = \left(\frac{LCR_L}{LCR_Ls^2 + Ls + R_L(1-D)^2}\right)[\frac{1}{C}(1-D) \quad s]\begin{bmatrix} \frac{1}{L} \\ 0 \end{bmatrix}$$

$$G(s) = \left(\frac{LCR_L}{LCR_Ls^2 + Ls + R_L(1-D)^2}\right)\left[\frac{1}{LC}(1-D)\right]$$

$$G(s) = \frac{R_L(1-D)}{LCR_Ls^2 + Ls + R_L(1-D)^2} = \frac{\frac{1}{LC}(1-D)}{s^2 + \frac{1}{CR_L}s + \frac{1}{LC}(1-D)^2}$$

$$\boldsymbol{G(s) = \frac{\widehat{V}_o(s)}{\widehat{V}_{in}(s)} = \frac{R_L(1-D)}{R_LLCs^2 + Ls + R_L(1-D)^2}}$$

APPENDIX IV

MATLAB CODES

LQR SYSTEM

```
%Step Response for open-loop system
>> A=[0 -4000; 80 -8];
>>B=[10000; 0];
>>C=[0 1];
>>D=[0];
>>sys=ss(A,B,C,D);
>> step(sys)
>> title('Step Response of the Open-loop system')
>> %check stability
>> eig(A)

ans =   1.0e+02 *-0.0400 + 5.6567i
                 -0.0400 - 5.6567i

>> %Check controllability
CO=ctrb(A,B)
CO =  10000          0
          0     800000
>> rank(CO)
ans =     2

>> %Check Observability
OB =     0     1
           80    -8

>> rank(OB)
ans =     2

>> Q=C'*C;
>> R=1;
ns=2;
ny=1;
[K,P,E]=lqr(A,B,Q,R)
K =     0.1033    0.6667
P =      0.0000    0.0001
          0.0001    0.0014
E =   1.0e+02 * -5.2041 + 7.6863i
                 -5.2041 - 7.6863i
>> Acl=A-B*K
Acl = 1.0e+04 *-0.1033   -1.0667
                  0.0080   -0.0008
>> sys1=ss(Acl,B,C,D);
>> step(sys1)
>> grid on
>> hold on
>> Q = 5*C'*C;
>> [K,P,E]=lqr(A,B,Q,R)
K =    0.1722    1.8543
P =      0.0000    0.0002
          0.0002    0.0049
E =1.0e+03 * -0.8652 + 1.0337i
                 -0.8652 - 1.0337i
>> Q = 5*C'*C;
>> [K,P,E]=lqr(A,B,Q,R)
K = 0.1722    1.8543
P =      0.0000    0.0002
          0.0002    0.0049
E =1.0e+03*-0.8652 + 1.0337i
                 -0.8652 - 1.0337i
>> Ac2=A-B*K
Ac2 =1.0e+04*-0.1722   -2.2543
                  0.0080   -0.0008
>> sys2=ss(Ac2,B,C,D);
>> step(sys2)
>> Q = 0.5*C'*C;
[K,P,E]=lqr(A,B,Q,R)
K =    0.0804    0.4044
P = 1.0e-03*   0.0080    0.0404
                  0.0404    0.8128
E =1.0e+02*  -4.0617 + 6.9638i
                 -4.0617 - 6.9638i

>> Q=C'*C;
>> R=1;
ns=2;
ny=1;
[K,P,E]=lqr(A,B,Q,R)
K =     0.1033    0.6667
P =      0.0000    0.0001
          0.0001    0.0014
E =   1.0e+02 * -5.2041 + 7.6863i
                 -5.2041 - 7.6863i
```

```
>> Q = 0.8*C'*C;
[K,P,E]=lqr(A,B,Q,R)
K =    0.0955    0.5702
P =       0.0000    0.0001
          0.0001    0.0012
E =  1.0e+02 * -4.8160 + 7.4290i
                -4.8160 - 7.4290i

>> Ac3=A-B*K
Ac3 =  1.0e+03 *-0.9552   -9.7024
                0.0800   -0.0080
>> Ac4=A-B*K
Ac4 = 1.0e+03 *-0.9552   -9.7024
                0.0800   -0.0080
>> sys4=ss(Ac4,B,C,D);
step(sys4)
>> title('Step Response for different values of
Q22')
>> legend('Q22 = 1','Q22 = 5','Q22 = 0.5','Q22
= 0.8')

>> x=xout1;plot(x(:,1))
grid on
legend('Reference signal', 'Output signal',
'Control signal', 'Error signal')
title('Time response using LQR control')
ylabel ('Output signal')
```

MRAC SYSTEM

```
>> x=xout;
>> plot(x(:,1))
>> grid on
>> ylabel('Output signal')
>> title('Step response for MRAC-only control
scheme')
>> legend('Reference
(y_m)','Γ=0.2','Γ=0.3','Γ=0.4','Γ=0.5','Γ=0.8','Γ
=1.0')

>> x=xout;
plot(x(:,1))
grid on
title('Control signal for different adaptation
gain values')
legend('Γ=0.2','Γ=0.3','Γ=0.4','Γ=0.5','Γ=0.8','Γ
=1.0')
ylabel('Control signal')

>> x=xout;
plot(x(:,1))
grid on
title('Error signal for different adaptation gain
values')
legend('Γ=0.2','Γ=0.3','Γ=0.4','Γ=0.5','Γ=0.8','Γ=
1.0')
ylabel('Error signal')

>> x=xout;
plot(x(:,1))
grid on
title('Parameter estimation for different
adaptation gain values')
legend('Γ=0.2','Γ=0.3','Γ=0.4','Γ=0.5','Γ=0.8','Γ=
1.0')
ylabel('Update signal (θ_1)')

>> x=xout;
plot(x(:,1))
grid on
title('Parameter estimation for different
adaptation gain values')
legend('Γ=0.2','Γ=0.3','Γ=0.4','Γ=0.5','Γ=0.8','Γ=
1.0')
ylabel('Update signal (θ_2)')
```

LQR-MRAC SYSTEM

```
>> x=xout;
plot(x(:,1))
grid on
legend('Reference
(y_m)','Γ=0.5','Γ=1.0','Γ=10.0','Γ=100.0')
title('Step response for LQR-MRAC system
with varying adaptation gains (Γ)')
ylabel('Output signal')


>> x=xout;
plot(x(:,1))
grid on
title('LQR-MRAC control signals for different
adaptation gain values')
legend('Γ=0.5','Γ=1.0','Γ=10.0','Γ=100.0','Γ=200
.0')
ylabel('Control signal')
```

```
>> x=xout;
plot(x(:,1))
grid on
title('LQR-MRAC control Error signals for
different adaptation gain values')
legend('Γ=0.5','Γ=1.0','Γ=10.0','Γ=100.0','Γ=200.0')
ylabel('Error signal')

>> x=xout;
plot(x(:,1))
grid on
title('LQR-MRAC control signals for different
adaptation gain values')
legend('Γ=0.5','Γ=1.0','Γ=10.0','Γ=100.0','Γ=200.0')
ylabel('Control signal')

>> x=xout;
plot(x(:,1))
grid on
legend('Reference
(y_m)','Γ=0.5','Γ=1.0','Γ=10.0','Γ=100.0')
title('Step response for LQR-MRAC system with
varying adaptation gains (Γ)')
ylabel('Output signal')

>> x=xout;
plot(x(:,1))
grid on
title('LQR-MRAC parameter estimation for
different adaptation gain values')
legend('Γ=0.5','Γ=1.0','Γ=10.0','Γ=100.0','Γ=200.0')
ylabel('Update law (θ_1)')

>> x=xout;
plot(x(:,1))
grid on
title('LQR-MRAC parameter estimation for
different adaptation gain values')
legend('Γ=0.5','Γ=1.0','Γ=10.0','Γ=100.0','Γ=200.0')
ylabel('Update law (θ_2)')

>> %Result comparison for different control
models
>> x=xout;
>> plot(x(:,1))
>> grid on
>> legend('LQR-MRAC (y_m)','LQR-MRAC
(y_p)','MRAC-only(y_m)','MRAC-oly(y_p)','LQR-
only','No-controller')
>> title('Step response for different control models
@ Γ=0.5')
>> ylabel('Output signal')

>> %Result comparison for different control models
x=xout;
plot(x(:,1))
grid on
legend('LQR-MRAC (y_m)','LQR-MRAC (y_p @
Γ=50)','MRAC-only (y_m) @ Γ=1.9','MRAC-only
(y_p)','LQR-only','No-controller')
title('Step response for different control models')
ylabel('Output signal')
```

DETERMINING THE INDUCTANCE

```
>> v0=80;
vr=0.02;
r=25;
f=20*(10^3);
d=0:0.01:1.0;
x=v0/(vr*r*f);
y=r/(2*f);
C=x.*d;
L=y.*d.*(1-d).^2;
plot(d,L,'b');
>> grid on
>> xlabel('Duty ratio')
>> ylabel('Inductance (Henry)')
>> title('inductance over duty cycle')
```

DETERMINING THE CAPACITANCE

```
>> v0=80;
vr=0.02;
r=25;
f=20*(10^3);
d=0:0.01:1.0;
x=v0/(vr*r*f);
y=r/(2*f);
C=x.*d;
L=y.*d.*(1-d).^2;
plot(d,C,'b');
grid on
xlabel('Duty ratio')
ylabel('Capacitance (Farad)')
title('Capacitance over duty cycle')
```